

Copyright
by
Jessica E. Momb
2009

**The Dissertation Committee for Jessica E. Momb Certifies that this is the approved
version of the following dissertation:**

**An Investigation of a Quorum-Quenching Lactonase
from *Bacillus thuringiensis***

Committee:

Walter Fast, Supervisor

David Hoffman

Kenneth Johnson

Christian Whitman

Yan Jessie Zhang

**An Investigation of a Quorum-Quenching Lactonase
from *Bacillus thuringiensis***

by

Jessica E. Momb, B.S.

Dissertation

Presented to the Faculty of the Graduate School of
The University of Texas at Austin
in Partial Fulfillment
of the Requirements
for the Degree of

Doctor of Philosophy

The University of Texas at Austin

December 2009

Dedication

I would like to dedicate this work to two important people in my life, my husband Michael and my mother Kathy. I thank Michael for his love, support, humor and good nature. I thank Kathy for her love, strength, and for always inspiring me to be a better person.

Acknowledgements

The printed pages of this dissertation hold far more than the culmination of years of study. These pages also reflect the relationships with many generous and inspiring people I have met since beginning my graduate work. I thank each person for their contribution to my life and career.

To my advisor Walter Fast, a gracious mentor who demonstrates that any problem must be considered from all possible angles, and to always trust your data even if the results are unexpected.

To past and present Fast Lab members for their friendship, contributions to this work and thoughtful insights.

To all my committee members for their helpful suggestions and for taking time out of their busy schedules for me.

To my undergraduate professors for inspiring me to do research and offering me the opportunity to teach chemistry to others, especially Jeffrey Schineller, William Wood and Jacob Varkey.

**An Investigation of a Quorum-Quenching Lactonase
from *Bacillus thuringiensis***

Publication No. _____

Jessica Momb, Ph.D.

The University of Texas at Austin, 2009

Supervisor: Walter Fast

Gram-negative bacteria use *N*-acyl homoserine lactones (AHLs) to sense population density and regulate gene expression, including virulent phenotypes. The quorum-quenching AHL lactonase from *Bacillus thuringiensis* cleaves the lactone ring of AHLs, disabling this mode of gene regulation. Despite the potential applications of this enzyme as an antibacterial weapon, little was known about its lactone ring-opening mechanism. As a member of the metallo- β -lactamase superfamily, AHL lactonase requires two divalent metal ions for catalysis. NMR experiments confirm that these metal ions are also involved in proper enzyme folding. The chemical mechanism of ring opening was explored using isotope incorporation studies, and hydrolysis was determined to proceed via a nucleophilic attack by a solvent-derived hydroxide at the carbonyl of the lactone ring. A transient, kinetically significant metal-leaving group interaction was detected in steady-state kinetic assays with AHL lactonase containing alternative divalent metal ions hydrolyzing a sulfur-containing substrate. High-resolution crystal structures

implicated two residues in substrate binding and hydrolysis, Tyr194 and Asp108. Site-directed mutagenesis of these residues followed by steady-state kinetic studies with wild-type and mutant enzymes hydrolyzing a spectrum of AHL substrates revealed that mutations Y194F and D108N significantly affect catalysis. Combining these results allows the proposal of a detailed hydrolytic mechanism. The binding site for the *N*-acyl hydrophobic moiety was probed using steady-state kinetics with a variety of naturally occurring and non-natural AHL substrates, and these studies indicate that AHL lactonase will accept a broad range of homoserine lactone containing substrates. Crystal structures with AHL substrates and non-hydrolyzable analogs reveal two distinct binding sites for this *N*-acyl group. Based on the ability of this enzyme to accommodate a variety of substrates, AHL lactonase was shown to have the ability to quench quorum sensing regulated by a newly discovered class of homoserine lactone signal molecules possessing an *N*-aryl group using a bioassay. Steady-state kinetic studies confirm that this class of signal molecules are indeed substrates for AHL lactonase.

Table of Contents

List of Tables.....	xiii
List of Figures.....	xiv
List of Schemes.....	xvi
Chapter 1 Introduction.....	1
Quorum Sensing in Gram-negative Bacteria.....	1
Quorum-Quenching is an Effective Antibacterial Strategy.....	5
AHL Lactonase is a Member of the Metallo- β -Lactamase Superfamily.....	9
Chapter 2 Investigation of the Metal Center of <i>Bacillus thuringiensis</i> AHL Lactonase. .	12
Introduction.....	12
Experimental Methods.....	15
Expression and Purification of the Maltose Binding Protein-AHL Lactonase Fusion Protein.....	15
^1H NMR Spectroscopy of Dinuclear Zinc and Apo AHL Lactonase.....	18
Synthesis of <i>N</i> -Hexanoyl-L-homoserine Lactone (C6-HSL).....	18
Enzyme-Catalyzed Incorporation of ^{18}O from H_2^{18}O into the <i>N</i> -Hexanoyl-L-Homoserine Product.....	19
^1H NMR Spectroscopy of Reaction Products After Hydrolysis in D_2O	20
Synthesis of <i>N</i> -Hexanoyl-DL-homocysteine Thiolactone (C6-HCTL).....	21
Expression and Purification of Metal-Substituted AHL Lactonases	22
Kinetic Assay of AHL Lactonase Activity.....	22

Crystallization, Data Collection and Processing, Model Building and Refinement of Product-Bound Dizinc and Dicobalt AHL Lactonases.....	23
Synthesis of Ring-opened Products and Determination of Product Inhibition Constants.....	23
Results.....	24
¹ H NMR Spectroscopy of Dinuclear Zinc AHL Lactonase and Apo AHL Lactonase	24
Enzyme-Catalyzed Incorporation of ¹⁸ O from H ₂ ¹⁸ O Into the <i>N</i> -Hexanoyl-L-Homoserine Product	26
¹ H NMR Spectroscopy of Reaction Products After Hydrolysis in D ₂ O.....	28
Expression and Purification of Metal-Substituted AHL Lactonases	29
Steady-State Kinetics of Metal-Substituted AHL Lactonases.....	30
Crystallization, Data Collection and Processing, Model Building and Refinement of Product-Bound Dizinc and Dicobalt AHL Lactonases	35
Discussion.....	38
Chapter 3 Role of Active Site Residues in the AHL Lactonase Catalytic Mechanism.....	48
Introduction.....	48
Experimental Methods	51
Construction of the Expression Vector for Maltose Binding Protein MBP-D108N AHL Lactonase Fusion Protein.....	51
Construction of the Expression Vector for Cleavable Maltose Binding Protein MBP-Y194F AHL Lactonase Fusion Protein.....	51
Expression and Purification of Metal-Substituted AHL Lactonases.....	52
Circular Dichroism Spectroscopy of AHL Lactonase.....	54

Kinetic Assay of AHL Lactonase Activity.....	56
Results.....	58
Protein Purification and Characterization.....	58
Circular Dichroism of Wild Type and Mutant AHL Lactonases.....	59
Steady-State Hydrolysis Kinetics.....	60
Discussion.....	62
Chapter 4 Substrate Preference and Promiscuity of AHL Lactonase.....	74
Introduction.....	74
Methods.....	75
Construction of the Expression Vector for Cleavable Maltose Binding Protein MBP-A206W, G207W and G207D AHL Lactonase Fusion Proteins.....	75
Expression and Purification of Metal-Substituted AHL Lactonases.....	76
Circular Dichroism Spectroscopy of AHL Lactonase.....	77
Synthesis of <i>N</i> -Pentanoyl-L-Homoserine Lactone (C5-HSL).....	79
Synthesis of <i>N</i> -Decanoyl-L-Homoserine Lactone (C10-HSL).....	80
Kinetic Assay of AHL Lactonase Activity.....	81
Synthesis of <i>N</i> -Octanoyl-L-Homoserine Lactone (C8-HSL).....	81
Synthesis of <i>N</i> -Dodecanoyl-L-Homoserine Lactone (C12-HSL).....	82
Synthesis of <i>N</i> -Tetradecanoyl-L-Homoserine Lactone (C14-HSL).....	83
Synthesis of <i>trans</i> -(<i>N</i> -Hexanoyl)-Aminocyclopentanol (<i>trans</i> -ACP).....	84
Synthesis of <i>cis</i> -(<i>N</i> -Hexanoyl)-Aminocyclopentanol (<i>cis</i> -ACP).....	86

Crystallization, Data Collection and Processing, Model Building and Refinement of Product-Bound Dizinc and Dicobalt AHL Lactonases.....	87
Determination of IC_{50} Values for <i>cis</i> and <i>trans</i> Substrate Analogs.....	87
Results.....	88
Protein Purification and Characterization.....	88
Circular Dichroism Spectroscopy of AHL Lactonase.....	88
Steady-state Hydrolysis Kinetics With Acyl Pocket Mutants.....	89
Steady-state Hydrolysis Kinetics with Wild Type Dicobalt and Dizinc AHL Lactonases.....	94
Determination of IC_{50} Values for Substrate Analogs.....	96
Crystallization, Data Collection and Processing, Model Building and Refinement of Dicobalt Wild Type and Y194F Mutant AHL Lactonases With <i>cis</i> -ACP, <i>trans</i> -ACP and C10-HSL.....	99
Discussion.....	102
Chapter 5 AHL Lactonase Hydrolyzes a New Class of Quorum-Sensing Signals.....	107
Introduction.....	107
Methods.....	109
Synthesis of <i>N</i> -(Cinnamoyl)-L-Homoserine Lactone (cinnamoyl-HSL).....	109
Expression and Purification of Metal-Substituted AHL Lactonases.....	110
Kinetic Assay of Cinnamoyl-HSL Hydrolysis.....	111
Mass Spectral Analysis of Products Formed in the AHL Lactonase Reaction.....	111

Bioassay for Quorum Quenching Using the <i>R. palustris</i> Quorum Sensing System	111
Results.....	112
Protein Purification and Characterization	112
Kinetic Analysis of Cinnamoyl-HSL Hydrolysis.....	113
Mass Spectral Analysis of Products Formed in the AHL Lactonase Reaction.....	115
Bioassay for Quorum Quenching of the <i>R. palustris</i> Quorum Sensing System.....	115
Discussion.....	117
References.....	123
Vita.....	133

List of Tables

Table 2.1 Metal content of purified monomeric AHL lactonase grown in minimal medium with alternative divalent metal ions.....	30
Table 2.2 Steady-state kinetic constants for hydrolysis of substrates with oxygen (C6-HSL) or sulfur (C6-HCTL) leaving groups by AHL lactonase disubstituted with indicated metal ions.....	31
Table 3.1 Calculated secondary structure content of AHL lactonase variants.....	56
Table 3.2 Steady-state kinetic constants for C6-HSL hydrolysis by dizinc and dicobalt AHL lactonase variants.....	60
Table 3.3 Steady-state kinetic constants for C6-HCTL hydrolysis by dicobalt AHL lactonase variants.....	62
Table 4.1 Primers used for Quikchange mutagenesis.....	76
Table 4.2 Calculated secondary structure content of AHL lactonase variants.....	79
Table 4.3 Steady-state kinetic constants for substrate hydrolysis by dicobalt AHL lactonase variants.....	93
Table 4.4 Steady state kinetic constants for AHL hydrolysis by dizinc AHL lactonase..	95
Table 4.5 Steady state kinetic constants for AHL hydrolysis by dicobalt AHL lactonase.....	96
Table 4.6 Inhibiton constants for hydrolysis of C6-HSL in the presence of <i>trans</i> - and <i>cis</i> -ACP.....	98
Table 5.1 Kinetic parameters and substrate discrimination energies for hydrolysis of indicated substrates by dizinc AHL lactonase.....	113
Table 5.2 Kinetic parameters and substrate discrimination energies for hydrolysis of indicated substrates by dicobalt AHL lactonase.....	114

List of Figures

Figure 1.1 Structure of the <i>Vibrio fischeri</i> quorum sensing signal, N-3-(oxohexanoyl) homoserine lactone (3-oxo-C6-HSL).	2
Figure 1.2 The LuxIR controlled quorum sensing circuit of <i>Vibrio fischeri</i>	3
Figure 1.3 Variation of AHL structures used by Gram-negative bacteria.....	4
Figure 2.1 Naturally occurring (C6-HSL) and synthetic (C6-HCTL) substrates used for crystallographic studies and to detect a kinetic thio effect.	14
Figure 2.2 One-dimensional ¹ H NMR spectra of dizinc and apo AHL lactonase.....	26
Figure 2.3 C6-HSL hydrolyzed by AHL lactonase in a mixture of 50% H ² ₁₈ O and 50% H ₂ ¹⁶ O.....	28
Figure 2.4 Product inhibition of dicadmium AHL lactonase by ring opened C6-HSL and C6-HCTL.....	33
Figure 2.5 Ring-opened C6-HSL and C6-HCTL bound at the metal center of dicobalt AHL lactonase.....	36
Figure 2.6 Ring-opened C6-HSL and C6-HCTL bound at the metal center of dizinc AHL lactonase.....	37
Figure 2.7 Metal binding ligands for dizinc and dicobalt AHL lactonases.....	45
Figure 3.1 CD spectra of dicobalt AHL lactonase	55
Figure 3.2 Metal ligand arrangement in unliganded and C6-Hse bound dizinc AHL lactonase.....	70
Figure 3.3 Metal ligand arrangement in unliganded and C6-Hse bound dicobalt AHL lactonase.....	71
Figure 4.1 CD spectra of dicobalt AHL lactonases	78

Figure 4.2 <i>trans</i> -(<i>N</i> -Hexanoyl)-aminocyclopentanol (<i>trans</i> -ACP).....	84
Figure 4.3 <i>cis</i> -(<i>N</i> -hexanoyl)-aminocyclopentanol (<i>trans</i> -ACP).....	86
Figure 4.4 Structures of AHL substrates used to probe the sidechain binding site of AHL lactonase.....	90
Figure 4.5 Binding of the hexanoyl chain of C6-HSL in AHL lactonase.....	91
Figure 4.6 Inhibition by substrate analogs.....	97
Figure 4.7 Overlay of the structures of <i>trans</i> -ACP bound to wild type dicobalt AHL lactonase and Y194F mutant AHL lactonase.....	100
Figure 4.8 Overlay of the structures of <i>trans</i> -ACP bound to wild type dicobalt AHL lactonase and Y194F mutant AHL lactonase.....	101
Figure 4.9 Overlay of wild type dicobalt AHL lactonase complexed with C6-Hse and dicobalt Y194F AHL lactonase complexed with C10-Hse.....	102
Figure 5.1 <i>N</i> -(<i>p</i> -coumaroyl)-L-homoserine lactone (<i>pC</i> -HSL) and <i>N</i> -(cinnamoyl)-L-homoserine lactone (cinnamoyl-HSL), novel ArHL signaling agents.....	108
Figure 5.2 Assay for cinnamoyl-HSL hydrolysis using the <i>P. aeruginosa</i> pRpaR-pRpaI::lacZ reporter strain.	116
Figure 5.3 Structural overlay of ring-opened cinnamoyl-HSL with ring-opened C6-HSL in complex with dizinc AHL lactonase.....	120

List of Schemes

Scheme 1.1 Enzymatic AHL signal degradation.....	6
Scheme 2.1 Four potential ring opening mechanisms for AHL lactonase catalysis.....	41
Scheme 3.1 AHL lactonase catalytic mechanism proposed by Kim et al.....	49
Scheme 3.2 Ring opening of C6-HSL catalyzed by AHL lactonase.....	56
Scheme 3.3 Proposed catalytic mechanism for hydrolysis by AHL lactonase.....	67

Chapter 1 Introduction

QUORUM SENSING IN GRAM-NEGATIVE BACTERIA

The ability of bacteria to communicate via a language of chemical signals was first identified in the early 1970s through studies of the marine bacterium *Vibrio fischeri*, an organism whose quorum sensing system is considered to be the paradigm for communication in most Gram-negative bacteria (1, 2). *V. fischeri* is a bioluminescent marine bacterium known to colonize the light organ of the Hawaiian squid *Euprymna scolopes*. Inside the light organ of this squid, *V. fischeri* is able to grow to a high cell density, resulting in induction of the expression of genes required for bioluminescence. The relationship between *V. fischeri* and *E. scolopes* is mutually beneficial, providing the bacteria with a nutrient rich environment while the bacteria produce light, enabling the host squid to mask its shadow and hide from predators (3).

V. fischeri utilizes the chemical signal 3-oxo-*N*-(tetrahydro-2-oxo-3-furanyl) hexanamide, a compound more commonly referred to as *N*-3-(oxohexanoyl) homoserine lactone or 3-oxo-C6-HSL (Figure 1.1) (4). This chemical signal is able to permeate the cell membrane and accumulate in the growth medium (5). 3-oxo-C6-HSL is produced constitutively at a basal level, and at low cell densities exists in low concentrations. As cell growth increases, 3-oxo-C6-HSL accumulates and increases in concentration. At a critical concentration of 10 nM (5), the 3-oxo-C6-HSL concentration is sufficient to

effect transcription of the luciferase operon, which contains the genes for light production (1).

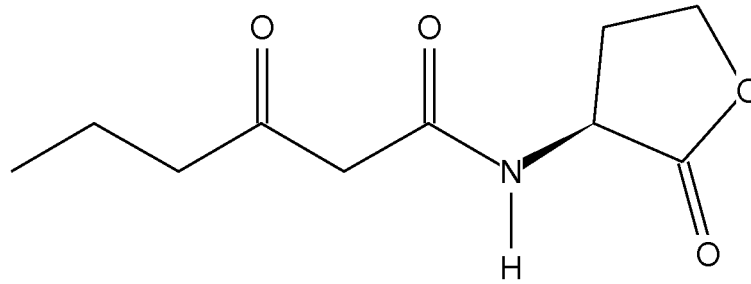


Figure 1.1 Structure of the *Vibrio fischeri* quorum sensing signal, *N*-3-(oxohexanoyl) homoserine lactone (3-oxo-C6-HSL).

The luciferase operon (*luxICDABE*) is required for light production and is under the control of two proteins, LuxI and LuxR (Figure 1.2) (6). The *luxI* gene encodes an AHL synthase that is responsible for production of the AHL signal 3-oxo-C6-HSL (4, 6). The product of the *luxR* gene is a transcriptional activator that binds the promoter of the *lux* operon, activating transcription of light production genes in addition to *luxI*, which is also encoded in this operon (7). When LuxR binds 3-oxo-C6-HSL, this complex forms a dimer (8) which is then able to bind to the promoter, causing expression of the *lux* operon (Figure 1.2) (9). Thus, activation of the *lux* operon creates a positive feedback loop,

flooding the environment with 3-oxo-C6-HSL, reaching a concentration of approximately 200 nM, and rapidly switching the entire population into light production mode (5).

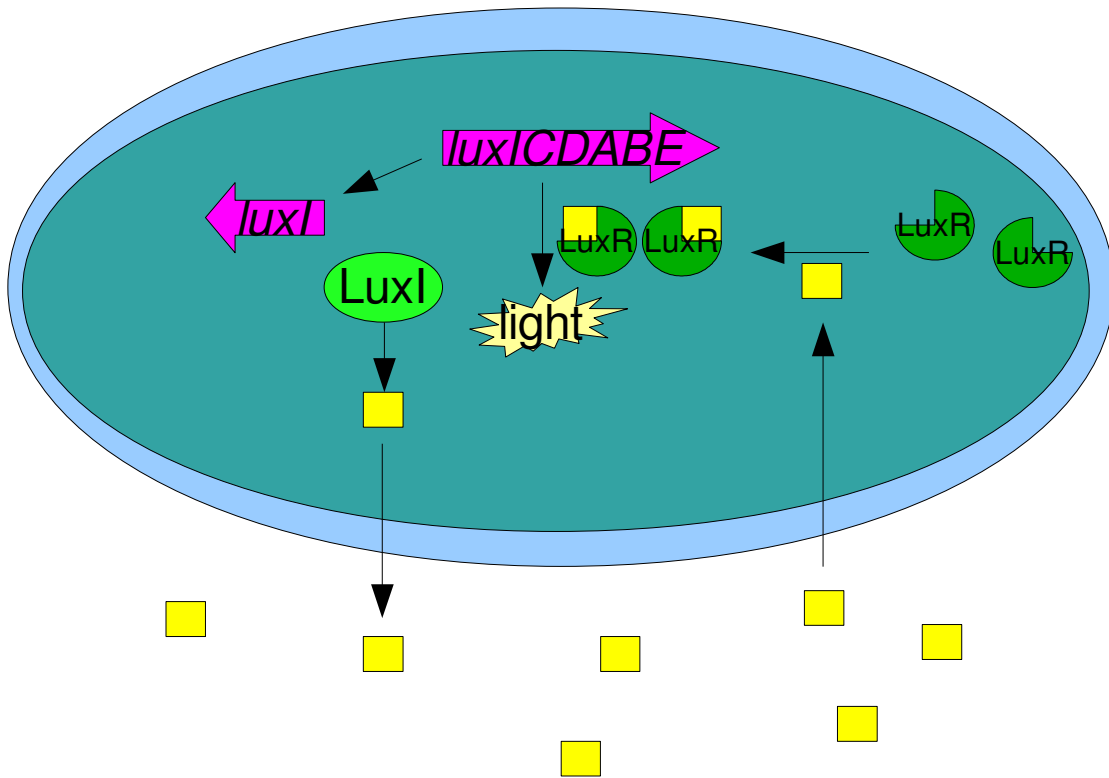


Figure 1.2 The LuxIR controlled quorum sensing circuit of *Vibrio fischeri*. Yellow boxes represent 3-oxo-C6-HSL. Upon binding the AHL signal molecule, LuxR dimerizes and is able to bind the promoter of the *lux* operon, causing expression of *luxI*, resulting in a positive-feedback loop where 3-oxo-C6-HSL production increases rapidly.

Similar quorum-sensing systems comprised of LuxIR-type proteins and *N*-acyl homoserine lactone (AHL) signals are employed by many species of Gram-negative

bacteria (10, 11). There is a large amount of diversity in the *N*-acyl chain of AHLs used for signaling (Figure 1.3), with the length varying from 4 to 16 carbons in length (10). In addition, there may be variation in substituents on the acyl chain, such as the 3-oxo moiety seen in 3-oxo-C6-HSL (10).

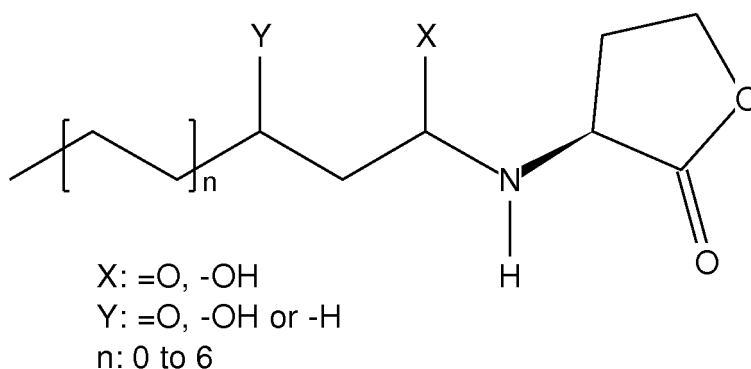


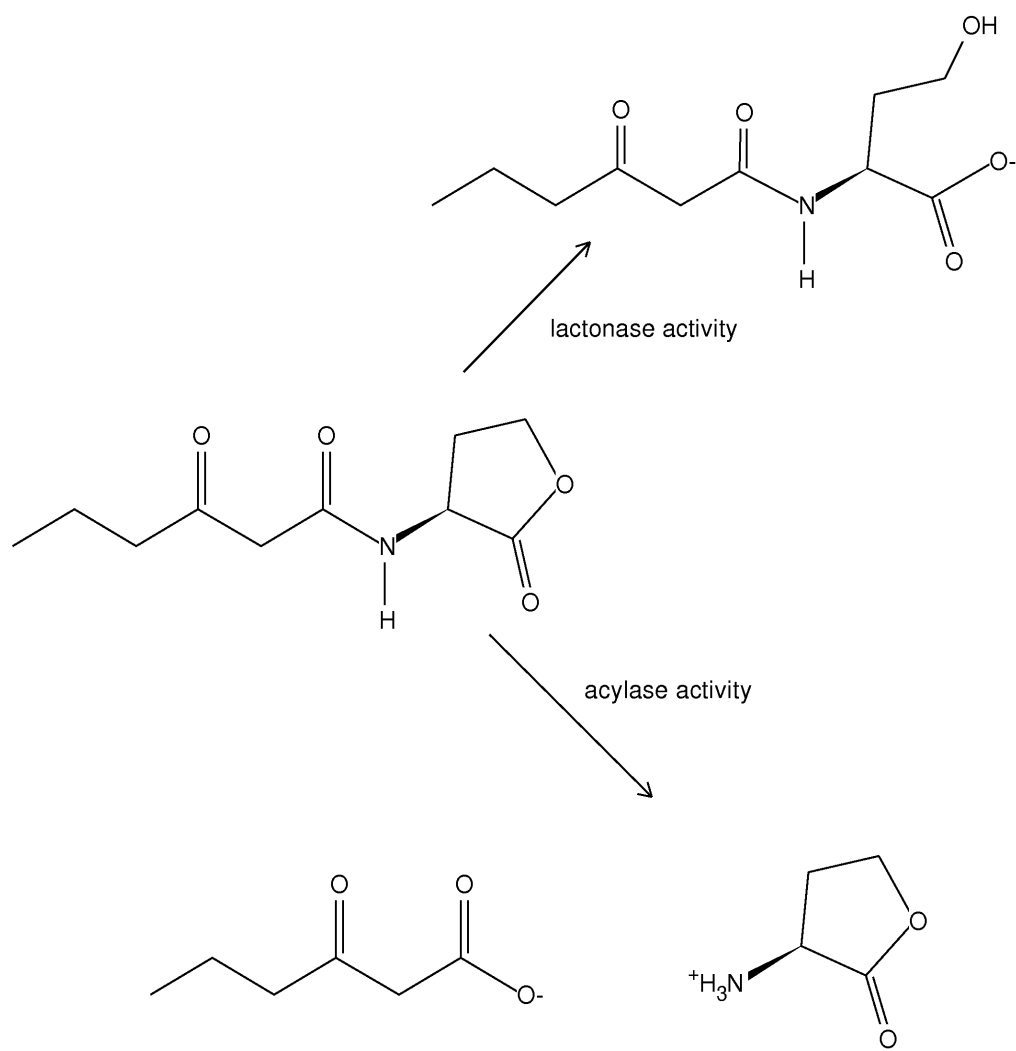
Figure 1.3 Variation of AHL structures used by Gram-negative bacteria.

Quite a few of these quorum-sensing systems are involved in the control of pathogenic activities that are harmful to the host, as opposed to the symbiotic relationship seen between *V. fischeri* and its squid host. For example, the human pathogen *Pseudomonas aeruginosa* controls biofilm formation and virulence factor production via a two-component AHL quorum sensing system (12). Another human pathogen, *Serratia marcescens*, uses AHL dependent quorum sensing to control swarming motility and protease production, among other functions (13). Many quorum-sensing controlled processes such as pathogenic and virulent phenotypes are not worthwhile for a single

bacterium to engage in, but benefit a community of bacteria. Quorum sensing allows bacteria to evade the host immune response while the bacterial population grows large enough to resist these responses.

QUORUM-QUENCHING IS AN EFFECTIVE ANTIBACTERIAL STRATEGY

Since quorum sensing is linked to pathogenicity, it is sensible to look at disruption of these systems as potential therapy for infection. The recent discovery of enzymes capable of modifying AHL signals offers promise as a new approach for control of bacterial growth, as a new therapeutic or as an adjuvant to existing antibacterial treatments. Two routes for enzymatic AHL degradation are known to operate currently via lactonase or acylase pathways (Scheme 1.1).



Scheme 1.1 Enzymatic AHL signal degradation

Enzymatic AHL signal degradation in bacteria was first reported in 2000, with the discoveries of an AHL lactonase from *Bacillus thuringiensis* and an AHL acylase from *Variovorax paradoxus* (14, 15). Since these first reports of AHL signal degradation,

many more homologs of acylase and lactonase enzymes have been found in bacteria, eukarya and archaea living in a variety of environments, indicating that degradation of this class of molecules is important across all classes of life (16).

Some AHL producers produce their own lactonases and acylases, such as *A. tumefaciens*, whose zinc-dependent lactonase AttM is involved in the shutdown of quorum sensing after quorum sensing controlled plasmid transfer (17). While *B. thuringiensis* does not possess its own quorum-sensing system, it may use AHL lactonase to inhibit quorum sensing by competing bacteria, or perhaps to inhibit the production of antibacterial tetramic acids (18). AHL-mediated quorum-sensing is known to control production of natural antifungals in species such as *Burkholderia cepacia* (19), and the quinolone class of quorum sensing signals utilized by Gram-positive bacteria are known to exhibit antibacterial activity against Gram-positive species (20). An enzyme capable of inactivating AHLs would provide an organism with a weapon against quorum-sensing related attacks from competitors. It is probably no coincidence, then, that many organisms known to produce AHL degrading enzymes are found in environments where AHL-producers also flourish.

Bacillus thuringiensis, which produces the AHL lactonase that is the focus of the studies described here, resides in soil and on the surface of plants. Many plant-associated bacteria such as *Pseudomonas aeruginosa* and *Erwinia carotovora* utilize AHLs to regulate pathogenic and symbiotic behaviors that occur between microbes and their plant

hosts (21). In such an environment, AHL degradation would confer a competitive advantage. Investigation of a *B. thuringiensis* mutant strain lacking AHL lactonase did in fact show that the survival rate was decreased in comparison to the wild-type organism growing in the pepper rhizosphere (22).

AHL-degrading enzymes have been proven to be effective in the attenuation of virulence in a variety of circumstances, for example coculture of AHL degrading and AHL producing species results in reduction of AHL accumulation and attenuation of virulence (14, 23, 24). Application of a purified quorum quenching acylase to cultures of *P. aeruginosa* resulted in a reduction of virulence factor production, but did not reduce cellular growth (25). Expression of the AHL lactonase from *Bacillus thuringiensis* in the plant pathogen *E. carotovora* resulted in reduced levels of AHL, decreased pectolytic enzyme activities, and attenuated disease symptoms caused by the pathogen on potato, eggplant, cabbage, carrots and celery (14). Transgenic expression of this enzyme in the human pathogen *Pseudomonas aeruginosa* reduced accumulation of the long AHL signal 3-oxo-C12-HSL and prevented accumulation of the short AHL signal C4-HSL, resulting in a decrease in swarming motility and virulence factor production (26). Despite these promising results, little was known about the catalytic mechanism of this hydrolytic enzyme, prompting our investigation into the mechanism of *B. thuringiensis* AHL lactonase.

AHL LACTONASE IS A MEMBER OF THE METALLO- β -LACTAMASE SUPERFAMILY

AHL lactonase (or AiiA, for autoinducer inactivator A) was first recognized as a member of the metallo- β -lactamase (M β L) superfamily based on sequence alignments (14). Proteins comprising the metallo- β -lactamase (M β L) superfamily are present in all three domains of life and show remarkable diversity, and members of this family are known to catalyze a wide variety of reactions (27). This variety includes at least 17 different activities ranging from nitric oxide and oxygen reduction as well as cleavage of C-O, C-N, C-S, S-O, P-O and possibly P-N bonds (28). A significant number of these M β Ls are implicated in clinically relevant processes such as bacterial antibiotic resistance mechanisms, anticancer drug detoxification and processing of mRNA (28). This abundance of clinically important family members makes this superfamily the subject of a large amount of ongoing study.

Incredible diversity has been observed among the identity and number of occupants of the active site metal centers of M β Ls. Examples include mononuclear and dinuclear proteins, mononuclear proteins with the metal ion bound at an alternative site, dinuclear proteins with both metals bound within close proximity to each other in a cocatalytic site and two-metal proteins where a second metal-binding site is distant but allosterically linked to the active site (29, 30). Most M β Ls are thought to bind zinc at their signature conserved metal binding motif HxHxDH~H~D~H (14), although some

examples have been noted to bind the alternative metals iron and manganese *in vivo* (31, 32). Although the metal stoichiometry and placement requirements for some MβLs are still debated (30), all members of this superfamily that have been studied in detail display a metal requirement (30, 33).

Initial studies on *B. thuringiensis* AHL lactonase suggested that this enzyme did not require metal ions, despite the presence of the known metal-binding motif (34). Subsequent investigations into the metal requirement of AHL lactonases have shown that this enzyme does in fact require two divalent metal ions for catalysis (34-38), and the claim that metal ions were not a requirement were based on data from a protein preparation, ostensibly contaminated by inactive, metal-free protein (34, 35). This revelation prompted our investigations to address the role of the metal center in proper folding of AHL lactonase, investigate the chemical mechanism of ring opening, probe substrate interactions with the metal center during catalytic hydrolysis and look at substrate preference of this enzyme. These are the topics of this dissertation - a brief summary of our findings is discussed below.

The involvement of metal ions in the proper folding and catalytic mechanism of AHL lactonase is investigated in Chapter 2. Using one-dimensional ¹H NMR, we show that two metal equivalents are required for protein folding. Isotopic labeling experiments yield insight into the chemical ring-opening mechanism, and incorporation of alternative metals along with steady-state kinetic studies using natural and synthetic substrates allow

tracking of a transient metal-leaving group interaction. Finally, a collaboration with the Petsko/Ringe group (Brandeis University) afforded high resolution crystal structures of product-bound dizinc and dicobalt AHL lactonases that indicate an interaction between the leaving group and the metal center. In Chapter 3, site-directed mutagenesis and steady-state kinetics are used to probe the roles of two important active-site residues, Tyr194 and Asp108. Combined with the results presented in Chapter 2, a catalytic mechanism for ring opening is proposed where Tyr194 stabilizes a tetrahedral intermediate and Asp108 acts as a proton shuttle. In Chapter 4 investigations of the acyl binding site through site-directed mutagenesis, synthesis of alternative substrates and substrate analogs, steady-state kinetics and crystal structures obtained with our collaborators are described. Lastly, in Chapter 5 we discover the activity of AHL lactonase against a new class of *N*-aryl homoserine lactone quorum sensing molecules using an *in vivo* bioassay and steady-state kinetics.

Chapter 2 Investigation of the Metal Center of *Bacillus thuringiensis* AHL Lactonase

INTRODUCTION

The first detailed study of the specificity and kinetics of AHL lactonase (AiiA) from *Bacillus thuringiensis* claimed that, despite the presence of the metal-binding motif conserved throughout the metallo- β -lactamase (M β L) superfamily, this enzyme does not require metal ions for catalysis (34). Subsequent studies from the Fast lab (35) and others (37) have confirmed the necessity of metal ions for successful catalysis of lactone hydrolysis by AHL lactonase. These studies, however, did not address the role of the required metal center in the hydrolytic mechanism. The role of these metal ions may be structural in nature, helping the enzyme to properly fold, or they may occupy a site in an a pre-folded structure, performing a purely catalytic role. Roles in catalysis could include stabilizing a negative charge by acting as a Lewis acid, positioning of the substrate for efficient attack, and/or lowering the pK_a of the nucleophilic metal bound hydroxide as is seen in catalytic mechanisms of members of the M β L superfamily (39). Of course, the metal center may serve both structural and catalytic roles for AHL lactonase. In order to address these questions, a one-dimensional ¹H NMR experiment was performed with the metal-bound and apo AHL lactonase to determine whether the enzyme remains folded or unfolds upon removal of metal ions.

To further study the possible roles of metal ions during catalysis, collaborative crystallographic experiments between the Fast lab and the Petsko-Ringe lab (Brandeis University) were undertaken. These reveal interesting interactions between the ring-opened products of two AHL lactonase substrates, *N*-hexanoyl-L-homoserine lactone (Figure 2.1, C6-HSL) and the *N*-hexanoyl-DL-homocysteine thiolactone (Figure 2.1, C6-HCTL). C6-HSL is a naturally occurring AHL substrate, while C6-HCTL is not known to be produced by any organism, and is a racemic mixture as a result of the synthetic method used to obtain it. Co-crystallization of these compounds with dizinc and dicobalt substituted AHL lactonase reveals interaction of the product with the metal center, prompting investigation into transient metal-substrate interactions during catalysis. These types of interactions have been detected in other M β L superfamily members, for example the dinuclear metal center of L1 M β L from *Stenotrophomonas maltophilia* (40, 41) has been shown to be involved in leaving group stabilization.

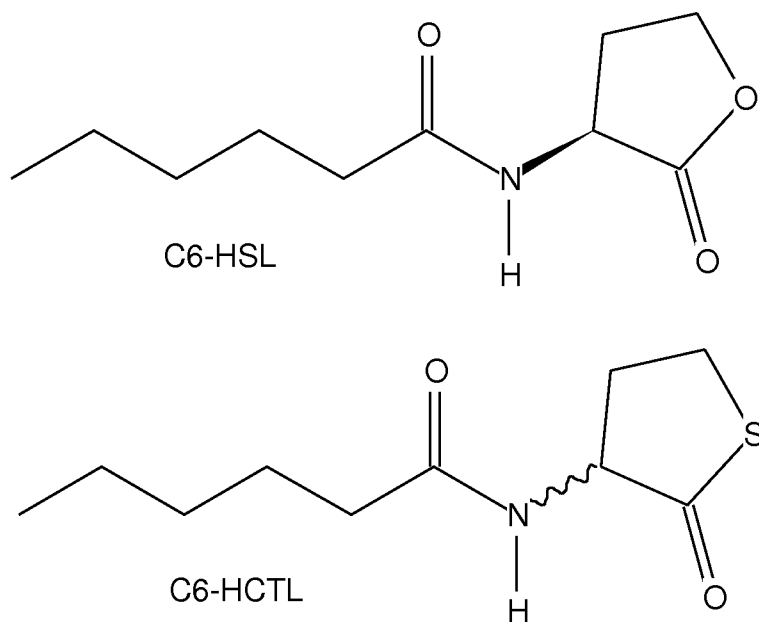


Figure 2.1 Naturally occurring (C6-HSL) and synthetic (C6-HCTL) substrates used for crystallographic studies and to detect a kinetic thio effect.

The stable isotope interaction studies described herein confirm that the ring oxygen of the AHL molecule acts as a leaving group during hydrolytic ring opening, and this opening proceeds through an addition-elimination pathway. This result allowed the exploitation of the different leaving groups of C6-HSL and C6-HCTL (Figure 2.1) in combination with variation in thiophilicities of alternative metal ions incorporated into AHL lactonase to detect a kinetic thio effect during hydrolytic ring opening by AHL lactonase.

EXPERIMENTAL METHODS

Expression and Purification of the Maltose Binding Protein-AHL Lactonase Fusion Protein

Protein expression and purification were accomplished using methods previously established by the Fast Lab (35). *E.coli* DH5 α E cells transformed with the plasmid pMAL-t-aiiA (35) were incubated with shaking at 37 °C in Terrific broth (TB) supplemented with 0.2% glucose and 50 μ g/mL ampicillin. Growth was continued until cell density reached an OD₆₀₀ of 0.5-0.7, at which time expression of recombinant maltose binding protein MBP-AHL lactonase fusion protein (MBP-AHL) was induced by addition of 0.3 mM IPTG. Expression was allowed to continue for an additional 16 h at 25 °C. Cells were then harvested by centrifugation and either lysed by sonication as described below or washed with 20 mM Tris-HCl buffer and 5 mM NaCl, pH 7.4 for storage at -20 °C until needed.

All purification procedures were performed at 4 °C unless otherwise indicated. A BioLogic LP protein purification system (Bio- Rad, Hercules, CA) was employed for all chromatographic procedures. A cell pellet obtained from a 1 L culture was resuspended in 100 mL of column buffer (20 mM Tris-HCl buffer, 200 mM NaCl, pH 7.4) and subjected to sonication with six pulses of 30 s each with 120 s cooling intervals. Cell debris was removed by centrifugation at 34,500 g for 30 min. Protein concentration of the resulting supernatant was determined using the Bio-Rad protein assay kit (Bio-Rad),

calibrated with bovine serum albumin (BSA) as the standard. The supernatant was subsequently diluted to 1.5 mg/mL with column buffer and loaded onto a column of amylose-agarose resin (2.5 x 10 cm , New England Biolabs) at a flow rate of 0.5 mL/min. After washing with 1- 2 column volumes of column buffer, the fusion protein was eluted with 10 mM maltose in column buffer. Eluted fractions containing fusion protein were identified using SDS-PAGE, combined and placed in Spectra/Por dialysis tubing with a molecular weight cutoff (MWCO) of 12,000-14,000 Da (Spectrum Laboratories, Rancho Dominguez, CA) and dialyzed overnight against buffer A (20 mM Tris-HCl buffer, pH 7.4, 5 mM NaCl) and 2mM dithiothreitol at 4 °C. The dialyzed protein was loaded onto a DEAE-Sepharose FF column (1.5 x 15 cm) equilibrated with buffer A and subsequently washed with 200 mL of buffer A made to 160 mM NaCl. Elution was accomplished by varying the NaCl concentrations from 160 to 250 mM. The active fraction of the MBP-AHL lactonase fusion protein observed to elute at a conductivity near 19 mS/cm (approximately 180-190 mM NaCl), and the remaining proteins including apo MBP-AHL lactonase were eluted at higher salt concentrations with a conductivity near 26 mS/cm as previously described (35).

Specific Proteolysis of MBP-AHL Lactonase and Subsequent Purification of Untagged AHL Lactonase

Fractions containing active MBP-AHL lactonase were concentrated using an Amicon Ultra-15 (10,000 MWCO) centrifugal filter device (Millipore, Billerica, MA).

The resulting concentrated fusion protein was diluted to 1 mg/mL in a buffer consisting of 50 mM Tris-HCl, pH 8, 160 mM NaCl, 1 mM DTT, and 4% (w/w) TEV protease (42, 43). Specific proteolysis of MBP-AHL lactonase was carried out at 10 °C overnight (16-20 h) with slow gentle shaking. Reaction products were characterized using SDS- PAGE to ensure cleavage. To purify the cleaved AHL lactonase, protein cleavage products were diluted with an equal volume of buffer A and applied to a DEAE-Sepharose FF column (1.5 x 10 cm). The MBP fragment and TEV protease both eluted from the column using 160 mM NaCl in buffer A. Untagged AHL lactonase eluted using 170 mM NaCl in buffer A. Lastly, to remove any trace amounts of uncleaved MBP-AHL lactonase, the eluate was passed through a small amylose- agarose affinity column (1.5 x 10 cm) and untagged AHL lactonase was collected in the flow-through and wash fractions. To assess the final metal content of the purified protein, protein samples and their associated dialysis buffers were analyzed using inductively coupled plasma mass spectrometry (ICP-MS; Department of Geological Sciences, The University of Texas at Austin). Equivalents of metal ion per enzyme were determined by subtracting the concentration of zinc found in dialysis buffers from the zinc concentrations of the protein samples and dividing by the protein concentration.

¹H NMR Spectroscopy of Dinuclear Zinc and Apo AHL Lactonase

Dinuclear zinc AHL lactonase (final concentration of 1.6 mg/mL) was prepared as described previously and dialyzed (12-14 kDa MWCO, Spectrapor) against Chelex (Bio-Rad)-treated KH₂PO₄ buffer (20 mM, pH 7.4), with addition of D₂O (10%, v/v). Samples of apo AHL lactonase (final concentration of 1.6 mg/mL) were prepared by dialyzing metal containing AHL lactonase against two changes of 4 L volumes of 2 mM 1,10-phenanthroline in 20 mM Hepes buffer containing 5 mM NaCl and 2 mM DTT, pH 7.0, over a 40 h period as previously described (35). Native PAGE was used to monitor removal of metal ions due to the difference in mobilities between apo and metal-bound AHL lactonase (35). Following dialysis, the apo-enzyme was concentrated and exchanged into the same buffer described above using a 1,10-phenanthroline treated Amicon Ultra-15 (10,000 MWCO) centrifugal filter device (Millipore, Billerica, MA). One-dimensional (1D) ¹H NMR spectra of the dizinc and apo proteins were recorded with the assistance of Dave Hoffman (University of Texas at Austin) using a 500 MHz Varian Inova NMR spectrometer equipped with a triple-resonance probe and z-axis pulsed field gradient. In each case, the NMR signal from the solvent was suppressed by presaturation.

Synthesis of *N*-Hexanoyl-*L*-homoserine Lactone (C6-HSL)

All synthetic reagents were purchased from Sigma-Aldrich Chemical Co. (St. Louis, MO). In a procedure similar to those previously described (44, 45), triethylamine

(23 mmol) was added to a stirred suspension of (*S*)- α -amino- γ -butyrolactone hydrobromide (10 mmol) in dimethylformamide (24 mL) at 0 °C. Hexanoyl chloride (14 mmol) was added dropwise, and the reaction was allowed to come to room temperature with continued stirring for 2 h. Solvent was removed by rotary evaporation with heating at ≤ 40 °C. The residue was dissolved in CH₂Cl₂ and washed sequentially with 1 M Na₂SO₄ solution (3 x 20 mL) and saturated NaCl solution (1 x 20 mL). The organic layer was dried over anhydrous MgSO₄, and solvents were removed by rotary evaporation. The final compound was further purified either by recrystallization from ethyl acetate and petroleum ether or by column chromatography on silica gel using ethyl acetate as the mobile phase. The product was obtained in 60% yield: $R_f = 0.50$ in ethyl acetate; $T_m = 133$ - 136 °C (uncorrected); ¹H NMR (300 MHz, CDCl₃) δ 0.90 (t, 3 H), 1.29-1.35 (m, 4 H), 1.61-1.71 (m, 2 H), 2.06-2.18 (m, 1 H), 2.21-2.28 (m, 2 H), 2.82-2.91 (m, 1 H), 4.25-4.34 (m, 1 H), 4.47 (d, 1 H), 4.51-4.60 (m, 1 H), 6.06 (s, 1 H); ¹³C NMR (75 MHz, CDCl₃) 14.15, 22.60, 25.35, 30.91, 31.60, 36.40, 49.50, 66.36, 174.01, 175.83; EI-HRMS $MH^+_{calc} = 200.1287$, $MH^+_{obs} = 200.1293$; $[\alpha]^{20^\circ C}_{D, methanol} = -29.4^\circ$.

Enzyme-Catalyzed Incorporation of ¹⁸O from H₂¹⁸O into the *N*-Hexanoyl-L-Homoserine Product

A reaction buffer (1 mL) containing 50% H₂¹⁸O and 50% H₂¹⁶O was prepared by mixing KH₂PO₄ buffer (40 mM, 0.47 mL) in H₂¹⁶O (pH 7.4) with H₂¹⁸O (95%, 0.53 mL).

To this solution was added *N*-hexanoyl-L-homoserine lactone (0.5 M, 20 μ L) in a methanol stock solution. AHL lactonase (6.5 μ g) was added, and the mixture was allowed to react at room temperature for 1 h after which the reaction was stopped by freezing the sample in liquid N₂ and the solvent removed under vacuum using a speedvac (Eppendorf). The remaining solid residue was redissolved in D₂O (99.9%, 1 mL) and incubated at 25 °C for 1 day in order to rule out nonenzymic exchange of H₂¹⁸O into the product before being analyzed by ¹³C NMR spectroscopy to determine the resulting peaks for product: ¹³C NMR (D₂O, 500 MHz) δ 13.39, 21.86, 25.21, 30.71, 35.93, 58.84, 62.70, 72.27, 177.05, 179.11, 179.13.

¹H NMR Spectroscopy of Reaction Products After Hydrolysis in D₂O

Products resulting from enzymic and nonenzymic hydrolysis of C6-HSL in 99.9% D₂O (Cambridge Isotope Laboratories) and KH₂PO₄ buffer (20 mM, pH 7.86) were compared. The pH was measured using a standard electrode and corrected using the equation $pD = pH + 0.4$ (46). Substrate was added from a stock solution of C6-HSL (0.5 M in methanol-*d*4). Nonenzymic alkaline hydrolysis of C6-HSL (83.3 mM) was carried out in the buffer described above upon addition of NaOH (105 mM, 1.25 equiv). ¹H NMR spectroscopy was performed using a Varian 300 MHz spectrometer before and after hydrolysis. A comparison of the peak integration values for the terminal methyl group in the C6 alkyl chain (3H, 0.9 ppm) and the lactone ring's α proton (1H, 4.3 and

4.1 ppm for the closed and open lactone, respectively) was used to determine whether exchange between hydrogen and solvent deuterium occurs at the α position. Investigation of the enzymic reaction utilized C6-HSL (20 mM) in the same deuterated buffer solution described above. ^1H NMR spectroscopy was carried out on the sample prior to addition of the enzyme. After addition of dizinc AHL lactonase (0.48 mg/mL), the solution was incubated (25 °C), and ^1H NMR spectra were obtained at various time points (1, 2, and 20 h). Comparison of the peak integration values for the terminal methyl group in the C6 alkyl chain and for the lactone α proton was completed as described above.

Synthesis of *N*-Hexanoyl-DL-homocysteine Thiolactone (C6- HCTL)

All synthetic reagents were purchased from Sigma-Aldrich Chemical Co. (St. Louis, MO). In a procedure similar to that reported elsewhere (45), triethylamine (3.0 mL, 21 mmol) was added to a stirred suspension of racemic DL-homocysteine thiolactone hydrochloride (3.0 g, 20 mmol) in dimethylformamide (350 mL) at 0 °C. Hexanoyl chloride (3.2 mL, 23 mmol) was added dropwise, and the mixture was allowed to react at room temperature with stirring for 1.5 h. Solvent was removed by rotary evaporation with heating at ≤ 50 °C. The residue was dissolved in 2-propanol and purified by column chromatography on silica gel using 2-propanol as the mobile phase. The solvent was removed by rotary evaporation at 20 °C. The remaining residue was dissolved in CH_2Cl_2 and washed sequentially with saturated NaHCO_3 , KHSO_4 (1 M), and saturated NaCl. The

organic layer was dried over anhydrous MgSO_4 , followed by removal of solvent by rotary evaporation to leave the final product, which shows as one spot by TLC: $R_f = 0.83$ in 2-propanol; $T_m = 50\text{-}53$ °C (uncorrected); ^1H NMR (300 MHz, $\text{DMSO-}d_6$) δ 0.86 (t, 3H), 1.25 (m, 4H), 1.48 (m, 2H), 2.04-2.12 (m, 3H), 2.36 (m, 1H), 3.25 (m, 1H), 3.35 (m, 1H), 4.57 (m, 1H), 8.12 (broad, 1H); ^{13}C NMR (75 MHz, $\text{DMSO-}d_6$) δ 13.86, 21.86, 24.85, 26.68, 30.18, 30.86, 35.17, 58.04, 172.30, 205.50; EI-HRMS $\text{MH}^+_{\text{calc}} = 216.0980$, $\text{MH}^+_{\text{obs}} = 216.1060$.

Expression and Purification of Metal-Substituted AHL Lactonases

Metal-substituted AHL lactonases were expressed and purified by P.W. Thomas from the Fast Lab according to published protocols (47).

Kinetic Assay of AHL Lactonase Activity

Kinetic assays for hydrolysis of C6-HSL and C6-HCTL by metal-substituted AHL lactonases were performed according to published protocols (35, 47) by P.W. Thomas from the Fast Lab.

Crystallization, Data Collection and Processing, Model Building and Refinement of Product-Bound Dizinc and Dicobalt AHL Lactonases

Crystallization, data collection, processing, model building and structure refinement of product-bound dizinc and dicobalt AHL lactonases was performed using methods similar to those described (36, 48) using purified protein prepared by P.W. Thomas from the Fast Lab and C6-HSL and C6-HCTL prepared as described above.

Synthesis of Ring-opened Products and Determination of Product Inhibition Constants

To prepare *N*-hexanoyl-L-homoserine (C6-Hse), the starting lactone C6-HSL (118 μmol in 255 μL methanol) was treated with one equivalent of NaOH (in 235 μL water) and mixed briefly at room temperature. The pH was adjusted to 7.5 with measured additions of HCl (0.1 M) and NaOH (0.1 M) before use in kinetic experiments. Ring opening was confirmed by comparison to standards using TLC on silica (isopropanol: C6-HSL $R_f = 0.65$; C6-Hse $R_f = 0.50$) and by ^{13}C NMR (75 MHz, methanol- d_4) δ 14.31, 23.46, 26.68, 32.58, 37.03, 37.23, 53.73, 60.25, 175.74, 178.98. *N*-Hexanoyl-DL-homocysteine (C6-Hcy) was prepared in a procedure similar to that given by Duerre et al (49). Briefly, the starting thiolactone C6-HCTL (50 μmol in 100 μL methanol) was treated with 7.5 equivalents of NaOH (in 75 μL water) and incubated for 5 min at 37° C. The reaction was stopped by addition of 6 equivalents of HCl (in 100 μL water) and the final pH was adjusted to 7.6 using NaOH (0.1 M) and HCl (0.1 M) and used immediately

in order to avoid disulfide formation. Ring opening was confirmed by comparison to standards using TLC on silica (isopropanol: C6-HCTL $R_f = 0.83$; C6-Hcy $R_f = 0.57$) by ^{13}C NMR (75 MHz, 50% D_2O / 50% methanol- d_4) δ 14.21, 21.52, 22.99, 26.31, 31.94, 36.89, 37.57, 54.40, 176.65, 178.42; and also by thiol titration using 5,5'-dithiobis-(2-nitrobenzoic acid).

Determination of product inhibition constants was performed by P.W. Thomas of the Fast lab using a phenol red based spectrophotometric assay (35). Initial rates of C6-HSL (240 μM) hydrolysis by dicadmium AHL lactonase (18 nM) were determined at pH 7.4, 28 $^\circ\text{C}$ in the presence of increasing concentrations of either product, C6-Hse or C6-Hcy, and plotted as a percent of the activity measured in absence of either product.

RESULTS

^1H NMR Spectroscopy of Dinuclear Zinc AHL Lactonase and Apo AHL Lactonase

To investigate the effect of removal of metal ions from AHL lactonase on protein folding, 1D ^1H NMR spectra were obtained for dizinc and apo AHL lactonase. 1D ^1H NMR spectroscopy is a tool commonly employed for qualitative determination of whether a protein is folded or unstructured (50, 51). Comparison of the ^1H NMR spectra for dizinc and apo AHL lactonase (Figure 2.2) reveals differences in downfield shifted resonances typical of folded proteins (50, 51). The dizinc AHL lactonase appears to be well-folded, exhibiting peaks for backbone amides shifted downfield by 8.5 ppm.

Following removal of the metal ions, most of these downfield peaks disappear with the appearance of broader features near 8.3 ppm, which is the characteristic shift of backbone amides in random coils. The use of low concentrations (2 mM) of chelator, in addition to the removal of these chelators prior to obtaining the ^1H NMR spectrum, make it unlikely that the chelator is responsible for the unfolding. In addition, reintroduction of metal ions has been shown to restore catalytic activity (35). These results are consistent with destabilization of AHL lactonase structure, resulting in enzyme unfolding, upon removal of active site metal ions.

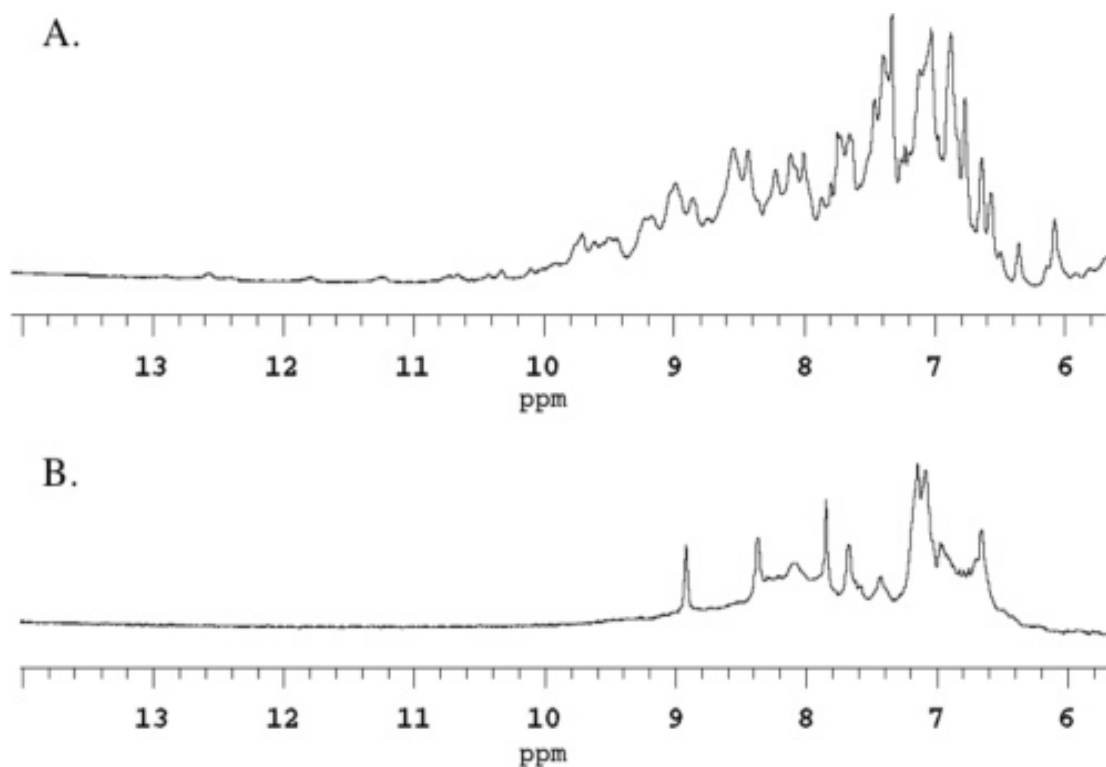


Figure 2.2 One-dimensional ^1H NMR spectra of dizinc and apo AHL lactonase. Following removal of the metal ions, most of the downfield peaks disappear while broader features appear near 8.3 ppm, the characteristic shift of backbone amides in random coils.

Enzyme-Catalyzed Incorporation of ^{18}O from H_2^{18}O Into the *N*-Hexanoyl-L-Homoserine Product

Taking advantage of a known isotope-induced shift in the ^{13}C resonance for the carbon adjacent to the site of ^{18}O incorporation (52), AHL lactonase was allowed to hydrolyze C6-HSL in a mixture of 50% H_2^{18}O and 50% H_2^{16}O during a one hour incubation. Following this, the samples were dried, resuspended in D_2O and allowed to

incubate for one day to rule out nonenzymic exchange with H_2^{18}O before analysis. The appearance of a characteristic ^{18}O isotope-induced ^{13}C shift (Figure 2.3) indicates that nonenzymic incorporation of oxygen did not occur during the D_2O incubation following enzymic cleavage. This is consistent with studies of oxygen exchange reactions with acetic acid in water which found that exchange is acid catalyzed, and exchange occurs very slowly with pH values greater than 6.0 (53). Following incubation of C6-HSL with AHL lactonase, a ^{13}C resonance peak appears for the γ methylene carbon at 72.272 ppm and a split peak is seen for the ring carbonyl carbon at 179.108 and 179.132 ppm, shown in Figure 2.3. The magnitude of this new upfield isotope shift at 179 ppm is consistent with incorporation of one ^{18}O atom into the product carboxylate (52), appearing 0.024 ± 0.004 ppm relative to the resonance position of the unlabeled ^{16}O -containing product.

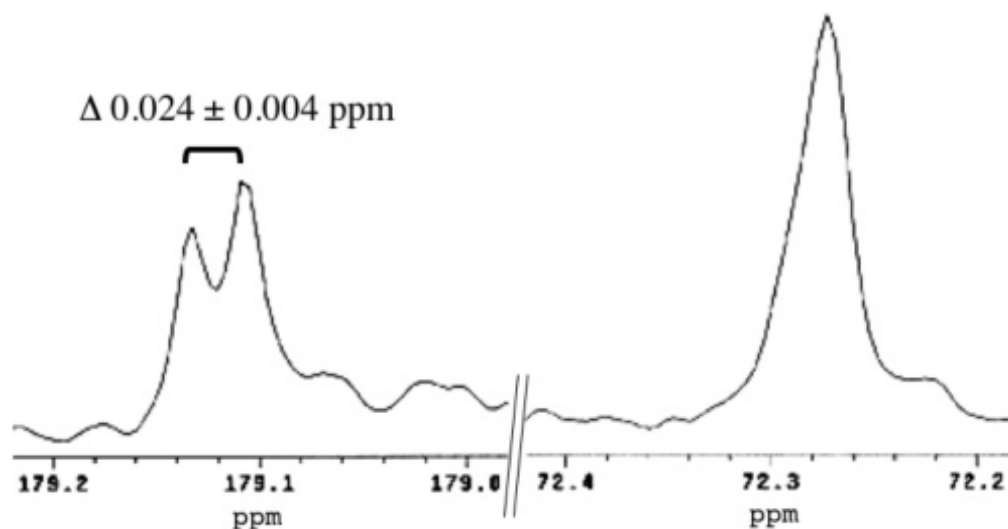


Figure 2.3 C6-HSL hydrolyzed by AHL lactonase in a mixture of 50% H_2^{18}O and 50% H_2^{16}O . The ^{13}C resonance peak for the γ methylene carbon at 72.272 ppm is on the right, and the split peak for the ring carbonyl carbon at 179.108 and 179.132 ppm is displayed on the left. The magnitude of the upfield isotope shift observed at 179 ppm is 0.024 ± 0.004 ppm relative to the resonance position of the unlabeled ^{16}O -containing product, consistent with incorporation of one ^{18}O atom into the product carboxylate.

^1H NMR Spectroscopy of Reaction Products After Hydrolysis in D_2O

To address the possibility that there is exchange of the lactone α proton during catalysis, nonenzymic and AHL lactonase-catalyzed hydrolysis of C6-HSL were completed in deuterated buffer and the reaction products analyzed by ^1H NMR spectroscopy. Comparison of the peak integration values for the protons of the terminal methyl group of the hexanoyl chain and the α proton shows a roughly 3:1 ratio for both reactions. The protons from the methyl group were chosen because their corresponding

peak is well-resolved, and they are not expected to exchange with solvent, allowing their value to be set equivalent to three. Prior to hydrolysis in the nonenzymic control reaction, the methyl protons (3.0 H, 0.73 ppm) integrated with a 3:1 ratio with the α proton (1.1 H, 4.25 ppm) of the substrate. Following addition of hydroxide, characteristic chemical shifts indicated ring opening was complete, and the methyl protons (3.0 H, 0.71 ppm) integrated with approximately the same ratio with the α proton of the product (0.8 H, 4.06 ppm). Similarly, in the enzyme-catalyzed reaction, complete hydrolysis was observed at the first time point (1 h) and the methyl protons (3.0 H, 0.72 ppm) integrated with a 3:1 ratio with the α proton of the product (0.9 H, 4.08 ppm). The enzyme-catalyzed reaction was also analyzed at two additional time points (2 and 20 h) to ensure no further reaction is taking place. At these points, the methyl protons (2 h, 3.0 H, 0.72 ppm; 20 h, 3.0 H, 0.73 ppm) and the product's α proton (2 h, 1.1H, 4.08 ppm; 20 h, 1.2 H, 4.10 ppm) remained in a ratio of 3:1, confirming that there is no significant exchange of the α proton with solvent deuterium during turnover.

Expression and Purification of Metal-Substituted AHL Lactonases

Untagged AHL lactonase (29 kDa) containing alternative metals was successfully purified from cells grown in minimal media supplemented with a salt of the desired metal ion. Yields from 2L expression cultures were greatest when the induction medium was supplemented with CoCl_2 (40 mg), followed by ZnSO_4 (7 mg). MBP-AHL lactonase

fusion proteins (73 kDa) were purified with similar yields from media supplemented with MnSO_4 (22 mg) or CdCl_2 (10 mg). Confirmation of the metal identity and number of equivalents per enzyme was accomplished using ICP-MS, and it can be seen in Table 2.1 that approximately two equivalents of the supplemented metal ion are bound per monomer. The reproducibility of these procedures was confirmed by carrying out multiple independent expression and purification procedures.

Metal Supplement	Equivalents Manganese	Equivalents Cobalt	Equivalents Zinc	Equivalents Cadmium
MnSO_4	1.8	< 0.01	0.1	0.06
CoCl_2	< 0.01	1.9	0.2	< 0.01
ZnSO_4	< 0.01	< 0.01	2.0	< 0.01
CdCl_2	< 0.01	< 0.01	0.04	2.0

Table 2.1 Metal content of purified monomeric AHL lactonase grown in minimal medium with alternative divalent metal ions.

Steady-State Kinetics of Metal-Substituted AHL Lactonases

Steady-state rate constants for hydrolysis of C6-HSL and C6-HCTL by AHL lactonase at 28 °C and pH 7.4 were obtained using a previously described phenol-red based spectrophotometric assay (35). Over the time course used for calculating initial rates (typically 0.2 min), progress curves remained linear for hydrolysis by AHL lactonase disubstituted with manganese, cobalt, zinc, or cadmium (Table 2.2).

Concentrations of substrates in these experiments were at least 5-fold higher than K_M values except in the instance of C6-HCTL hydrolysis by dizinc AHL lactonase, where limited aqueous solubility and a high K_M did not allow increasing C6-HCTL concentration above 40 mM substrate. Variation of the metal center does not provide an obvious correlation upon inspection of the steady-state rate constants (Table 2.2). For hydrolysis of C6-HSL, k_{cat} values increase with metal substitution in the order $Zn^{2+} \ll Mn^{2+} < Cd^{2+} < Co^{2+}$ while K_M values decreased in the order $Zn^{2+} \gg Co^{2+} > Cd^{2+} > Mn^{2+}$. For hydrolysis of the sulfur-containing C6-HCTL substrate, increasing k_{cat} values upon substitution are observed in the order $Zn^{2+} < Cd^{2+} \ll Co^{2+} < Mn^{2+}$ while K_M values are observed to decrease in the order $Zn^{2+} > Co^{2+} > Mn^{2+} > Cd^{2+}$. In general, these values for the steady-state rate constants do not show an obvious correlation with Lewis acid strength or thiophilicity of the substituted metal ions.

Metal Supplement	C6-HSL			C6-HCTL			$\frac{k_{cat}(O)}{k_{cat}(S)}$	$\frac{K_M(O)}{K_M(S)}$
	$k_{cat} (s^{-1})$	$K_M (mM)$	$k_{cat}/K_M (M^{-1}s^{-1})$	$k_{cat} (s^{-1})$	$K_M (mM)$	$k_{cat}/K_M (M^{-1}s^{-1})$		
MnSO ₄	330±20	0.18±0.04	1.8 x 10 ⁶	500±20	0.39±0.05	1.3 x 10 ⁶	0.66±0.07	0.4±0.2
CoCl ₂	510±10	0.36±0.04	1.4 x 10 ⁶	198±8	6.7±0.7	2.9 x 10 ⁴	2.6±0.2	0.054±0.006
ZnSO ₄	91±3	5.6±0.6	1.6 x 10 ⁴	4.1±0.7	36±10	114	22±5	0.16±0.06
CdCl ₂	480±20	0.24±0.03	2.0 x 10 ⁶	5.0±0.5	0.12±0.02	4.2 x 10 ⁴	100±20	2.0±0.6

Table 2.2 Steady-state kinetic constants for hydrolysis of substrates with oxygen (C6-HSL) or sulfur (C6-HCTL) leaving groups by AHL lactonase disubstituted with indicated metal ions.

If we instead compare the ratio of rate constants for the oxygen- and sulfur-containing substrates (O:S ratios in Table 2.2), however, a pattern begins to emerge. Comparison of the O:S ratio of k_{cat} values allows isolation of the effects of metal substitution on the rate limiting step, assuming that the metal substitution does not affect the enzyme structure or catalytic mechanism of hydrolysis. The O:S ratio of k_{cat} values for C6-HSL and C6-HCTL hydrolysis vary by 150-fold and follow a clear trend in the order of $Mn^{2+} < Co^{2+} < Zn^{2+} < Cd^{2+}$. This ranking corresponds to the trend seen with small molecule thiols binding to metal ions ($Mn^{2+} < Co^{2+} < Zn^{2+} < Cd^{2+}$) (54, 55). This correlation indicates that there is an increased interaction with the thiol leaving group upon substitution to a more thiophilic metal, and this interaction causes a slowing of k_{cat} . This is evidence for a catalytic role for metal ions as they are observed to interact with the leaving group in a kinetically significant fashion.

The possibility that the thio effect may have been due to product inhibition instead of being associated with transient interactions during turnover should be considered. In order to address this possibility, the ring-opened products *N*-hexanoyl-homoserine (C6-Hse) and *N*-hexanoyl-homocysteine (C6-Hcy) were prepared and their inhibition constants determined for hydrolysis of C6-HSL by dicadmium substituted AHL lactonase. The dicadmium substituted variant was chosen because the thio effect is most significant on its k_{cat} values [$k_{cat}(O)/k_{cat}(S) = 100$] as indicated by the values in Table 2.2. Using these inhibition constants, the effect of product inhibition on initial hydrolysis

rates can be calculated. In Figure 2.4, percent activity as measured in the presence of either C6-Hse or C6-Hcy is plotted.

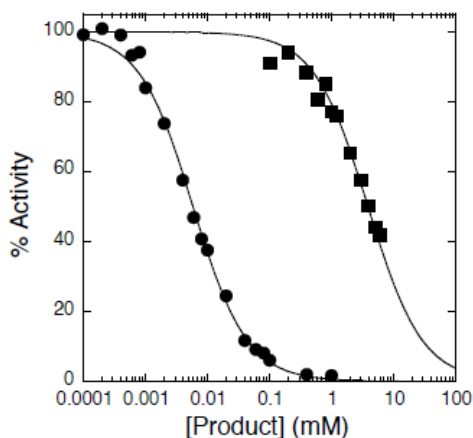


Figure 2.4 Product inhibition of dicadmium AHL lactonase by ring opened C6-HSL and C6-HCTL. IC_{50} values were determined for inhibition of C6-HSL hydrolysis by dicadmium AHL lactonase in the presence of either C6-Hcy (●) or C6-Hse (■).

Inhibition curves from Figure 2.4 may be fit using equation (1) and a Hill coefficient (h) equal to one to determine the IC_{50} value for each product (56).

$$\% \text{ Activity} = 100 - \left\{ \frac{100}{1 + (IC_{50} \div [I]^h)} \right\} \quad (1)$$

IC_{50} values for inhibition by C6-Hcy and C6-Hse were calculated to be 5.9 ± 0.2 μM and 3.9 ± 0.2 mM , respectively. Using the assumption that these compounds behave

as competitive inhibitors, equation (2) was used to calculate K_i values for C6-Hcy and C6-Hse as $3.0 \pm 0.1 \mu\text{M}$ and $2.0 \pm 0.1 \text{ mM}$ (57).

$$IC_{50} = K_i(1 + [S]/K_M) \quad (2)$$

During investigation of C6-HSL and C6-HCTL hydrolysis by dicadmium substituted AHL lactonase, the highest concentrations of substrate used (C6-HSL, 2 mM and C6-HCTL, 10 mM) showed linear absorbance decreases over the first 0.3 minutes from which initial rates were calculated. During this time, 53 μM of C6-Hse or 16 μM of C6-Hcy products were produced. Assuming that the back reaction of ring closure is minimal, and substituting K_M for K_S and K_i for K_P , the contribution of product inhibition to these initial rates can be calculated using equation (3) (58).

$$\frac{v}{V_{\max}} = \frac{[S]}{K_S(1 + [P]/K_P) + [S]} \quad (3)$$

Under these conditions, product inhibition for both substrates was calculated to be less than 7% of the observed rate. This effect is not only less than the experimental error, it is also much less than the 100-fold magnitude of the observed thio effect, so product inhibition may be ruled out as the cause of the thio effect on k_{cat} values.

Crystallization, Data Collection and Processing, Model Building and Refinement of Product-Bound Dizinc and Dicobalt AHL Lactonases

Dizinc and dicobalt AHL lactonase were cocrystallized with 4-25 mM C6-HSL or 10-25 mM C6-HCTL. AHL lactonase can be inhibited by ring-opened products, as a result co-crystallization with substrate affords crystal structures with product bound. Four crystal structures were obtained: dizinc AHL lactonase and C6-Hse (1.4 Å resolution), dizinc AHL lactonase and C6-Hcy (1.3 Å resolution), dicobalt AHL lactonase and C6-Hse (1.53 Å resolution), and dicobalt AHL lactonase and C6-Hcy (1.74 Å resolution). In both of the dizinc AHL lactonase structures, product is observed with the thiol or alcohol leaving group not coordinated to the metal center. In contrast, in the dicobalt AHL lactonase structures, the C6-Hse alcohol or C6-Hcy thiol are ligated to cobalt-2 (Co₂, Figure 2.5). It is interesting to note that the thiol group of the non-natural substrate C6-HCTL interacts with the metal center in the dicobalt AHL lactonase, but not in the dizinc enzyme (Figure 2.6), because in most other examples of thiol-inhibited enzymes in the MβL superfamily, the sulfur atom either bridges both zinc ions or directly binds zinc-2 (Zn₂) (59-63).

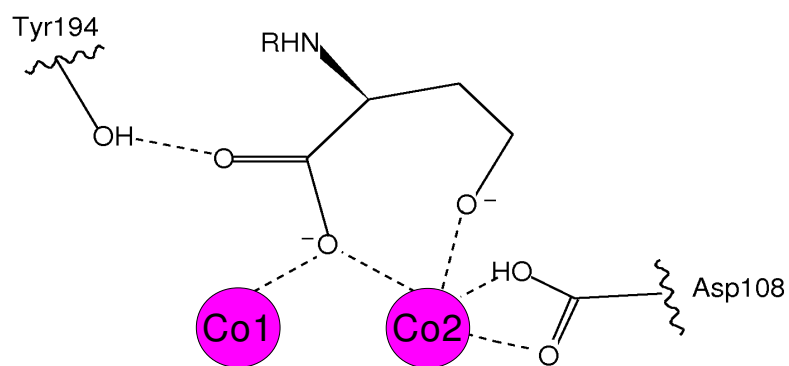
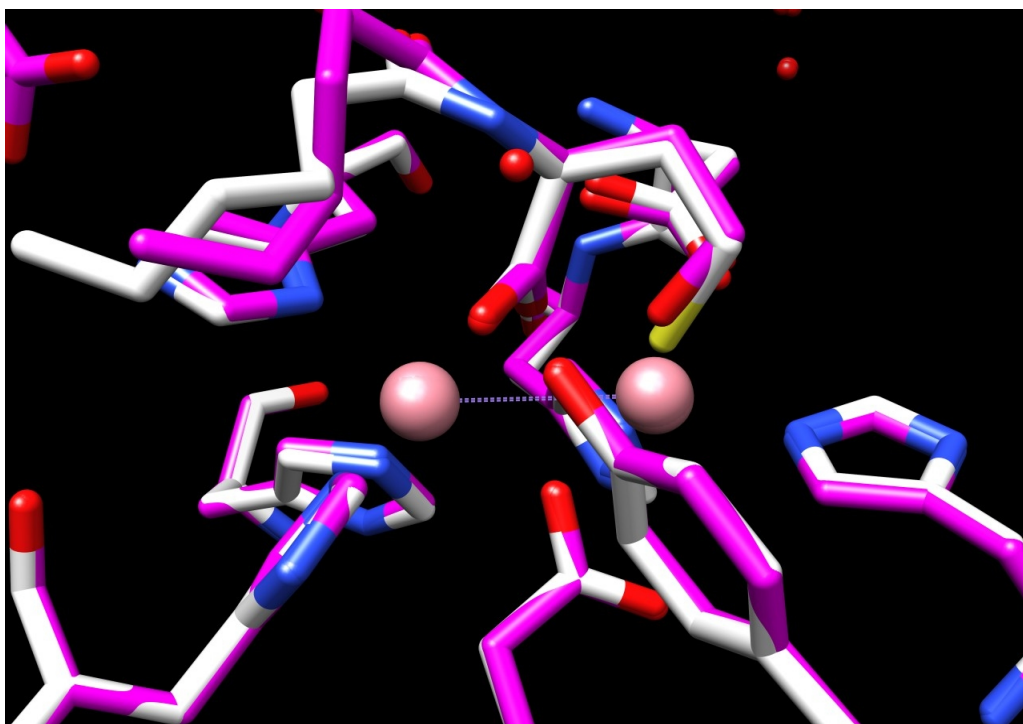


Figure 2.5 Ring-opened C6-HSL and C6-HCTL bound at the metal center of dicobalt AHL lactonase. Top: Overlaid crystal structures of C6-Hse (pink) and C6-Hcy (white) in complex with AHL lactonase. Figure prepared using UCSF Chimera (64). Bottom: Schematic of product-metal center interactions. The alcohol and thiol groups of the ring-opened products are seen interacting with Co2 of the metal center.

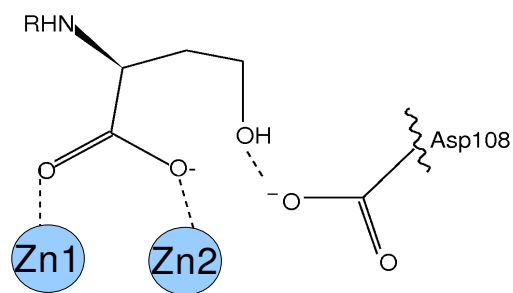
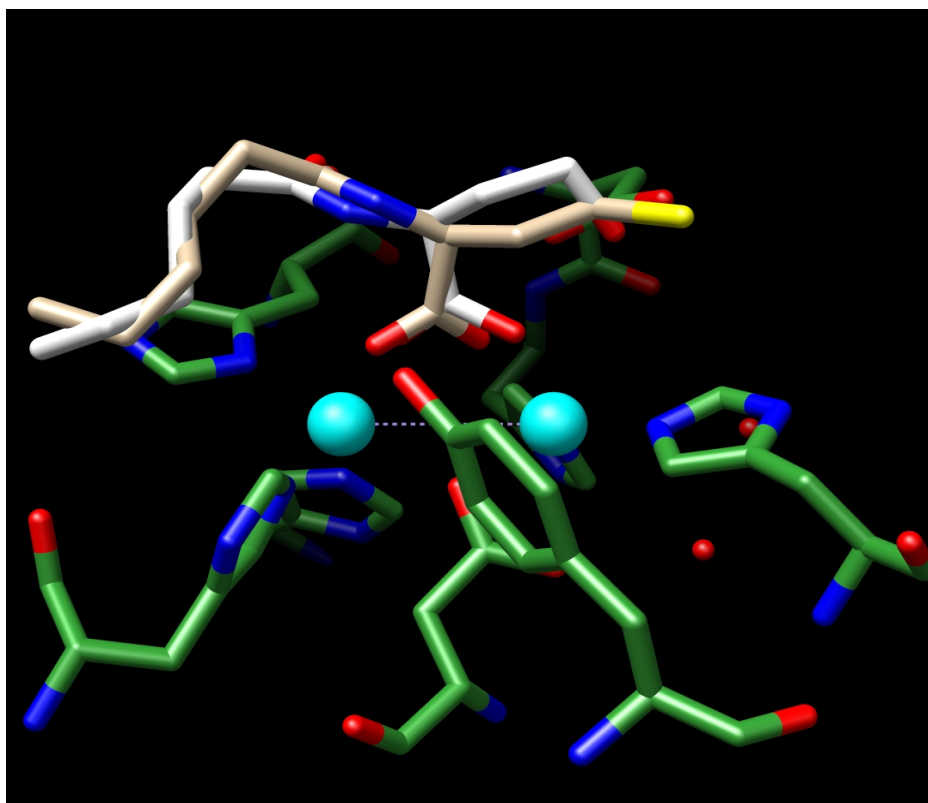


Figure 2.6 Ring-opened C6-HSL and C6-HCTL bound at the metal center of dizinc AHL lactonase. Top: Overlaid crystal structures of C6-Hse (white) and C6-Hcy (beige) in complex with AHL lactonase. Figure prepared using UCSF Chimera (64). Bottom: Schematic of product-metal center interactions. The alcohol and thiol groups of the ring-opened products are no longer interacting with Zn2 of the metal center.

DISCUSSION

The first detailed study of AHL lactonase from *Bacillus thuringiensis* proposed that, despite the presence of a conserved metal-binding motif, there was not an absolute requirement for metal ions in catalysis by AHL lactonase (34). Subsequent studies on this enzyme have shown that 2 equivalents of zinc copurify with AHL lactonase (35, 48, 37), and the presence of these metal ions is required for catalytic activity (35). These studies did not address what role the metal ions serve for AHL lactonase. The metal ions may contribute to the structural integrity of the enzyme, participate in catalysis, or provide a combination of these effects. If the metal ions contribute to the structural integrity of AHL lactonase, removal of the metal ions should destabilize the fold of the protein. If the metal center serves a predominantly catalytic role, it could potentially be removed without significant perturbation to the overall protein fold.

To investigate of the importance of metal binding in stabilization of the fold of AHL lactonase, ¹H NMR spectra of dizinc AHL lactonase and apo AHL lactonase (with no bound metal ions) were compared. One-dimensional ¹H NMR spectroscopy is a common method employed to detect gross changes in protein folding (50, 51). The spectra presented in Figure 2.2 reveal distinct differences between these two enzyme states. The spectrum of dizinc AHL lactonase exhibits many defined peaks downfield of 8.5 ppm, which is the region indicating backbone amide protons in folded proteins (50).

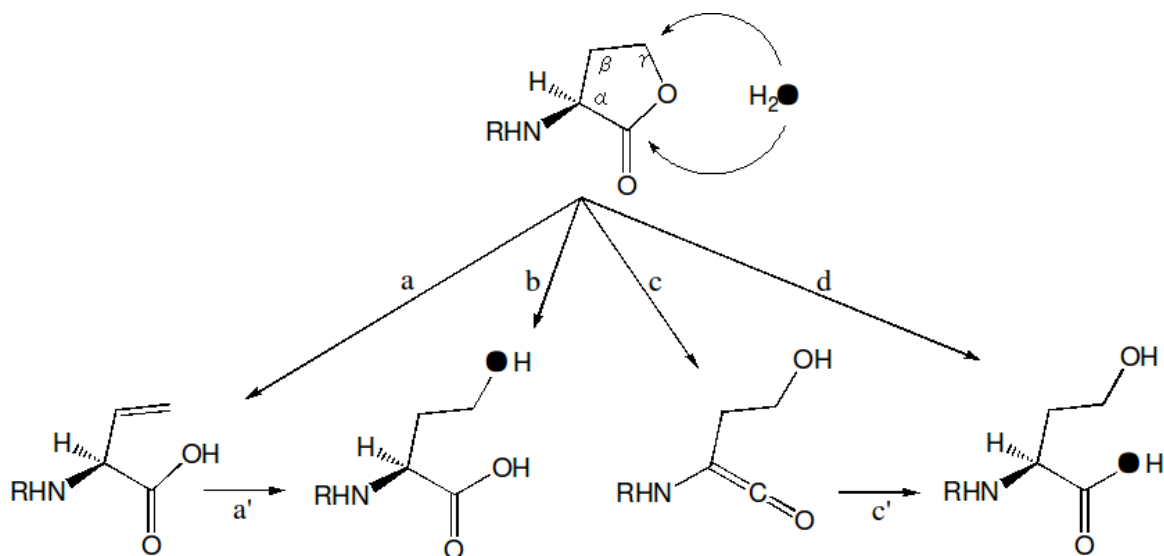
The spectrum of apo AHL lactonase, in contrast, exhibits peaks which are broader and less resolved. In this state, the peaks occur mainly near 8.3 ppm, indicating that there is a loss of structural integrity upon removal of metal ions (65). This result supports a structural role for the dinuclear metal center of AHL lactonase. Crystal structures of this enzyme are consistent with this finding, revealing that the dizinc center aids in bridging two pseudosymmetrical halves of the overall $\alpha\beta\beta\alpha$ fold (37, 38). Reconstitution of apo AHL lactonase with zinc produces low yields and is slow to reach equilibrium (35), consistent with the involvement of metal ions in protein folding, rather than acting as a cofactor that binds to a pre-folded enzyme. A similar reliance on metal ions for proper folding has been observed with other metallo- β -lactamase superfamily members (66, 65).

The structural role that metal ions serve for AHL lactonase does not exclude them from performing a catalytic role as well. Before investigation of the involvement of the metal center in hydrolysis, it was necessary to elucidate the mechanism used to perform ring opening. The common pathway for alkaline ester hydrolysis is via an addition-elimination pathway, rather than an elimination-addition pathway. The reactivities of lactone rings are known to vary from those of their open-chain ester counterparts, however (67). An example of this is seen with lactone rings containing fewer than eight carbon atoms, in this case the lactone ring is forced into a *cis* configuration, rather than the lower energy *trans* configuration adopted by open-chain esters. As a result, these

lactones are observed to hydrolyze 200-fold faster than the analogous open-chain esters (67, 68).

The AHL lactonase-catalyzed ring opened product had previously been identified by mass spectrometry (35), but the nature of the ring opening mechanism had not been examined in detail. Lactone hydrolysis may occur through the obvious mechanism involving nucleophilic attack of hydroxide at the carbonyl of the lactone ring, but other pathways should be considered. For example, an elimination mechanism has been observed for the enzyme catalyzed ring opening of type B streptogramin macrolactones (69). Studies on nonenzymatic open chain ester hydrolysis indicate that ring opening can proceed through a ketene intermediate when an ionizable α proton is present (70, 71). Notably, under nonenzymic acidic conditions, *N*-benzoylhomoserine lactone has been found to open between the methylene carbon and the ring oxygen rather than between the carbonyl carbon and the ring oxygen (72).

AHL lactonase possesses an active site containing two strong Lewis acids in addition to a metal-bound preformed hydroxide ion (38), making an *a priori* prediction of an acidic or alkaline pathway for lactone hydrolysis problematic. To address this issue, four potential ring opening mechanisms were considered and investigated (Scheme 2.1).



Scheme 2.1 Four potential ring opening mechanisms for AHL lactonase catalysis.

Pathway (a) depicts elimination of the acetate group of the lactone ring. While this alkene species has not been detected in previous studies of reaction products (35, 34, 73), if elimination is followed by a hydration step (path a'), the expected ring opened product will be observed. Direct attack of hydroxide at the γ carbon (path b) with the acetate acting as the leaving group will also result in opening of the lactone ring. Deprotonation at the α position with concomitant elimination of the alcohol (path c) would produce a ketene which would readily react with water (path c') forming ring-opened product. Direct attack of hydroxide at the lactone carbonyl with the accompanying alcohol leaving group (path d) would produce the open product.

Both pathways a and b incorporate solvent oxygen into the product alcohol while pathways c and d involve oxygen incorporation into the carboxylate of the ring-opened product. We exploited this difference to narrow down the potential mechanisms. C6-HSL was hydrolyzed by AHL lactonase in a buffered solution of 50% H₂¹⁸O and 50% H₂¹⁶O. The resulting product was analyzed by natural abundance ¹³C NMR spectroscopy, revealing a small but reproducible change in the shift of the carbon adjacent to the incorporated oxygen (52). The γ carbon of the AHL lactonase hydrolyzed product exhibited only a single symmetrical peak (Figure 2.3), indicating that there was no ¹⁸O label attached. The product's carbonyl carbon peak, on the other hand, is split into two, with approximately 50% of the sample shifted upfield by 0.024 ± 0.004 ppm, indicating that the ¹⁸O label is incorporated into the product at this site. The magnitude of this ¹⁸O-induced isotope shift agrees with that observed previously with carboxylic acids and indicates that only one ¹⁸O atom is incorporated into the product (52).

Incorporation of solvent oxygen into the product carboxylate rather than into the alcohol rules out pathways a and b (Scheme 2.1). The remaining pathways c and d may be distinguished by studying whether there is exchange of the α proton during hydrolysis. Pathway c predicts that the α proton readily exchanges with solvent during formation of the ketene while pathway d predicts that this proton will be retained at this position. After hydrolysis of C6-HSL by AHL lactonase in buffer consisting of 95% H₂O, ¹H NMR spectroscopy was performed to examine the number of protons remaining at this position.

The product's α proton integrates well with the three protons of the terminal methyl group of the alkyl chain, exhibiting a 1:3 stoichiometry. This indicates that there is no significant proton exchange at this position during catalysis, favoring pathway d as the correct mechanism. These results do not completely rule out the possibility that a general base, which is not in rapid equilibrium with solvent, may catalyze both removal of the α proton as well as reprotonation of the ketene. The high pK_a of the α proton, however, as well as the solvent accessibility of the active site (38) make this possibility unlikely. Overall, isotope labeling patterns are consistent with the addition-elimination mechanism depicted in pathway d of Scheme 2.1, with attack of a solvent-derived hydroxide occurring at the carbonyl carbon of the lactone ring and the associated elimination of an alcohol leaving group.

The metal requirement of AHL lactonase has been shown to be required for folding, and thus catalysis (35), however these studies did not address potential catalytic roles for the metal center in catalysis. A majority of the M β L superfamily members utilize active site metal ions during catalysis (28). One structure of AHL lactonase complexed with homoserine lactone indicates ligand-metal contacts (37), and although this structure likely represents a nonproductive complex, it may indicate that the metal center interactions with substrate are important. As a result of establishing that the leaving group during catalytic ring opening is an alcohol (or thiol), we were able to use a kinetic thio effect experiment to detect metal-leaving group interactions during AHL

lactonase ring opening. Thio effect experiments have precedent in the studies of metal-assisted phosphoester hydrolysis (74) and hydrolysis of thionolactams (75), thioureas (76) and thiono-peptides (54, 77) by metallohydrolases. The studies described here differ somewhat from previous studies because the sulfur for oxygen substitution is made at the leaving group position rather than at the carbonyl.

Measurement of the rates of hydrolysis of lactone and thiolactone substrates by AHL lactonase substituted with metals of varying thiophilicity allowed us to determine if there is a metal ion-leaving group interaction. If there is no interaction between the leaving group and the metal center, then no change is expected in the ratio of hydrolysis rates for the lactone and thiolactone substrates (O:S ratio) upon metal substitution. If a kinetically significant interaction occurs between the leaving group and the metal center during hydrolysis, then it is a reasonable assumption that the ratio of hydrolysis rates will vary in tandem with the thiophilicity of the active site metals.

Steady-state kinetic constants were determined for the hydrolysis of C6-HSL and C6-HCTL by AHL lactonase containing 2 equiv each of four different metal ions (Tables 2.1 and 2.2): Mn^{2+} , Co^{2+} , Zn^{2+} , and Cd^{2+} . The O:S ratios of K_M do not show a correlation with the thiophilicity of the substituted metals, but such an interaction is not necessarily anticipated. On the other hand, a strong correlation is seen with the O:S ratios of k_{cat} values and the active site metal ion thiophilicity. The ranking of O:S k_{cat} ratios for metal-substituted AHL lactonase (Table 2.2: $Cd^{2+} > Zn^{2+} > Co^{2+} > Mn^{2+}$)

correlates well with the the thiophilicity ranking of these metals ($\text{Cd}^{2+} > \text{Zn}^{2+} > \text{Co}^{2+} > \text{Mn}^{2+}$) (78). X-ray absorption fine spectroscopy (EXAFS) studies indicate that there are identical coordination spheres for dizinc and dicobalt lactonase (Figure 2.7), indicating that the observed differences in reactivity between dizinc and dicobalt AHL lactonase are likely due to intrinsic differences in each metal's properties rather than changes in the protein structure (35, 47).

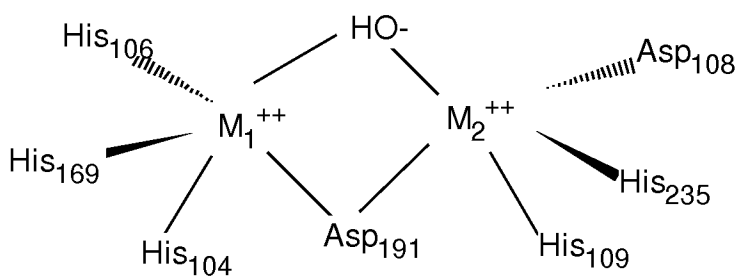


Figure 2.7 Metal binding ligands for dizinc and dicobalt AHL lactonases. M_1 and M_2 indicate metal ion positions 1 and 2.

The values from Table 2.2 show that Mn^{2+} substituted AHL lactonase hydrolyzed the thiolactone more rapidly under substrate-saturating conditions than the oxygen-containing species, despite the fact that the Mn^{2+} is expected to be the least thiophilic species. In a similar trend, the Cd^{2+} substituted enzyme, expected to be the most thiophilic species, hydrolyzed the oxygen-containing lactone faster than the thiolactone. The observation that the most thiophilic metal displays the slowest rate for thiolactone

hydrolysis suggests that breaking the leaving group-metal bond may be at least partially rate-limiting during steady-state turnover. Other metallo- β -lactamase enzymes have shown similar rate-limiting metal ion-leaving group interactions (40), and additionally, crystal structures of dicobalt and dizinc AHL lactonase with C6-Hse and C6-Hcy show differences in interactions between the alcohol or thiol and metal-2 (Co₂ or Zn₂ in Figures 2.5 and 2.6), providing additional support for this leaving group-metal center interaction during turnover.

These metal-substitution studies have revealed that substitution of AHL lactonase with different metal ions can enhance catalysis. The Cd²⁺-substituted enzyme exhibits a 5-fold increase in k_{cat} , a 23-fold decrease in K_M , and a corresponding 125-fold increase in k_{cat}/K_M for hydrolysis of a naturally occurring substrate, C6-HSL, as compared with the dizinc enzyme. In fact, the dizinc enzyme was the least effective catalyst in the studies described here, despite the fact that zinc appears to be the optimal metal ion required for catalysis by a related metallo- β -lactamase (79) and, without supplementation, zinc is the major metal species incorporated into heterologously expressed AHL lactonase in rich media (35), although the native metal utilized by this enzyme is unknown. Alternative metal incorporation may provide a route to a more effective quorum-quenching therapeutics. Dicadmium AHL lactonase is orders of magnitude faster than other reported quorum-quenching enzymes. For example, the dicadmium variant of AHL lactonase is 2600-fold more efficient at hydrolyzing C6-HSL compared to a lactonase

obtained from directed evolution of a phosphotriester-like-lactonase from *Mycobacterium avium* (80).

In conclusion, these experiments have shown that the dinuclear metal site of AHL lactonase is required for structural and catalytic purposes by AHL lactonase. Investigation of AHL ring opening reveals that hydrolysis proceeds via an addition-elimination mechanism where a solvent-derived hydroxide attacks at the carbonyl of the lactone ring while an alcohol leaving group is eliminated. This leaving group was shown to interact with the metal center by observation of a kinetic thio effect. Along with crystal structures showing that metal-2 of dicobalt AHL lactonase is ligated to the alcohol (or thiol) of the ring opened product, this thio effect is consistent with a role for the metal center in stabilization of the leaving group, aiding in the facilitation of bond cleavage. Supplementation of AHL lactonase with alternative metals can enhance its catalytic activity, suggesting that preparing different metalloforms may be a viable route to the development of more effective quorum-quenching agents.

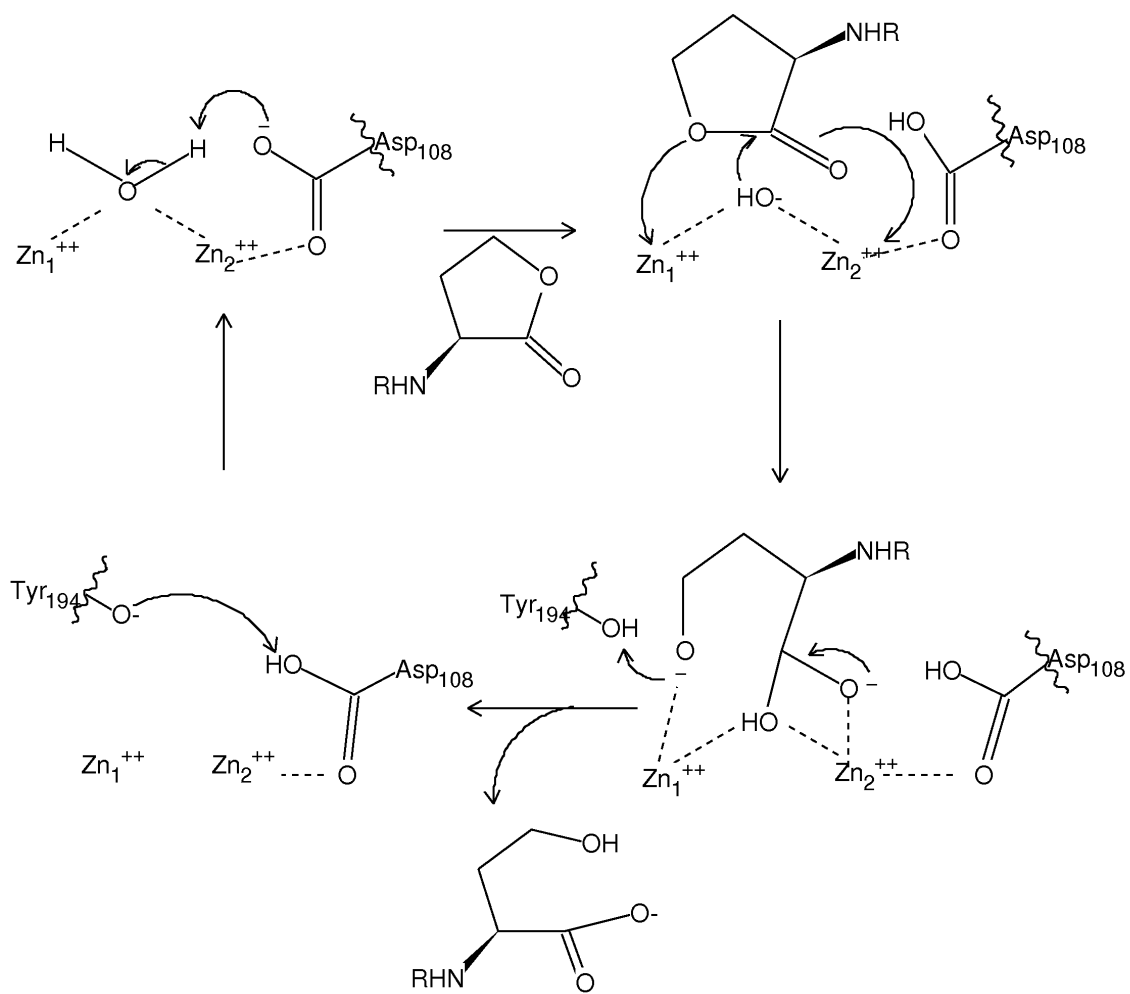
Chapter 3 Role of Active Site Residues in the AHL Lactonase Catalytic Mechanism

INTRODUCTION

The active site of AHL lactonase includes a dinuclear metal ion center bound by the signature metal-binding motif of the metallo- β -lactamase superfamily HxHxDH~H~D~H (81, 82). This metal center has been confirmed as essential to catalysis (35, 37), and based on crystallographic data and a kinetic thio effect study, it appears that the leaving group alcohol makes a transient interaction with metal-2 of the dinuclear metal center of AHL lactonase during catalytic turnover (47).

The dicobalt and dizinc AHL lactonase structures introduced in Chapter 2 provided us with a high-resolution glimpse into the active site, and the opportunity to discover what residues may be involved in catalytic ring opening. These structures are important because the first reported structure did not contain any bound substrate or inhibitor (36), making it difficult to determine which residues were important in the catalytic mechanism. A subsequent dizinc AHL lactonase structure was reported with the competitive L-homoserine lactone bound (37). The binding mode of L-homoserine lactone reported in this structure is rotated approximately 180° compared to binding modes observed in the enzyme-substrate and enzyme-product complex structures of related metallo- β -lactamase superfamily members (30, 81, 83, 59), and is likely due to

the lack of the *N*-acyl hydrophobic group typically found in AHL substrates. Using this complex, a catalytic mechanism for ring opening was proposed, with Asp108 abstracting a proton from the metal-bound water and Tyr194 acting as a general acid to protonate the leaving group (Scheme 3.1) (37).



Scheme 3.1 AHL lactonase catalytic mechanism proposed by Kim et al (37).

The product-bound dizinc (48) and dicobalt AHL lactonases reveal that ring-opened AHLs bind in an orientation consistent with other members of the M β L superfamily, with the ring oxygen over metal-2 and the carbonyl oxygen over metal-1.

The crystal structure of AiiB from *Agrobacterium tumefaciens*, another M β L superfamily member with known lactonase activity, was crystallized with phosphate coordinated to the metal center (38). This phosphate ion interacts in a bidentate fashion with the metal center, with the remaining two oxygens coordinated to Tyr216 and Asp115 (which correspond to Tyr194 and Asp108, respectively, in AHL lactonase), suggesting that Tyr194 may help stabilize a tetrahedral adduct formed during catalysis. This role would be consistent with observed product orientation in AHL lactonase (48), but not with the mechanism proposed by Kim et al (37). In L1 metallo- β -lactamase from *Stenotrophomonas maltophilia*, an active site (Tyr228) has been proposed to participate as a member of an oxyanion hole (83), but later studies implicate this residue as being involved in substrate binding - however, these effects are highly substrate dependent (84). It is interesting to note that a similar mechanism where a glutamate within a zinc-binding motif acts as a general base while an active site tyrosine stabilizes a tetrahedral intermediate has been observed in an unrelated metalloprotease from *Erwinia chrysanthemi* (85).

In this chapter, site-directed mutagenesis and steady-state kinetic studies are used to probe the roles of Tyr194 and Asp108, and in combination with information gleaned

from the previously introduced dizinc and dicobalt product bound AHL lactonase crystal structures, we propose a detailed catalytic mechanism for the AHL lactonase from *Bacillus thuringiensis*.

EXPERIMENTAL METHODS

Construction of the Expression Vector for Maltose Binding Protein MBP-D108N AHL Lactonase Fusion Protein

Construction of the expression vector for the maltose binding protein MBP-D108N AHL lactonase fusion protein was performed by T. Schaller of the Fast Lab.

Construction of the Expression Vector for Cleavable Maltose Binding Protein MBP-Y194F AHL Lactonase Fusion Protein

An expression vector for expression of the Y194F mutant was constructed using the Quikchange kit (Stratagene, La Jolla, CA). The sequence of the forward mutagenic primer, was 5'-CGATTGATGCATCGttcACGAAAGAGAATTTTGAATGAAGTGTGC-3', and the sequence of the reverse mutagenic primer was 5'-GCACACTTCATTCAAATTCTCTTTCGTgaaCGATGCATCAATCG-3', with the mutagenic codons are indicated in lowercase. Both forward and reverse primers (125 ng) were combined with template (100 ng of pMal-t-AiiA plasmid) (35), dNTPs (each at a final concentration of 200 μ M), and Pfu polymerase (2.5 units). The reaction mixture was brought to a volume of 50 μ L by the addition of reaction buffer and subjected to the

following thermocycler program: 95 °C for 30 s, 17 cycles at 95 °C for 30 s, 55 °C for 1 min, and 68 °C for 7 min and 30 s, followed by 68 °C for 10 min. DpnI restriction enzyme was added and allowed to react for 2 h at 37 ° C. The digested mixture was transformed into competent *E. coli* Top10 (5 µL into 50 µL of cells). Transformed cells were selected by plating onto LB supplemented with ampicillin (50 µg/mL). The mutation was verified by fully sequencing the gene insert (DNA Core Facility, The University of Texas).

Expression and Purification of Metal-Substituted AHL Lactonases

Cobalt and zinc were incorporated into AHL lactonase using previously developed expression conditions (47). *E. coli* BL21(DE3) cells harboring either the pMAL-D108N or pMAL-t-aiiA Y194F expression plasmid (35) were incubated with shaking at 37 °C in M9 minimal medium [Na_2HPO_4 (47 mM), KH_2PO_4 (22 mM), NaCl (8.5 mM), NH_4Cl (18.7 mM), MgSO_4 (2.0 mM), CaCl_2 (0.1 mM), and glucose (0.4%, w/v)] supplemented with ampicillin (100 µg/ mL) until cells reached an OD_{600} of 0.5-0.7. Cells were harvested by centrifugation and then resuspended in fresh M9 minimal medium containing IPTG (0.3 mM), ampicillin (100 µg/mL), and either ZnSO_4 or CoCl_2 (0.5 mM). Induction was continued at 25 °C with shaking for an additional 16 h, followed by harvesting by centrifugation at 8275g and 4 °C for 7 min. Cell pellets from 2 L of expression culture were resuspended in 50 mL of Tris-HCl buffer (20 mM, pH 7.4)

with NaCl (5 mM) and stored at -20 °C until they were used. Unless otherwise noted, all purification procedures were carried out at 4 °C. A BioLogic LP protein purification system (Bio-Rad, Hercules, CA) was employed for all chromatographic procedures. Thawed cell pellets were resuspended in 200 mL of Tris-HCl buffer (10 mM, pH 7.4) with NaCl (5 mM). After resuspension, cells were lysed by sonication, and cell debris was removed by centrifugation at 34500g for 30 min. The resulting supernatant was loaded onto a DEAE-Sepharose FF column (2.5 cm x 20 cm) equilibrated with buffer A [20 mM Tris-HCl and 5 mM NaCl (pH 7.4)]. After washing the column with 200 mL of buffer A made to 160 mM NaCl, protein was eluted with a linear salt gradient increasing to 250 mM NaCl in buffer A. Fractions containing active fusion protein typically eluted at a conductivity near 20 mS/cm (200 mM NaCl). Pooled fractions containing MBP-AHL lactonase fusion protein were portioned into two aliquots and loaded in parallel on two columns (2.5 cm x 10 cm) of amylose-agarose resin (New England BioLabs) maintaining a flow rate of 0.5 mL/min. After washing each column with 2 column volumes of buffer A made to 100 mM NaCl at a flow rate of 0.5 mL/min, the fusion protein was eluted at a flow rate of 1.0 mL/min with buffer A made to 100 mM NaCl and 10 mM maltose. The MBP-AHL lactonase fusion proteins prepared with ZnSO₄ or CoCl₂ were subsequently cleaved with tobacco etch virus protease, and the untagged enzyme was purified as described in Chapter 2. It has previously been demonstrated that AHL lactonase is monomeric (36) and that the presence of the MBP tag does not significantly affect

catalysis (35). The purity of each enzyme preparation was confirmed by SDS-PAGE and metal content was analyzed by ICP-MS (School of Geological Sciences, The University of Texas at Austin).

Circular Dichroism Spectroscopy of AHL Lactonase

Far UV-circular dichroism spectra of wild type and mutant dicobalt AHL lactonases were compared to assess changes in secondary structure upon mutation. For this experiment, proteins were transferred into sodium phosphate buffer (10 mM), pH 7.4 by buffer exchange (Amicon Ultra-4 10,000 kDa MWCO, Millipore), and made to final concentrations of 45-95 $\mu\text{g} / \text{mL}$ using the same buffer, as determined by the BCA protein assay kit (Pierce). Sodium phosphate buffer (10 mM), pH 7.4 was used as the baseline buffer used for all samples. CD spectra (190 – 240 nm, with a wavelength step of 0.1 nm) were obtained using five scans on a JASCO J-810 spectropolarimeter operating at room temperature. Ellipticity values at each wavelength for all five scans were averaged, and these averages were used in further analysis. Elliptical rotation was converted to molar ellipticity $[\theta]$, and is plotted versus wavelength for untagged wild type and Y194F AHL lactonase in Figure 3.1.

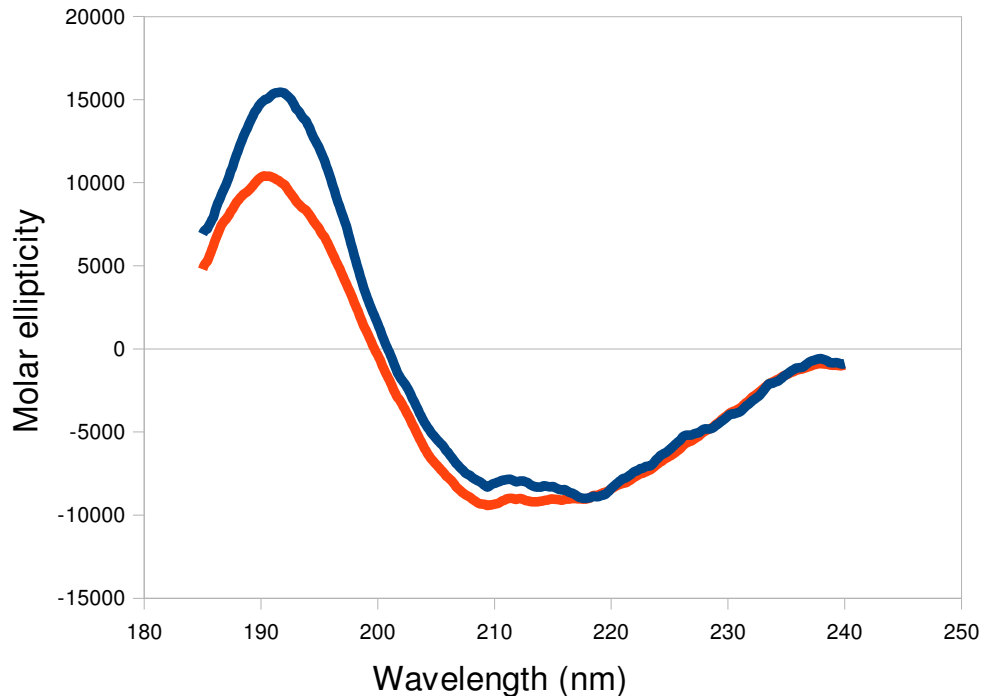


Figure 3.1 CD spectra of dicobalt AHL lactonase (wild type in blue, Y194F variant in orange). Far UV molar ellipticity $[\theta]$ (in units of degrees cm^2/dmol protein) are plotted against wavelength.

The CD spectra were analyzed for secondary structural content using the SELCON3 simulation program and data set SP175 (86) available at DICHROWEB (<http://www.cryst.bbk.ac.uk/cdweb/html/home.html>) (87, 88). Predicted alpha helix and beta sheet content are presented in Table 3.1. The generally accepted interpretation of normalized standard deviation (NRMSD) for CD data is that an NRMSD of less than 0.2 indicates the calculated structure is generally similar to the actual structure (88), and the values obtained here are within this cutoff. Indeed, the alpha and beta character of all samples are similar to those calculated for the crystal structure of dizinc AHL lactonase

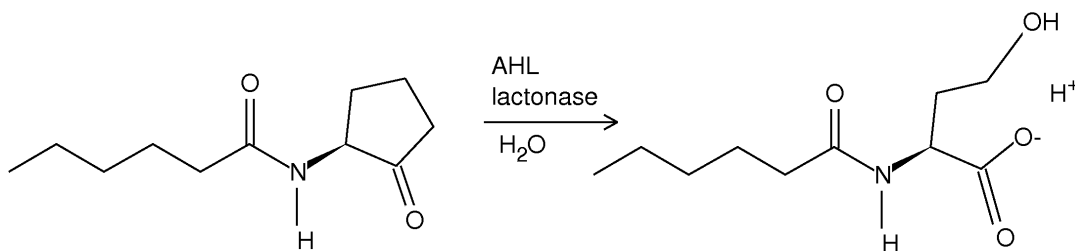
(36). The D108N mutant AHL lactonase is purified as a fusion protein that lacks a TEV protease cleavage site, and so is not included in this comparison.

	α -helix (%)	β -sheet (%)	Turns (%)	Unordered (%)	NRMSD
Wild Type	18	33	12	37	0.10
Y194F	18	33	11	37	0.09
calculated ^a	25	30	- ^b	-	-

Table 3.1 Calculated secondary structure content of AHL lactonase variants. ^afrom PDB ID 2A7M (36). ^bNot calculated.

Kinetic Assay of AHL Lactonase Activity

Hydrolysis of AHLs by AHL lactonase was followed using a previously reported colorimetric assay (35). This assay takes advantage of the loss of one proton during catalytic ring opening at pH values above the pK_a of the product's carboxylic acid (Scheme 3.2).



Scheme 3.2 Ring opening of C6-HSL catalyzed by AHL lactonase

It is possible to track the net production of protons continuously using the spectrophotometric pH indicator assay originally reported for measuring the activity of carbonic anhydrase and haloalkane dehalogenase (89-91). In these assays, the reactions are weakly buffered. The addition of a colorimetric pH indicator having a pK_a similar to the reaction pH incorporates the indicator as part of the buffer system. Alterations in proton concentration causes a change in the protonation state of the indicator, causing a color change that allows quantification of proton concentration by comparison with a standard curve. Typical assay conditions include 750 μL of 2x dye solution (2 mM buffer, 0.2 M Na₂SO₄, and indicator), 10-20 μL of enzyme, and 1-30 μL of 0.5 M substrate dissolved in methanol. Buffers and indicators must be chosen in tandem in order for the reaction pH and indicator pK_a to match (90). Previous studies on AHL lactonase using this assay identified ideal conditions for the assay at pH 7.4-7.6 (35). These assay conditions were used in the studies described in this manuscript. The indicator used here is phenol red, disappearance of the unprotonated species is followed at 557 nm. The final concentration of phenol red in the assay buffer is 40 μM. Initial rates of hydrolysis were measured over 20-60 seconds at 28 °C. Background hydrolysis was corrected for via the substitution of storage buffer for the enzyme solution. This observed background rate was subtracted from the rate observed with enzyme. A standard curve was constructed using known amounts of HCl in order to convert the

decrease in absorbance observed during enzymatic turnover to changes in proton concentration.

RESULTS

Protein Purification and Characterization

Wild-type and Y194F AHL lactonase were expressed, purified, and characterized for purity and metal content. When protein expression was completed using medium supplemented with ZnSO_4 , wild-type AHL lactonase was purified with 2.0 equiv of zinc, and Y194F with 1.9 equiv of zinc, with negligible amounts of other bound divalent metal ions. When expression cultures were supplemented with CoCl_2 , the wild-type protein contained 2.1 equiv of cobalt and 0.1 equiv of zinc, and Y194F contained 2.2 equiv of cobalt and 0.1 equiv of zinc with negligible amounts of other divalent metal ions. The D108N variant of AHL lactonase was cloned without a tobacco etch virus (TEV) protease cleavage site, and it was expressed, purified, and characterized with its N-terminal MBP fusion tag intact. Previous experiments have shown that the rates of hydrolysis exhibited by the fusion protein do not significantly differ from those of the untagged version (35). When expressed in medium supplemented with ZnSO_4 , the D108N MBP-AHL lactonase complex was found to contain 1.9 equiv of zinc. When expressed in medium containing a CoCl_2 supplement, the mutant contained 1.3 equiv of cobalt and 0.1 equiv of zinc. As described below, circular dichroism (CD) spectroscopy

indicated that there were no major structural perturbations induced by the Y194F mutation. The D108N mutant was purified as a fusion protein lacking a TEV cleavage site, so it was not included in the CD comparison.

Circular Dichroism of Wild Type and Mutant AHL Lactonases

There are slight differences in predicted α -helix and β -sheet content between wild-type and Y194F mutant enzymes (Figure 3.1), with the Y194F mutant displaying similarity to the wild type enzyme. The negative bands at 222 and 208 nm corresponding to α -helical character (92) overlap quite well, while more deviation is seen in the positive band near 198 nm corresponding to a portion of the β -sheet region (92). It is known that more strongly twisted β -sheets have a stronger 198 nm band (92), it is possible that the Y194F mutation cause slight changes in conformation that relax one or more strongly twisted β -sheets; these residues are adjacent to ends of the 10-12 strands.

The slight differences seen in circular dichroism spectra between wild type and Y194F enzymes may indicate a minor global change in conformation. However, they appear to have little impact at the active site of the enzyme, as is seen in crystal structures of the Y194F and Y194A enzymes (D. Liu and D. Ringe, unpublished data).

Steady-State Hydrolysis Kinetics

Substrate turnover of C6- HSL by the Y194F and D108N variants of dizinc AHL lactonase was quite slow as seen from the data presented in Table 3.2, with k_{cat}/K_M values two orders of magnitude lower than that of the wild-type protein.

enzyme	metal ^a	K_M (mM)	k_{cat} (s ⁻¹)	k_{cat}/K_M (M ⁻¹ s ⁻¹)
wild type ^b	ZnSO ₄	5.6±0.6	91±3	1.6 x 10 ⁴
Y194F	ZnSO ₄	2.1±0.5	0.31±0.02	1.5 x 10 ²
D108N	ZnSO ₄	1.6±0.6	1.4±0.1	8.8 x 10 ²
wild type	CoCl ₂	0.36±0.04	510±10	1.4 x 10 ⁶
Y194F	CoCl ₂	2.0±0.4	16.6±0.8	8.3 x 10 ³
D108N	CoCl ₂	0.09±0.04	3.5±0.1	3.9 x 10 ⁴

Table 3.2 Steady-state kinetic constants for C6-HSL hydrolysis by dizinc and dicobalt AHL lactonase variants. ^aMetal supplements added during protein expression. ^bValues taken from reference (47).

As seen in Table 2.2, dicobalt-substituted AHL lactonase from *B. thuringiensis* exhibits enhanced activity in comparison to the dizinc metalloform. This property was exploited in order to obtain more reliable kinetic parameters from these slower variants, by using dicobalt-substituted AHL lactonases to obtain kinetic parameters for AHL hydrolysis. X-ray absorption spectroscopy (47) and X-ray crystallography (48, 36) indicate very similar metal coordination environments for the dicobalt and dizinc

substituted lactonases, and a circular dichroism study reveals similar folds for the Y194F mutant compared to wild-type. Using dicobalt-substituted AHL lactonase, a 2-3 order of magnitude decrease in k_{cat}/K_M values is observed for the Y194F and D108N mutations (Table 3.2) in comparison to the values for the wild type enzyme. The majority of this effect is due to a decrease in k_{cat} values (30- 150 fold) rather than the modest changes in K_M values (4-6 fold), which is consistent with an important role for these residues in the lactone ring-opening mechanism.

Hydrolysis of the synthetic thiolactone substrate C6-HCTL was used to investigate the effects of the oxygen to sulfur substitution in the substrate's leaving group with wild-type and mutant AHL lactonases. The previously observed thio effect (Chapter 2) suggest that breaking a metal-thiol bond may be partially rate-limiting in wild-type lactonase. Comparison of the K_M and k_{cat} values for AHL hydrolysis by wild type and D108N mutant AHL lactonase reveals some interesting differences. Kinetic constants for hydrolysis of C6-HCTL and C6-HSL are affected similarly with the D108N mutation. For hydrolysis of C6-HCTL, K_M and k_{cat} values are decreased 5- and 180-fold, respectively. Hydrolysis of C6-HSL shows K_M and k_{cat} values decreased by 4- and 150-fold (Tables 3.2 and 3.3).

enzyme	K_M (mM)	k_{cat} (s ⁻¹)	k_{cat}/K_M (M ⁻¹ s ⁻¹)
wild type ^a	6.7±0.7	198±8	3.0 x 10 ⁴
Y194F	0.6±0.1	5.4±0.02	9.0 x 10 ³
D108N	1.3±0.2	1.11±0.04	8.5 x 10 ²

Table 3.3 Steady-state kinetic constants for C6-HCTL hydrolysis by dicobalt AHL lactonase variants. ^aValues taken from reference (35).

Upon mutation to the Y194F variant, a decrease in both K_M and k_{cat} (11- and 37-fold, respectively) is seen for hydrolysis of C6-HCTL compared to the wild type enzyme (Table 3.3). Hydrolysis of C6-HSL, however, showed an increase in K_M and a decrease in k_{cat} (6- and 30-fold, respectively, Table 3.3). The changes in K_M upon mutation may be due to changes in the substrate dissociation constant or changes in other microscopic rate constants. Values of k_{cat} for C6-HCTL hydrolysis by wild-type and mutant enzymes are approximately 3-fold lower than for C6-HSL, indicating that the effects of the oxygen for sulfur substitution are likely independent of the D108N and Y194F mutations. However, both mutants exhibited lower k_{cat} values in comparison to wild-type enzyme with C6-HSL and C6-HCTL substrates, indicating that the Asp108 and Tyr194 both contribute to rate-limiting steps during steady-state hydrolysis.

DISCUSSION

There is a large amount of diversity in the catalytic hydrolysis mechanisms used by metallo- β -lactamase superfamily members (81, 28, 39). This diversity makes

prediction of catalytic mechanisms difficult, necessitating investigation of active site residues experimentally. Product-bound structures of AHL lactonase indicate that the lactone ring of C6-HSL binds in an orientation similar to that seen in metallo- β -lactamases (48). This binding mode is different from that seen in L-homoserine lactone inhibited AHL lactonase, with the lactone ring rotated nearly 180° from that seen in the inhibited complex (37). A mechanism for AHL hydrolysis was previously proposed based on this complex, where Tyr194 behaves as a general acid to protonate the alcohol leaving group and Asp108 assists in deprotonation of a metal bound water (Scheme 3.1) (37). Although this mechanism is based on the inhibited structure, our subsequent crystal structures with product bound indicate that substrate likely binds in an alternate orientation, more similar to other M β L superfamily members.

In structures of product-bound AHL lactonase, the placement of two active site residues, Asp108 and Tyr194 suggest that they may participate in the catalytic mechanism. In addition to the structural evidence supporting a role in catalysis, quantum mechanical/molecular modeling hybrid studies support a binding mode similar to that seen in other M β L family members. Construction of a model based on the inhibited L-homoserine structure (37) showed that this complex was not stable and that this orientation likely represents a nonproductive inhibitory binding mode rather than an on-pathway reaction species (93). In contrast, a model based on the structure of the product-bound complex with the carbonyl oxygen of the lactone ring coordinated to Zn1 and the

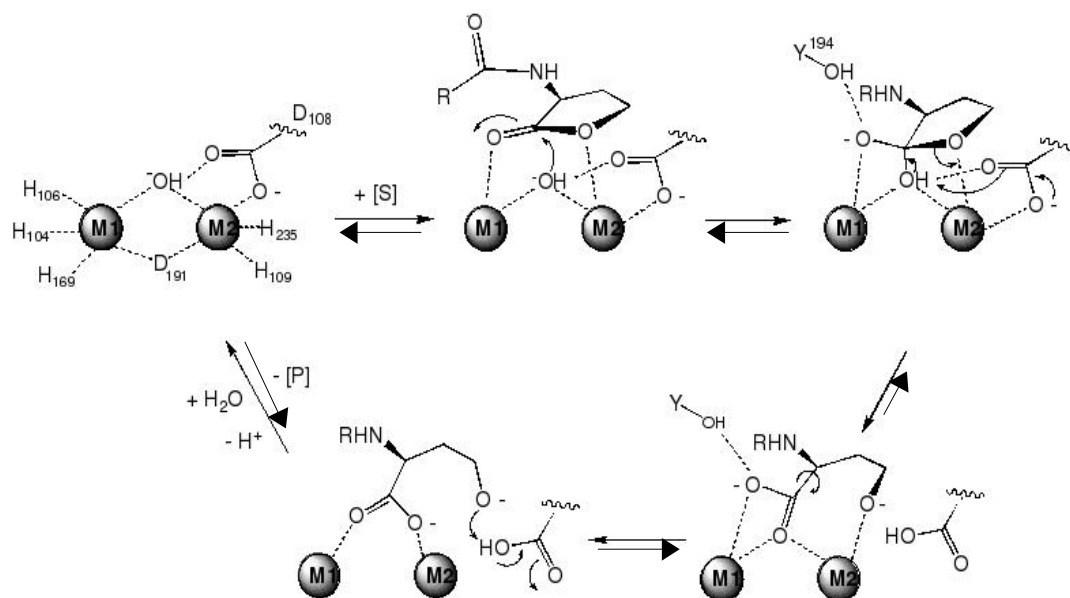
leaving group oxygen is coordinated to Zn²⁺ revealed that this alternative substrate binding mode was stable over a 1 ns simulation period (93). This simulation indicated important binding interactions between substrate and enzyme. In addition to oxygen-zinc interactions, the lactone ring's carbonyl oxygen was noted to interact with the phenol of Tyr194 (93). A molecular dynamics simulation with the Y194F variant confirmed the importance of this interaction; with this mutation the lactone ring binding mode was destabilized and the positioning was not optimized for catalysis (93). In contrast to the interactions seen between the lactone ring and the metal center, the interaction between the *N*-hexanoyl chain was much less stable, consisting of multiple transient interactions along the surface of the binding cavity (93). Despite the relative instability of the acyl chain binding, these interactions are important, as indicated by computational studies indicating instability (93) and inhibitory binding seen with L-homoserine, which lacks the acyl chain (37). The QM/MM model of the ES complex also shows that the zinc-bound hydroxide is located near the lactone carbonyl, indicating that binding produces a configuration for optimal attack by the nucleophile. Attack by the nucleophile will likely produce a tetrahedral intermediate that would collapse after cleavage of the C-O bond between the carbonyl carbon and the leaving group oxygen.

The interaction between the lactone carbonyl oxygen and Tyr194 may help to stabilize the tetrahedral adduct that occurs after attack of the nucleophilic hydroxide at the ring carbonyl. While molecular modeling studies indicate a role for Tyr194 in

arranging the substrate in a near-attack configuration, the role of this residue in lactone hydrolysis had not previously been established, despite its importance being suggested by multiple studies (37, 94). Steady-state kinetics of substrate hydrolysis by the Y194F variant shows k_{cat}/K_M values approximately 2 orders of magnitude lower than those seen with wild-type AHL lactonase, consistent with a role for this residue in binding and tetrahedral intermediate stabilization, as suggested by structural and computational studies (48, 93). This Y194F mutation displays a higher K_M value (6-fold) and a 30-fold slower k_{cat} value, indicating that removing the interaction with the phenol group has a large effect on catalysis and probably on binding as well, although K_M may not provide a direct measurement of the substrate's dissociation constant.

The role of Asp108 was previously proposed to participate in the deprotonation of a metal-bound water, however, this suggestion was based on an inhibitor bound structure of AHL lactonase (37). Crystal structures of dizinc- and dicobalt-substituted AHL lactonases show differences in product coordination upon variation of the metal center. With the dizinc AHL lactonase, both C6-Hse and C6-Hcy are observed with the leaving group alcohol or thiol in hydrogen-bonding distance to Asp108, which is no longer coordinated to Zn²⁺, as it was seen in the unliganded enzyme (36). Alternatively, when AHL lactonase is disubstituted with cobalt, the alcohol or thiol of C6-Hse and C6-Hcy are observed to remain coordinated to Co²⁺, as is Asp108. The D108N mutation replaces the acidic carboxylic acid group with asparagine, which is unlikely to donate a proton to

the leaving group. The effect of this mutation on catalysis is drastic, resulting in a 150-fold decrease in k_{cat} along with a more modest decrease (4-fold) in K_M , consistent with a significant role of this residue in catalysis. It is interesting to note that the sulfur-for-oxygen substitution in the leaving group of the lactone ring does not significantly alter the relative effects on K_M or k_{cat} values for either mutation in comparison to wild-type hydrolysis of the respective lactone and thiolactone substrates, with the thiolactone substrate being hydrolyzed about 3-fold slower than its oxygen-containing counterpart. Although the rate-limiting step has not been identified for AHL hydrolysis, the results seen with the Y194F and D108N mutations as well as substitution of the leaving group indicate that all of these changes likely contribute to the overall rate-limiting steps during steady-state catalysis.



Scheme 3.3 Proposed catalytic mechanism for hydrolysis by AHL lactonase.

Through the combination of all the available data, a detailed catalytic mechanism for *B. thuringiensis* can be proposed (Scheme 3.3) that contrasts with the previously suggested mechanism based on an inhibitor-bound structure (Scheme 3.1) (37). The requirement for a dinuclear metal center has been proven through ICP-MS metal analysis (35, 47), reconstitution studies (35), ¹H NMR (Chapter 2) as well as EXAFS (35, 47) and X-ray crystallography (37, 48). These experiments reveal that the resting enzyme includes two zinc (II) ions within close proximity of one another that aid in both catalysis (35) and folding (Chapter 2). Related metallo- β -lactamase family members are observed to bind with the less sterically hindered exo face of the lactam ring toward the metal

center. Similar binding is suggested by both X-ray crystallography of product-bound AHL lactonase (48) and molecular dynamics simulations of the ES complex (93), which show AHL substrates binding with the less sterically hindered re face of the lactone ring facing towards the dinuclear metal center of AHL lactonase. The positioning of the lactone group over the metal center is also similar to that seen with other metallo- β -lactamase superfamily members, with the carbonyl oxygen of the lactone ring located above Zn1 and the leaving group oxygen above Zn2. Site-directed mutagenesis, steady-state kinetics and molecular dynamics studies (93) indicate that the phenol group of Tyr194 interacts with the carbonyl oxygen of the lactone ring to stabilize binding and the tetrahedral intermediate formed after nucleophilic attack of the metal-bound hydroxide.

Upon binding in this orientation, the active site metal ions aid in polarization of the lactone, effecting an increase in the electrophilic nature of the carbonyl carbon of the lactone. As described in Chapter 2, NMR studies with isotopic labels have confirmed that opening of the lactone ring is achieved through an addition-elimination reaction with a solvent-derived hydroxide, presumably the zinc-bridging hydroxide, acting as the nucleophile. Metal ions are known to perturb the pK_a of water, this effect likely contributes to the variation in reaction rates seen with substitution of metal at the dinuclear center (47). The bound substrate is positioned for attack by this metal-bound hydroxide, which is also observed to coordinate to Asp108 (48). Upon substrate binding, the bridging hydroxide may increase in nucleophilicity by releasing one of the zinc ions,

as is seen with other dinuclear metallo hydrolases (95). Although little experimental evidence for active site rearrangement exists save for a slightly shorter distance between Zn1 and the oxygen of the metal bound hydroxide calculated for the ES complex (93).

After attack of the metal coordinated hydroxide, the resulting tetrahedral adduct may be stabilized by Zn1 and the phenol group of Tyr194. The decrease in k_{cat} values (Tables 3.2 and 3.3) and destabilization of the ES complex (93) seen with the Y194F variant supports a role for this residue in binding and intermediate stabilization. A related metallo- β -lactamase requires deprotonation to the dianionic form prior to bond cleavage (96), however, the lactone substrate is less stable than the lactam substrates investigated in that study. Collapse of the tetrahedral intermediate is likely assisted by Zn2, which is located in an optimal position to stabilize the developing negative charge on the leaving group. In addition to the kinetic thio effect described in Chapter 2, further evidence for this role is seen in the product bound dicobalt AHL lactonase crystal structures, where the leaving group is observed interacting with Co2. Intermediates which interact with the metal in position 2 have been observed in related metallo- β -lactamase superfamily members (97, 30). With coordination of the anionic leaving group to metal-2, the Asp108 interaction with metal-2 weakens, allowing for Asp108 to deprotonate the intermediate. In the dicobalt product bound structures, a new compensatory interaction is seen between Asp191 and Co2, most likely in order to maintain a preferred ligand ratio. Metal-dependent ligand preferences may be associated

with observed differences in reactivity with the cobalt and zinc substituted AHL lactonases as indicated by steady-state kinetics (Table 2.2). Upon comparison of free and unliganded enzyme, the dizinc lactonase appears to tolerate 5 or 6 ligands while (Figure 3.2) the dicobalt lactonase tries to maintain approximately 5 ligands, with long-range interactions occurring between Zn2 and both Asp191 and Asp108 in the product-bound structure (Figure 3.3).

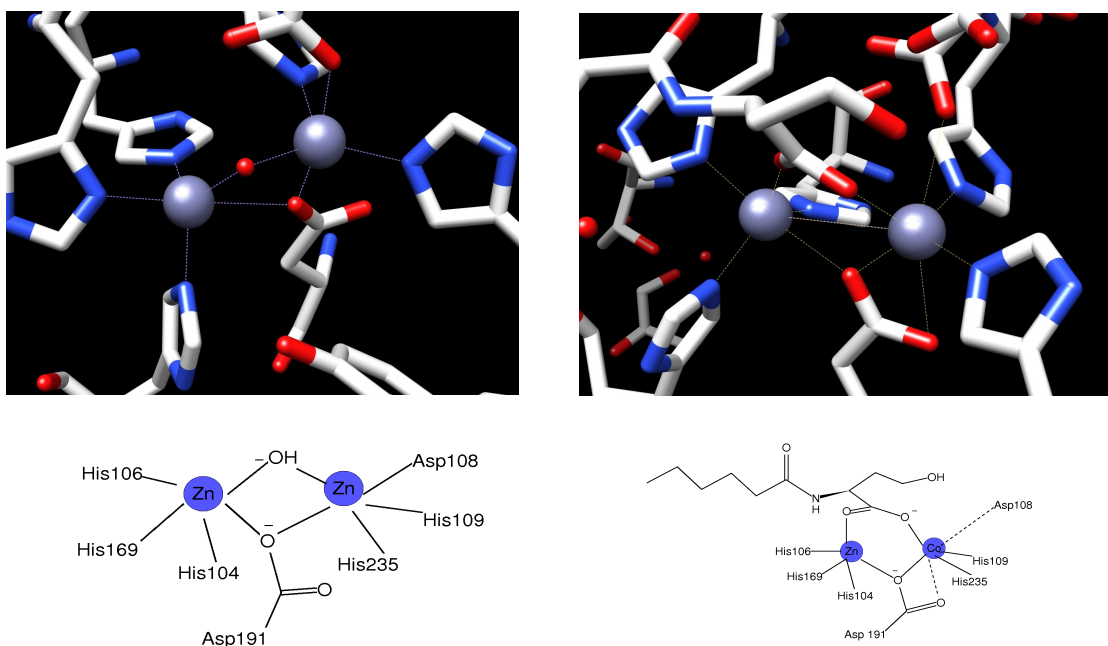


Figure 3.2 Metal ligand arrangement in unliganded and C6-Hse bound dizinc AHL lactonase.

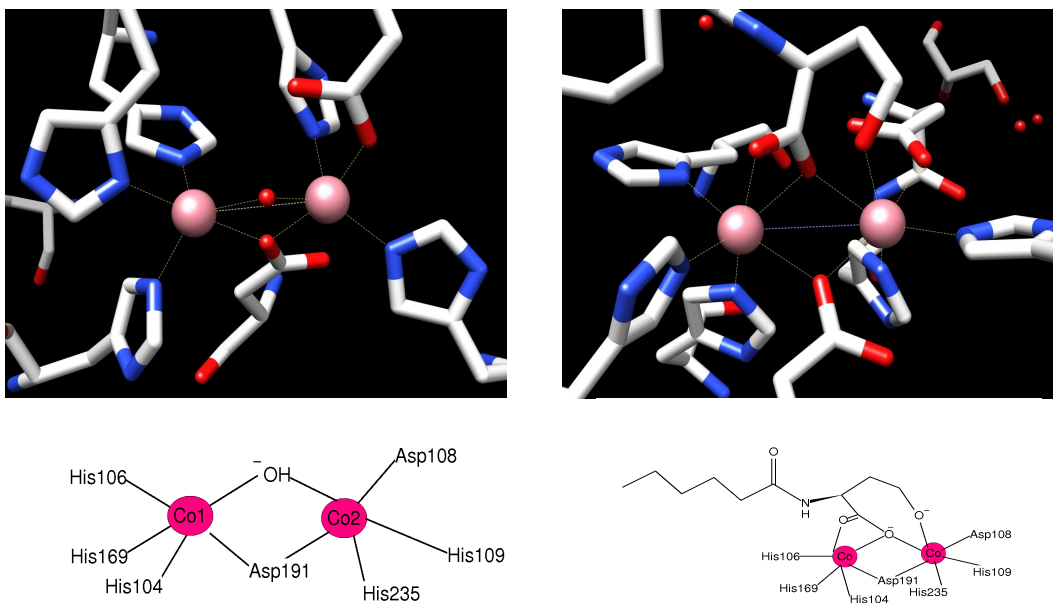


Figure 3.3 Metal ligand arrangement in unliganded and C6-Hse bound dicobalt AHL lactonase.

As Asp108 releases Co2 or Zn2, it is well placed to act as the general base for deprotonation, and in fact is seen coordinated to the bridging hydroxide in the X-ray structure of the free enzyme (38). The loss of coordination between Zn2 and Asp108 seen in the product-bound dizinc lactonase is also observed in a phosphate-bound structure of a related AHL lactonase (38) as well as in an M β L structure obtained at low pH (98). The disruption of an Asp-Zn interaction upon protonation of Asp has also been implicated in catalysis by a monozinc M β L (99). Steady-state kinetic studies on a D108N AHL lactonase mutant reveal a significant decrease in k_{cat} values (Table 3.2), supporting a role for Asp108 in catalysis, likely the deprotonation of the carboxylate of

the tetrahedral intermediate. Following deprotonation, the product's carboxylate is able to bridge the dinuclear metal site in a bidentate fashion, as seen in the dizinc product-bound lactonase (Figure 3.2). This bridging arrangement may be accompanied by a repositioning of the leaving-group oxygen so that the transient coordination to Co₂ or Zn₂ is released so that it can remove the proton from Asp108. The different binding orientations seen with product in the dizinc and dicobalt product-bound crystal structures are consistent with this proposal, as Asp108 is observed to release the metal ion with the leaving group, indicating that the movements of these moieties are related (Figure 3.2). Transfer of the proton to the leaving group regenerates the deprotonated Asp108, which can recoordinate Co₂ or Zn₂, facilitating product release. Proton shuttling by Asp108 follows a favorable pathway, as the proton is transferred between groups of successively higher pK_a values; the zinc-bound carboxyl donates to Asp108 and finally to the metal-bound leaving group. In a related metallo-β-lactamase, a homologous aspartate residue has been primarily implicated as a Zn₂ anchor (*100-103*). In AHL lactonase, however, the weak compensatory aniso-bidentate interaction with Asp191 that is seen in the dicobalt product-bound structure may allow Asp108 to leave Co₂ and act as a proton shuttle without deviation of the metal ion's position. Other metallo-β-lactamases do not possess a homolog to the bridging Asp191 residue, indicating that this bidentate interaction may be a uniquely important feature in the prevention of significant movement during catalysis (*30*). Although differences are seen in the mechanisms of the

diverse members of the metallo- β -lactamase superfamily, there are notable similarities that are shared: a dinuclear metal center, substrate orientation with the carbonyl oxygen over the metal ion in position one, and leaving group stabilization mediated by the metal ion in position 2.

Chapter 4 Substrate Preference and Promiscuity of AHL Lactonase

INTRODUCTION

The *N*-acyl moiety found in AHL substrates is important for proper substrate binding and hydrolysis as has been indicated by an activity assay showing that L-homoserine (which lacks an *N*-acyl substituent) is not hydrolyzed by AHL lactonase and in fact acts as a competitive inhibitor (37). A structure of AHL lactonase complexed with L-homoserine (37) shows this compound bound in an orientation 180° opposite of substrate binding seen in other metallo- β -lactamase superfamily members (30, 81, 83, 59). Crystal structures of AHL lactonase with the open-ring products C6-Hse and C6-Hcy, on the other hand, show product bound in an orientation more consistent with that seen in the M β L superfamily as discussed in Chapters 2 and 3.

The importance of this enzyme-substrate interaction prompted our investigation into the nature of the acyl binding pocket. The first crystal structures of AHL lactonase obtained in collaboration with the Petsko-Ringe group indicate that the hexanoyl sidechains of C6-Hse and C6-Hcy locate to a hydrophobic binding pocket containing Ala206 and Gly207. In this chapter, site-directed mutagenesis of these two residues, synthesis of alternative substrates and steady-state kinetics are used to test the proposed substrate binding model. Non-hydrolyzable substrate analogs were prepared as potential

inhibitors and crystal structures were obtained by our collaborators with these compounds bound. The interactions that were observed with these structures prompted us to obtain additional crystal structures with a longer-chain AHL, leading to the unexpected discovery of an additional substrate binding mode.

METHODS

Construction of the Expression Vector for Cleavable Maltose Binding Protein MBP-A206W, G207W and G207D AHL Lactonase Fusion Proteins

Expression vectors expressing A206W, G207W, and G207D mutants were obtained using the Quikchange kit (Stratagene, La Jolla, CA). Mutagenic primers used to obtain each mutant are given in Table 4.1. Briefly, both forward and reverse primers (125 ng) were combined with template (100 ng of pMal-t-AiiA plasmid) (35), dNTPs (each at a final concentration of 200 μ M), and Pfu polymerase (2.5 units). The reaction mixture was brought to a volume of 50 μ L by the addition of reaction buffer and subjected to the following thermocycler program: 95 $^{\circ}$ C for 30 s, 17 cycles at 95 $^{\circ}$ C for 30 s, 55 $^{\circ}$ C for 1 min, and 68 $^{\circ}$ C for 7 min and 30 s, followed by 68 $^{\circ}$ C for 10 min. DpnI restriction enzyme was added and allowed to react for 2 h at 37 $^{\circ}$ C. The digested mixture was transformed into competent *E. coli* Top10 (5 μ L into 50 μ L of cells). Transformed cells were selected by plating onto LB supplemented with ampicillin (50 μ g/mL). The plasmid expressing the G207D mutant gene was obtained in a similar manner as described above,

utilizing the appropriate primers described in Table 4.1, and the following thermocycler parameters: 95 °C for 2 min, 15 cycles at 95 °C for 30 s, 73 °C for 30 s, and 72 °C for 9 min, followed by 72 °C for 10 min. All mutations were verified by fully sequencing the gene inserts (DNA Core Facility, The University of Texas).

	primer sequence
A206W forward	5'-GAAGTGCCGTTctggGGATTTGATCCAGAATTAGCTTTATCT-3'
A206W reverse	5'-AGATAAAGCTAATTCTGGATCAAATCCccaGAACGGCACTTC-3'
G207W forward	5'-GAAGTGCCGTTTCGCAatggTTTGGATCCAGAATTAGCTTTATCT-3'
G207W reverse	5'-AGATAAAGCTAATTCTGGATCAAAccaTGCGAACGGCACTTC-3'
G207D forward	5'-GATGAAGTGCCGTTTCGCAgatTTTGGATCCAGAATTAGCT-3'
G207D reverse	5'-AGCTAATTCTGGATCAAAatcTGCGAACGGCACTTCATC-3'

Table 4.1 Primers used for Quikchange mutagenesis. Mutagenic codons are indicated in lowercase.

Expression and Purification of Metal-Substituted AHL Lactonases

Cobalt and zinc were incorporated into AHL lactonase using previously developed expression conditions as described in Chapter 3. Protein was purified from *E. coli* BL21(DE3) cells harboring the desired vector (pMAL-t-aiiA wild type (35), pMAL-t-aiiA A206W, pMAL-t-aiiA G207W, pMAL-t-aiiA G207D or pMAL-t-aiiA Y194F expression plasmid. Purification procedures did not require alteration from established protocols. The MBP-AHL lactonase fusion proteins prepared with ZnSO₄ or CoCl₂ were subsequently cleaved with tobacco etch virus protease, and the untagged enzyme was

purified as described in Chapter 2. It has previously been demonstrated that AHL lactonase is monomeric (36) and that the presence of the MBP tag does not significantly affect catalysis (6). The purity of each enzyme preparation was confirmed by SDS-PAGE and metal content was analyzed by ICP-MS (School of Geological Sciences, The University of Texas at Austin).

Circular Dichroism Spectroscopy of AHL Lactonase

Far UV-circular dichroism spectra of dicobalt variants of wild type and mutant AHL lactonases to assess changes in secondary structure upon mutation was accomplished in the same manner as described in Chapter 3. Sodium phosphate buffer (10 mM), pH 7.4 was used as the baseline buffer used for all samples. Molar ellipticity [θ] is plotted versus wavelength for untagged wild type, A206W, G207W and G207D dicobalt AHL lactonases in Figure 4.1.

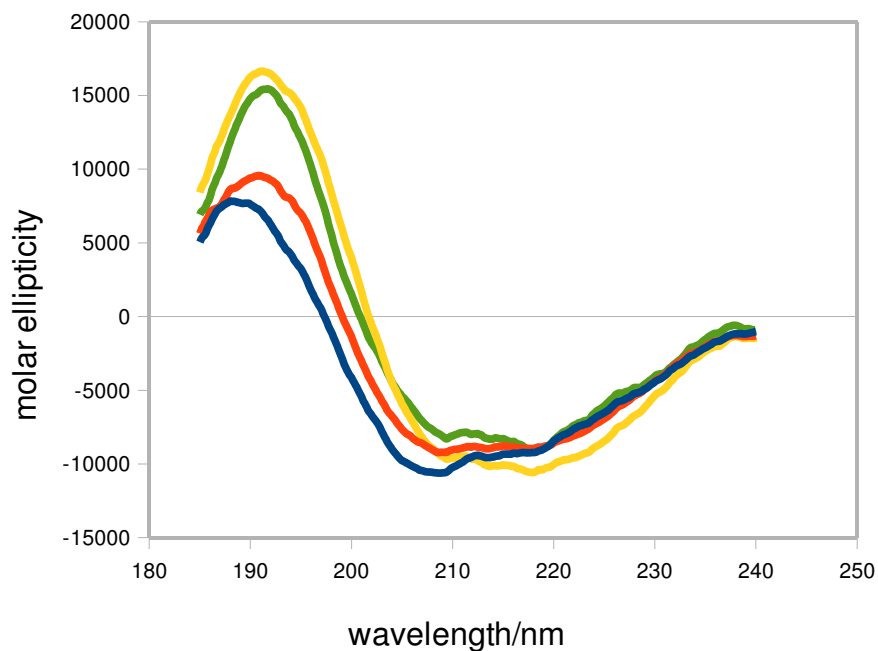


Figure 4.1 CD spectra of dicobalt AHL lactonases (G207W variant in gold, wild type in green, G207D variant in red, A206W variant in blue). Far UV molar ellipticity $[\theta]$ (in units of degrees cm^2/dmol protein) are plotted against wavelength.

The CD spectra were analyzed for secondary structural content as described in Chapter 3 using the SELCON3 simulation program and data set SP175 (86) available at DICHROWEB (<http://www.cryst.bbk.ac.uk/cdweb/html/home.html>) (87, 88). Predicted α helix and β sheet content are presented in Table 4.2. The generally accepted interpretation of normalized standard deviation (NRMSD) for CD data is that an NRMSD of less than 0.2 indicates the calculated structure is generally similar to the actual

structure (88), and the values obtained here are within this cutoff. Indeed, the alpha and beta character of all samples are similar to those calculated for the crystal structure of dizinc AHL lactonase (8).

	α -helix (%)	β -sheet (%)	Turns (%)	Unordered (%)	NRMSD
Wild Type	18	33	12	37	0.10
A206W	22	28	10	38	0.19
G207D	19	29	11	37	0.11
G207W	23	29	10	37	0.07
calculated ^a	25	30	- ^b	-	-

Table 4.2 Calculated secondary structure content of AHL lactonase variants. ^afrom PDB ID 2A7M (36). ^bNot calculated.

Synthesis of *N*-Pentanoyl-L-Homoserine Lactone (C5-HSL)

All synthetic reagents were purchased from Sigma-Aldrich Chemical Co. (St. Louis, MO). In a procedure similar to those previously described (44, 45), triethylamine (12 mmol) was added to a stirred suspension of (*S*)- α -amino- γ -butyrolactone hydrobromide (6.5 mmol) in dimethylformamide (50 mL) at 0 °C. Valeroyl chloride (7 mmol) was added dropwise. The reaction mixture was allowed to come to room temperature and stirred for 2 h. Solvent was removed by rotary evaporation with heating at ≤ 55 °C. The residue was dissolved in dichloromethane and washed sequentially with sodium sulfate (1 M, 2 \times 50 mL), saturated sodium bicarbonate (1 \times 50 mL), and

saturated sodium chloride (1 × 50 mL). The organic layer was dried over anhydrous magnesium sulfate, and solvent was removed by rotary evaporation. The final compound was further purified by recrystallization from ethyl acetate and petroleum ether (50:50, v/v): calculated yield 30%; $R_f = 0.49$ in ethyl acetate; mp 125-128 °C (uncorrected); ^1H NMR (300 MHz, CDCl_3) δ 0.88 (t, 3H), 1.29-1.36 (m, 2H), 1.55-1.63 (m, 2H), 2.08-2.15 (m, 1H), 2.22 (m, 2H), 2.75-2.82 (m, 1H), 4.21-4.30 (m, 1H), 4.40 (t, 1H), 4.46-4.59 (m, 1H), 6.18 (broad, N-H); ^{13}C NMR (75 MHz, CDCl_3) δ 13.72, 22.27, 27.46, 30.41, 35.83, 49.11, 66.09, 173.80, 175.70; EI-HRMS $\text{MH}^+_{\text{calc}} = 186.1130$, $\text{MH}^+_{\text{obs}} = 186.1133$; $[\alpha]^{20^\circ\text{C}}_{\text{D, methanol}} = -23^\circ$.

Synthesis of *N*-Decanoyl-*L*-Homoserine Lactone (C10-HSL)

All synthetic reagents were purchased from Sigma-Aldrich Chemical Co. (St. Louis, MO). In a procedure similar to those previously described (44, 45), triethylamine (12 mmol) was added to a stirred suspension of (*S*)- α -amino- γ -butyrolactone hydrobromide (5.7 mmol) in dimethylformamide (50 mL) at 0 °C. Decanoyl chloride (7 mmole) was added dropwise. The reaction mixture was allowed to come to room temperature and stirred for 75 min. Solvent was removed by rotary evaporation with heating at ≤ 55 °C. The residue was dissolved in dichloromethane and washed sequentially with sodium sulfate (1 M, 2 × 50 mL), saturated sodium bicarbonate (1 × 50 mL), and saturated sodium chloride (1 × 50 mL). The organic layer was dried over

anhydrous magnesium sulfate, and solvent was removed by rotary evaporation. The final compound was further purified by recrystallization from ethyl acetate and petroleum ether (50:50, v/v): calculated yield 46%; $R_f = 0.55$ in ethyl acetate; mp 127-130 °C (uncorrected); ^1H NMR (300 MHz, CDCl_3) δ 0.86 (t, 3H), 1.24 (m, 10H), 1.57 (m, 2H), 1.64 (m, 2H), 2.06-2.13 (m, 1H), 2.20-2.25 (m, 1H), 2.81-2.90 (m, 1H), 4.22-4.31 (m, 1H), 4.42-4.48 (m, 1H), 4.49-4.53 (m, 1H), 5.95 (broad, N-H); ^{13}C NMR (75 MHz, CDCl_3) δ 14.10, 22.65, 25.41, 29.19, 29.24, 29.29, 29.39, 30.74, 31.84, 36.20, 49.29, 66.11, 175.50, 173.76; EI-HRMS $\text{MH}^+_{\text{calc}} = 256.1913$, $\text{MH}^+_{\text{obs}} = 256.1915$; $[\alpha]^{20}_{\text{D, methanol}} = -23.5^\circ$.

Kinetic Assay of AHL Lactonase Activity

Hydrolysis of AHLs by AHL lactonase was followed using a previously reported colorimetric assay (6), as described in Chapter 3.

Synthesis of *N*-Octanoyl-L-Homoserine Lactone (C8-HSL)

All synthetic reagents were purchased from Sigma-Aldrich Chemical Co. (St. Louis, MO). In a procedure similar to those previously described (44, 45), triethylamine (11.5 mmol) was added to a stirred suspension of (*S*)- α -amino- γ -butyrolactone hydrobromide (5 mmol) in dimethylformamide (12 mL) at 0 °C. Octanoyl chloride (7 mmol) was added dropwise. The reaction mixture was allowed to come to room

temperature and stirred for one hour. Solvent was removed by rotary evaporation with heating at ≤ 55 °C. The residue was dissolved in dichloromethane (50 mL) and washed sequentially with sodium sulfate (1 M, 3 \times 40 mL), saturated sodium bicarbonate (1 \times 40 mL), and saturated sodium chloride (1 \times 40 mL). The organic layer was dried over anhydrous magnesium sulfate, and solvent was removed by rotary evaporation. The final compound was purified by flash column chromatography on silica in ethyl acetate. Calculated yield 90 %; R_f = 0.56 in ethyl acetate; mp 116-117 °C (uncorrected); ^1H NMR (300 MHz, CDCl_3) δ 0.84 (m, 3H), 1.17-1.40 (m, 8H), 1.61 (m, 2H), 2.12 (m, 1H), 2.22 (m, 2H), 2.24 (m, 1H), 4.24 (m, 1H), 4.44 (t, 1H), 4.55 (m, 1H), 6.20 (broad, N-H); ^{13}C NMR (75 MHz, CdCl_2) δ 14.30, 22.83, 25.69, 29.21, 29.40, 30.76, 31.89, 36.41, 49.43, 66.34, 174.13, 175.96; EI-HRMS $\text{MH}^+_{\text{calc}} = 228.1602$, $\text{MH}^+_{\text{obs}} = 228.1600$; $[\alpha]_{\text{D},\text{methanol}}^{20} = -24.7$ °C.

Synthesis of *N*-Dodecanoyl-*L*-Homoserine Lactone (C12-HSL)

All synthetic reagents were purchased from Sigma-Aldrich Chemical Co. (St. Louis, MO). In a procedure similar that previously described (44, 45), triethylamine (7 mmol) was added to a stirred suspension of (*S*)- α -amino- γ -butyrolactone hydrobromide (3 mmol) in dimethylformamide (10 mL) at 0 °C. Lauroyl chloride (4 mmol) was added dropwise. The reaction mixture was allowed to come to room temperature and stirred overnight. Solvent was removed by rotary evaporation with heating at ≤ 55 °C. The

residue was dissolved in dichloromethane (100 mL) and washed sequentially with sodium sulfate (1 M, 2 × 100 mL), saturated sodium bicarbonate (1 × 100 mL), and saturated sodium chloride (1 × 100 mL). The organic layer was dried over anhydrous magnesium sulfate, and solvent was removed by rotary evaporation. The final compound was further purified by recrystallization from ethyl acetate and petroleum ether (50:50, v/v): calculated yield 73 %; $R_f = 0.68$ in ethyl acetate; mp 130-133 °C (uncorrected); ^1H NMR (300 MHz, CDCl_3) δ 0.86 (t, 3H), 1.21-1.25 (m, 16H), 1.56-1.65 (m, 2H), 2.10 (m, 1H), 2.23 (m, 2H), 2.86 (m, 1H), 4.29 (m, 1H), 4.47 (t, 1H), 4.51 (m, 1H), 5.97 (broad, N-H); ^{13}C NMR (75 MHz, CDCl_3) δ 14.11, 22.66, 25.41, 29.19, 29.29, 29.29, 29.43, 29.43, 29.57, 30.73, 31.88, 36.20, 66.11, 173.76, 175.50; EI-HRMS $\text{MH}^+_{\text{calc}} = 284.2224$, $\text{MH}^+_{\text{obs}} = 284.2226$; $[\alpha]^{20}_{\text{D, methanol}} = -21.2^\circ$.

Synthesis of *N*-Tetradecanoyl-*L*-Homoserine Lactone (C14-HSL)

All synthetic reagents were purchased from Sigma-Aldrich Chemical Co. (St. Louis, MO). In a procedure similar to that previously described (44, 45), triethylamine (7 mmol) was added to a stirred suspension of (*S*)- α -amino- γ -butyrolactone hydrobromide (3 mmol) in dimethylformamide (10 mL) at 0 °C. Myristoyl chloride (4 mmol) was added dropwise. The reaction mixture was allowed to come to room temperature and stirred overnight. Solvent was removed by rotary evaporation with heating at ≤ 55 °C. The residue was dissolved in dichloromethane (100 mL) and washed sequentially with

sodium sulfate (1 M, 2 × 100 mL), saturated sodium bicarbonate (1 × 100 mL), and saturated sodium chloride (1 × 100 mL). The organic layer was dried over anhydrous magnesium sulfate, and solvent was removed by rotary evaporation. The final compound was further purified by recrystallization from ethyl acetate and petroleum ether (50:50, v/v): calculated yield 93 %; R_f = 0.74 in ethyl acetate; mp 112-118 °C (uncorrected); ^1H NMR (300 MHz, CDCl_3) δ 0.85 (t, 3H), 1.21-1.24 (m, 20H), 1.59-1.62 (m, 2H), 2.13 (m, 1H), 2.22 (m, 2H), 2.86 (m, 1H), 4.25 (m, 1H), 4.42 (t, 1H), 4.48 (m, 1H), 5.93 (broad, N-H); ^{13}C NMR (75 MHz, CDCl_3) δ 14.11, 22.68, 25.41, 29.33, 29.33, 29.63, 29.63, 29.63, 30.50, 30.50, 30.74, 31.91, 36.19, 49.30, 51.93, 66.11, 171.40, 173.78; EI-HRMS $\text{MH}^+_{\text{calc}} = 312.2543$, $\text{MH}^+_{\text{obs}} = 312.2539$; $[\alpha]^{20^\circ}_{\text{D, methanol}} = -27.8^\circ$.

Synthesis of *trans*-(*N*-Hexanoyl)-Aminocyclopentanol (*trans*-ACP, Figure 4.2)

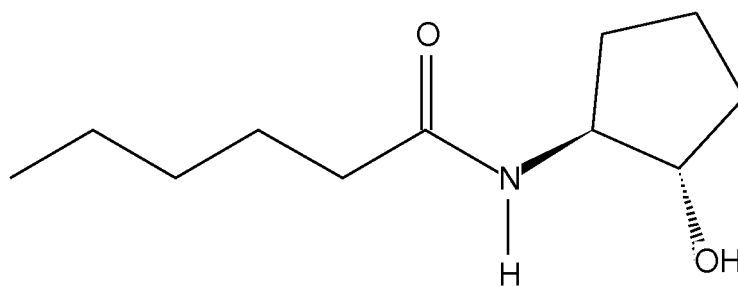


Figure 4.2 *trans*-(*N*-Hexanoyl)-aminocyclopentanol (*trans*-ACP)

All synthetic reagents were purchased from Sigma-Aldrich Chemical Co. (St. Louis, MO). Triethylamine (9 mmol) was added to a stirred suspension of *trans*-(1*S*,2*S*)-2-aminocyclopentanol hydrochloride (4.5 mmol) in dimethylformamide (20 mL) at 0 °C. Hexanoyl chloride (5 mmol) was added dropwise, after which time the reaction mixture was allowed to come to room temperature and stirred for 2 h. Solvent was removed by rotary evaporation with heating at ≤ 55 °C. The residue was dissolved in chloroform (50 mL) and washed sequentially with water (3 \times 50 mL), saturated sodium bicarbonate (1 \times 50 mL), and saturated sodium chloride (1 \times 50 mL). The organic layer was dried over anhydrous magnesium sulfate, run through activated carbon on a bed of celite to decolorize, then solvent was removed by rotary evaporation to afford the final compound as a white solid. Calculated yield 32%; $R_f = 0.5$ in ethyl acetate; mp = 73-74 °C (uncorrected); ^1H NMR (300 MHz, CDCl_3) δ 0.86 (3H, m), 1.35 (4H, m), 1.61 (4H, m), 1.68 (1H, m), 1.79 (1H, m), 2.03 (1H, m), 2.11 (1H, m), 2.18 (2H, m), 3.81 (1H, m), 3.92 (1H, m), 4.62 (1H, broad, OH), 5.60 (1H, broad, NH); ^{13}C NMR (75 MHz, CDCl_3) δ 13.87, 21.11, 22.33, 25.42, 30.16, 31.32, 32.34, 36.05, 60.82, 79.34, 175.85; EI-HRMS $\text{MH}^+_{\text{calc}} = 200.1654$, $\text{MH}^+_{\text{obs}} = 200.1651$.

Synthesis of *cis*-(*N*-Hexanoyl)-Aminocyclopentanol (*cis*-ACP, Figure 4.3)

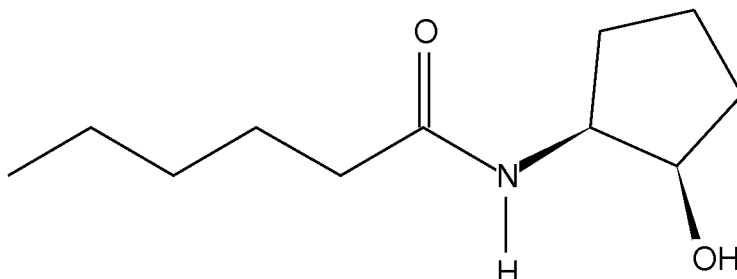


Figure 4.3 *cis*-(*N*-hexanoyl)-aminocyclopentanol (*trans*-ACP)

All synthetic reagents were purchased from Sigma-Aldrich Chemical Co. (St. Louis, MO). Triethylamine (9 mmol) was added to a stirred suspension of *cis*-(1*S*,2*R*)-2-aminocyclopentanol hydrochloride (4.5 mmol) in dimethylformamide (20 mL) at 0 °C. Hexanoyl chloride (5 mmol) was added dropwise, after which time the reaction mixture was allowed to come to room temperature and stirred for 1.5 h. Solvent was removed by rotary evaporation with heating at ≤ 55 °C. The residue was dissolved in chloroform (50 mL) and washed sequentially with water (3 \times 50 mL), saturated sodium bicarbonate (1 \times 50 mL), and saturated sodium chloride (1 \times 50 mL). The organic layer was dried over anhydrous magnesium sulfate, run through activated carbon on a bed of celite to decolorize, then solvent was removed by rotary evaporation to afford the final compound as a white solid. Calculated yield 30.5%; R_f = 0.51 in ethyl acetate; mp = 61-64 °C

(uncorrected); ^1H NMR (300 MHz, CDCl_3) δ 0.88 (3H, m), 1.32 (4H, m), 1.54 (4H, m), 1.73 (1H, m), 1.90 (1H, m), 1.99 (1H, m), 2.13 (2H, m), 2.28 (1H, m), 4.03 (1H, m), 4.16 (1H, m), 5.57 (1H, broad, OH), 5.92 (1H, broad, NH); ^{13}C NMR (75 MHz, CDCl_3) δ 13.92, 20.27, 22.38, 25.47, 29.10, 31.45, 32.89, 36.83, 53.96, 72.78, 173.42, ; EI-HRMS $\text{MH}^+_{\text{calc}} = 200.1654$, $\text{MH}^+_{\text{obs}} = 200.1651$.

Crystallization, Data Collection and Processing, Model Building and Refinement of Product-Bound Dizinc and Dicobalt AHL Lactonases

Crystallization, data collection, processing, model building and structure refinement of product-bound dizinc and dicobalt AHL lactonases was performed by D. Liu, C.F. Liu and D. Ringe of Brandeis University using methods similar to those described (36, 48) using wild type and Y194F mutant AHL lactonase purified as described above (wild type and Y194F mutant) and *cis*-ACP, *trans*-ACP or C10-HSL prepared as described above.

Determination of IC_{50} Values for *cis* and *trans* Substrate Analogs

IC_{50} values were determined for both *cis*- and *trans*-ACP substrate analogs for dicobalt wild type and Y194F mutant AHL lactonases using the pH-based assay described in Chapter 3. Initial velocity measurements were taken at varying inhibitor concentrations and a single C6-HSL substrate concentration. For untagged dicobalt AHL lactonase, a concentration of 17 nM enzyme was used with a substrate concentration of

0.4 mM C6-HSL. For untagged dicobalt Y194F AHL lactonase, a concentration of 420 nM enzyme was used with 1.5 mM C6-HSL as the substrate concentration.

RESULTS

Protein Purification and Characterization

Wild-type and Y194F AHL lactonase were expressed, purified, and characterized for purity and metal content as from M9 minimal medium supplemented with CoCl_2 as described in Chapter 3. The purified wild-type protein contained 2.1 equiv of cobalt and 0.1 equiv of zinc, and Y194F AHL lactonase contained 2.2 equiv of cobalt and 0.1 equiv of zinc with negligible amounts of other metal ions. The AHL lactonase acyl binding site mutants A206W, G207W and G207D variants were also well expressed in M9 minimal medium supplemented with CoCl_2 , purified, and characterized for purity and metal content. The purified A206W AHL lactonase mutant contained 2.0 equiv of cobalt and 0.2 equiv of zinc, the G207W mutant contained 2.1 equiv of cobalt and 0.1 equiv of zinc and the G207D mutant contained 1.3 equiv of cobalt and 0.1 equiv of zinc. All mutants purified with negligible amounts of other divalent metal ions.

Circular Dichroism Spectroscopy of AHL Lactonase

Circular dichroism spectroscopy confirmed that there were no major secondary structural perturbations induced by the acyl pocket mutations. Minor differences are seen

in predicted α -helix and β -sheet content between wild-type and acyl binding pocket mutant enzymes (Table 4.2), with the the G207D mutant displaying the most similarity to the wild type enzyme and the Ala or Gly to Trp (A206W and G207W) mutations having the largest. Negative bands corresponding to α -helical character are observed at 222 and 208 nm (15) and overlap quite well. More deviation, especially with the G207D and A206W mutants, is seen in the positive band near 198 nm corresponding to a portion of the β -sheet region (15). It is known that more strongly twisted β -sheets have a stronger 198 nm band (15), raising the possibility that the G207D and A206W mutations cause slight changes in conformation that relax one or more strongly twisted β -sheets. In fact, these residues are adjacent to ends of the β 10-12 strands, however this does not rule out the possibility that the differences arise from a more global change in conformation.

Steady-state Hydrolysis Kinetics With Acyl Pocket Mutants

The binding site for the *N*-acyl chain of the AHL substrates was probed through the use of dicobalt variants of AHL lactonase with single-point mutations in the binding pocket where the hexanoyl chain of C6-HSL and C6-HCTL is seen to bind in crystal structures (Chapters 2 and 3). Steady-state kinetic constants were obtained for the hydrolysis of substrates with five substitutions: γ -butyrolactone (GBL), *N*-pentanoyl-L-homoserine lactone (C5-HSL). *N*-decanoyl-L-homoserine lactone (C10-HSL), *N*-(*tert*-

butyloxycarbonyl)-DL-HSL (BOC-HSL), and *N*-(benzyloxycarbonyl)-L-HSL (CBZ-HSL). The structures of these substrates are given in Figure 4.4.

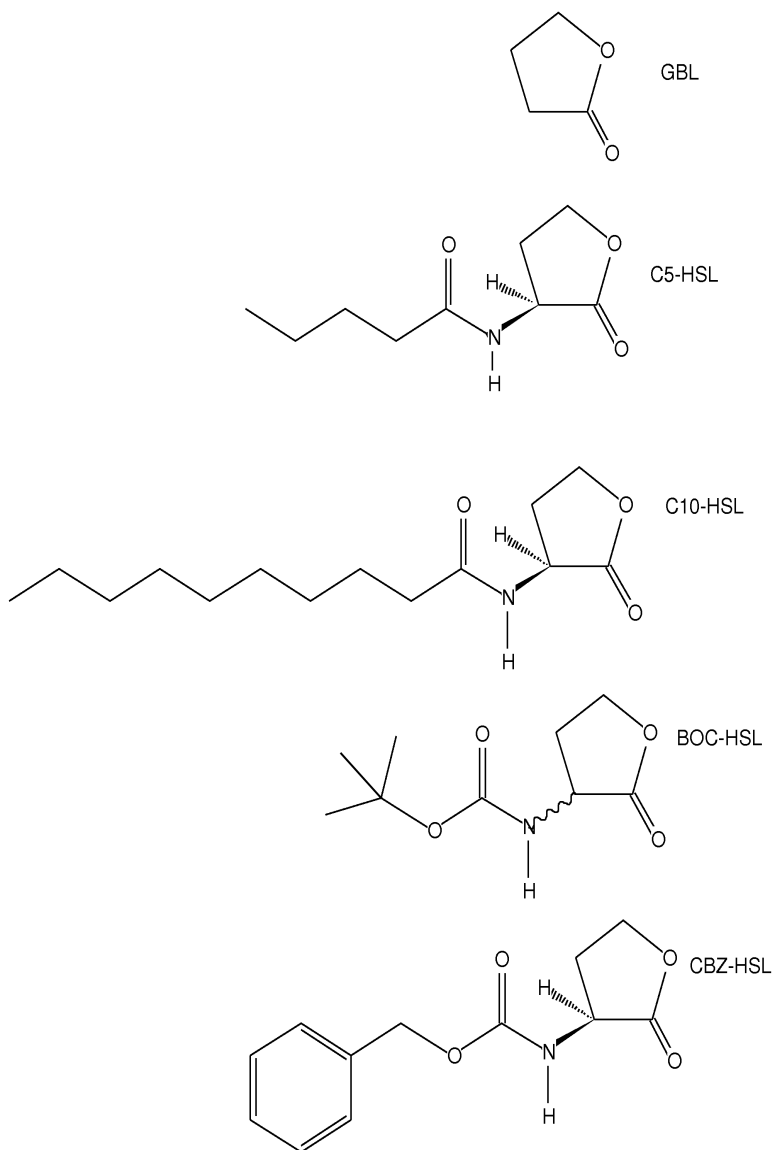


Figure 4.4 Structures of AHL substrates used to probe the sidechain binding site of AHL lactonase.

Site-directed mutagenesis was used to introduce hydrophobic (A206W and G207W) or charged (G207D) side chains at positions predicted to interact with the *N*-acyl chain of the bound substrate molecule based on the observed product bound structures (Figure 4.5).

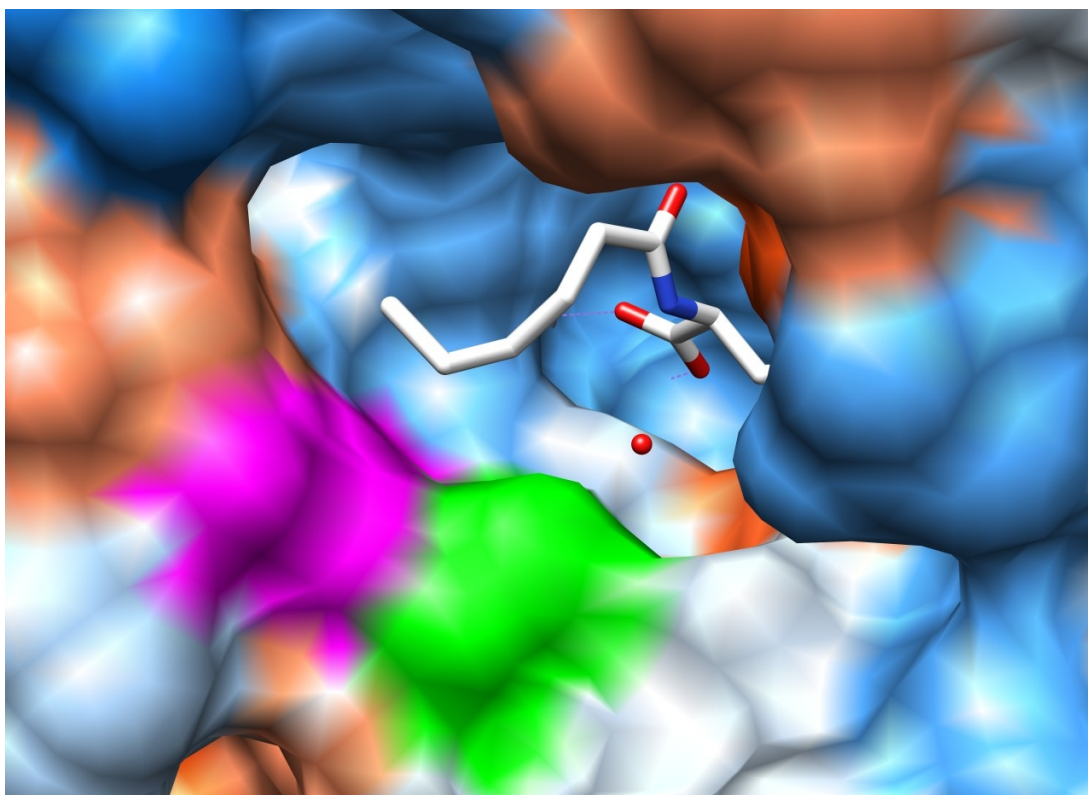


Figure 4.5 Binding of the hexanoyl chain of C6-HSL in AHL lactonase. Ala206 is indicated in green and Gly207 is indicated in pink. Figure prepared using UCSF Chimera (64).

These interactions are predicted to be weak and nonspecific based on QM/MM modeling of the enzyme-substrate complex, where the hexanoyl chain of C6-HSL exhibits significant movement (93). In order to maximize these predicted interactions, two large

nonconservative mutations (A206W and G207W) were introduced to increase the hydrophobicity of the binding pocket. Steady-state kinetic constants of C10-HSL and the shorter *N*-acyl compound C5-HSL reveals that hydrolysis of the longer chain compound C10-HSL displayed the highest k_{cat}/K_M values ($10^6 \text{ M}^{-1}\text{s}^{-1}$) for all mutants (Table 4.3). The k_{cat}/K_M values for C5-HSL were approximately 10-fold lower, with GBL by far acting as the poorest substrate with a k_{cat}/K_M value 5 orders of magnitude lower than those of substrates containing *N*-pentanoyl substitutions (Table 4.3).

enzyme	substrate	K_M (mM)	k_{cat} (s ⁻¹)	k_{cat}/K_M (M ⁻¹ s ⁻¹)	$\Delta\Delta G$ (kcal/mol)
wild type	GBL	303±40	5.9±0.5	20	0 ^a
A206W	GBL	200±15	3.4±0.1	17	0.1
G207W	GBL	115±15	3.3±0.1	30	-0.2
G207D	GBL	210±30	1.4±30	6	0.7
wild type	C5-HSL	0.8±0.1	490±30	6.1 x 10 ⁵	-6.1
A206W	C5-HSL	0.32±0.06	148±3	4.6 x 10 ⁵	-6.0
G207W	C5-HSL	0.7±0.1	263±7	3.8 x 10 ⁵	-5.8
G207D	C5-HSL	3.5±0.3	650±20	1.7 x 10 ⁵	-5.4
wild type	C10-HSL	0.15±0.02	650±20	4.3 x 10 ⁶	-7.3
A206W	C10-HSL	0.08±0.01	106±5	1.3 x 10 ⁶	-6.6
G207W	C10-HSL	0.015±0.002	123±4	8.2 x 10 ⁶	-7.7
G207D	C10-HSL	0.24±0.01	500±10	2.1 x 10 ⁶	-6.9
wild type ^b	BOC-HSL	3.8±0.3	185±4	4.9 x 10 ⁴	-4.6
wild type	CBZ-HSL	0.48±0.4	790±20	1.6 x 10 ⁶	-6.7

Table 4.3 Steady-state kinetic constants for substrate hydrolysis by dicobalt AHL lactonase variants. ^aThe differences in discrimination energy ($\Delta\Delta G$) were calculated using $\Delta\Delta G = RT\ln[(k_{cat}/K_M)_{WT:GBL} / (k_{cat}/K_M)_{enzyme:substrate}]$ (104).

^bValues obtained by P.W. Thomas of the Fast Lab.

The compounds BOC-HSL and CBZ-HSL, which are not known to be naturally produced by any organism, were processed efficiently with k_{cat}/K_M values comparable to those of naturally occurring AHLs. Despite their nonconservative nature, mutations in the *N*-acyl binding region (A206W, G207W, and G207D) exhibited only small changes in K_M values (< 2.6-fold) for hydrolysis of GBL, C5-HSL, or C10-HSL with the exception of two modest examples. The K_M value for C5- HSL hydrolysis by the charged mutant, G207D, was increased approximately 5-fold, and the K_M for C10-HSL hydrolysis by the hydrophobic mutant, G207W, was decreased approximately 10-fold, compared to that of the wild type. Changes in the resulting k_{cat}/K_M values for all mutants were <3.6-fold. Apparent substrate discrimination energies were calculated by comparing the k_{cat}/K_M values for each enzyme- substrate pair to the value for wild-type lactonase hydrolysis of GBL using the equation $\Delta\Delta G = RT\ln[(k_{cat}/K_M)_{WT:GBL} / (k_{cat} /K_M)_{enzyme:substrate}]$ (Table 4.3) (104).

Steady-state Hydrolysis Kinetics with Wild Type Dicobalt and Dizinc AHL Lactonases

Steady-state kinetic constants of acyl binding pocket mutants (Table 4.3) reveal that an *N*-acyl chain is required for effective hydrolysis of the lactone ring of the AHL substrate, as demonstrated by the k_{cat}/K_M value 5 orders of magnitude lower for GBL hydrolysis than for substrates containing *N*-pentanoyl substitutions. In order to further probe the nature of this requirement, steady-state kinetic parameters were determined for

substrates with a range of *N*-acyl substitutions from five to fourteen carbon atoms in length: *N*-pentanoyl-L-homoserine lactone (C5-HSL), *N*-octanoyl-L-homoserine lactone (C8-HSL), *N*-decanoyl-L-homoserine lactone (C10-HSL), *N*-dodecanoyl-L-homoserine lactone (C12-HSL) and *N*-tetradecanoyl-L-homoserine lactone (C14-HSL). Values of k_{cat}/K_M (Tables 4.4 and 4.5) indicate optimal chain lengths of 8 carbons for dizinc AHL lactonase and 10 carbons with dicobalt AHL lactonase. AHLs with chain lengths longer than 10 carbons were not hydrolyzed as efficiently as their shorter-chain counterparts. Due to insolubility of C12-HSL and C14-HSL, we were not able to reach enzyme saturation levels of substrate for some enzyme-substrate pairs. For this reason, only the limits for K_M and k_{cat} values for hydrolysis of C12-HSL by dicobalt AHL lactonase, and hydrolysis of C14-HSL by dicobalt and dizinc AHL lactonase are provided in Tables 4.4 and 4.5.

Substrate	K_M (mM)	k_{cat} (s ⁻¹)	k_{cat}/K_M (M ⁻¹ s ⁻¹)
C5-HSL	8.7±0.8	47±2	5.4 x 10 ³
C6-HSL	5.6±0.6	91±3	1.6 x 10 ⁴
C8-HSL	0.55±0.6	60±2	1.1 x 10 ⁵
C10-HSL	0.6±0.3	33±7	9.1 x 10 ⁴
C12-HSL	0.2±0.1	1.5±0.7	7500
C14-HSL	≥ 0.02	≤ 0.8	≤ 4 x 10 ⁴

Table 4.4 Steady state kinetic constants for AHL hydrolysis by dizinc AHL lactonase.

Substrate	K_M (mM)	k_{cat} (s ⁻¹)	k_{cat}/K_M (M ⁻¹ s ⁻¹)
C5-HSL	0.8±0.1	490±30	6.1 x 10 ⁵
C6-HSL	0.36±0.04	510±10	1.4 x 10 ⁶
C8-HSL	1.3±0.6	677±92	5.2 x 10 ⁵
C10-HSL	0.15±0.02	650±20	4.3 x 10 ⁶
C12-HSL	≥ 0.6	≤ 8	≤ 1.3 x 10 ⁴
C14-HSL	≥ 0.15	≤ 1	≤ 6.7 x 10 ³

Table 4.5 Steady state kinetic constants for AHL hydrolysis by dicobalt AHL lactonase.

Determination of IC_{50} Values for Substrate Analogs

Substrate analogs were prepared as potential inhibitors of AHL lactonase. The *trans*-ACP compound was designed with the thought that the hydroxyl of the cyclopentanoyl ring may displace the metal-bound hydroxide, and the hydroxyl of the *cis*-ACP ring may instead interact with Tyr194. Assuming competitive inhibition, IC_{50} values were obtained for *cis*- and *trans*-ACP (Figure 4.2 and 4.3) inhibition of dicobalt wild type and Y194F mutant AHL lactonases hydrolyzing C6-HSL.

In this assay, inhibitor concentration was varied while C6-HSL substrate concentration was held constant at 0.4 mM for wild type enzyme, 1.5 mM for Y194F mutant enzyme. These values were chosen to reflect the K_M values for the dicobalt enzymes [$K_M = 0.36 \pm 0.04$ mM for wild type lactonase (Table 4.6, $K_M = 2.0 \pm 0.4$ mM

for the Y194F mutant (Table 3.2)]. In Figure 4.6, percent activity for wild type and Y194F dicobalt AHL lactonases as measured in presence of *cis*- and *trans*-ACP inhibitors is plotted.

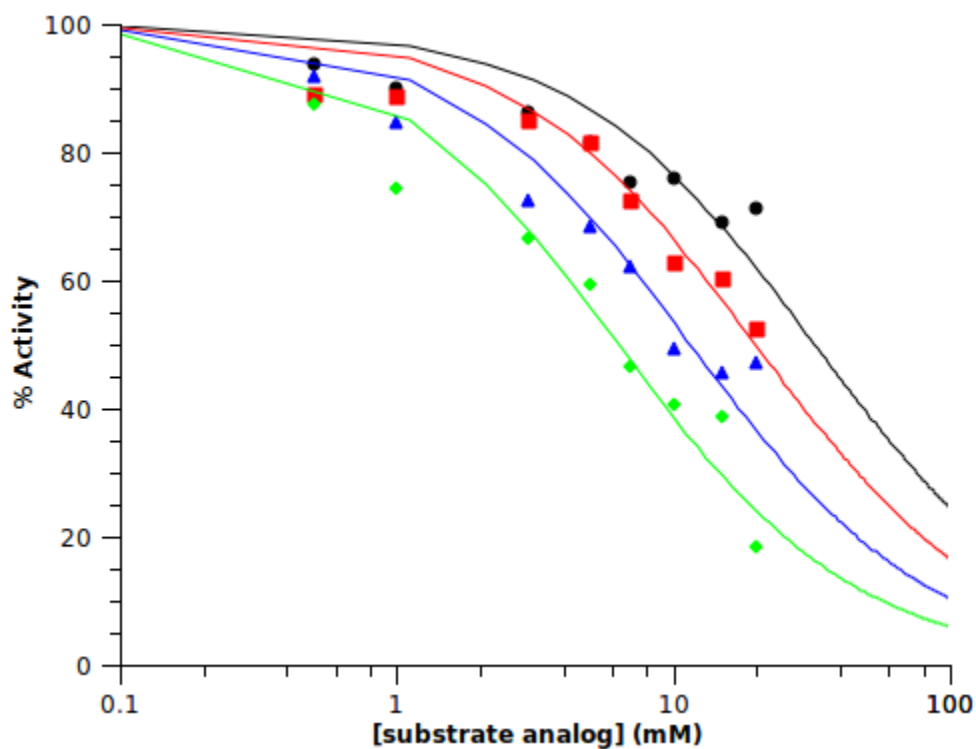


Figure 4.6 Inhibition by substrate analogs. IC_{50} values were determined for C6-HSL hydrolysis by wild-type dicobalt AHL lactonase in the presence of *cis*-ACP (blue) or *trans*-ACP (green) and Y194F dicobalt AHL lactonase with *cis*-ACP (red) and *trans*-ACP (black).

Percent activity was plotted against inhibitor concentration, and inhibition curves were fit using (1) with a hill coefficient (h) equal to one to determine the IC_{50} value for each analog, given in Table 4.6 (58).

$$\% \text{ Activity} = 100 - \{100/(1 + (IC_{50} \div [I]^h))\} \quad (1)$$

Enzyme	<i>trans</i> -ACP IC_{50} (mM)	<i>cis</i> -ACP IC_{50} (mM)
Wild type Co^{2+} AHL lactonase	8.1 ± 0.6	14 ± 1
Y194F mutant Co^{2+} AHL lactonase	≥ 25	≥ 24

Table 4.6 Inhibitor constants for hydrolysis of C6-HSL in the presence of *trans*- and *cis*-ACP.

At the concentrations tested, neither the *cis*- or *trans*-ACP substrate analog were able to inhibit the Y194F dicobalt AHL lactonase below 50% activity, allowing determination of only an estimated IC_{50} limit. For the wild-type dicobalt AHL lactonase, *trans*-ACP was an approximately 2-fold better inhibitor than the *cis*-ACP substrate analog.

Crystallization, Data Collection and Processing, Model Building and Refinement of Dicobalt Wild Type and Y194F Mutant AHL Lactonases With *cis*-ACP, *trans*-ACP and C10-HSL

The substrate analogs *cis*- and *trans*-ACP or the substrate C10-HSL were prepared and sent to our collaborators (D. Liu, C.F. Liu and D. Ringe) where these compounds were co-crystallized with wild-type or Y194F dicobalt AHL lactonases. AHL lactonase can be inhibited by the substrate analogs, and the complexes resulting from co-crystallization with them affords crystal structures with analog bound. A total of five crystal structures were obtained: dicobalt AHL lactonase with *trans*-ACP (1.55 angstroms), dicobalt AHL lactonase with *cis*-ACP (1.4 Å resolution), dicobalt Y194F AHL lactonase with *trans*-ACP (1.27 Å resolution), dicobalt Y194F AHL lactonase with *cis*-ACP (1.3 Å resolution) and dicobalt Y194F AHL lactonase with ring opened C10-HSL (1.5 Å resolution). All structures are of high resolution. The compounds did not behave as predicted, but the complexes still provide important information. Both of the structures containing *cis*-ACP contained electron density at the active site that was not well resolved, indicating that this analog likely binds to the active site in multiple conformations. Structures with *trans*-ACP show interesting differences between the wild type and Y194F mutant dicobalt lactonases. In the wild-type dicobalt structure, the hexanoyl tail of *trans*-ACP resides in the same hydrophobic patch where the product tail is observed to bind in C6-Hse and C6-Hcy product bound structures presented in Chapter 2 (Figure 4.7). In this structure, the hydroxyl group of *trans*-ACP forms a hydrogen bond

with the hydroxyl group of Tyr194 (Figure 4.8) rather than displacing the metal bound hydroxide as anticipated. In contrast, with the *trans*-ACP complex with the Y194F mutant, this bond is disrupted and the position of *trans*-ACP is shifted towards Co₂ by the remaining binding forces (Figure 4.8). Along with this shift, the acyl chain is observed to bind in an alternate, adjacent hydrophobic groove (Figure 4.7).

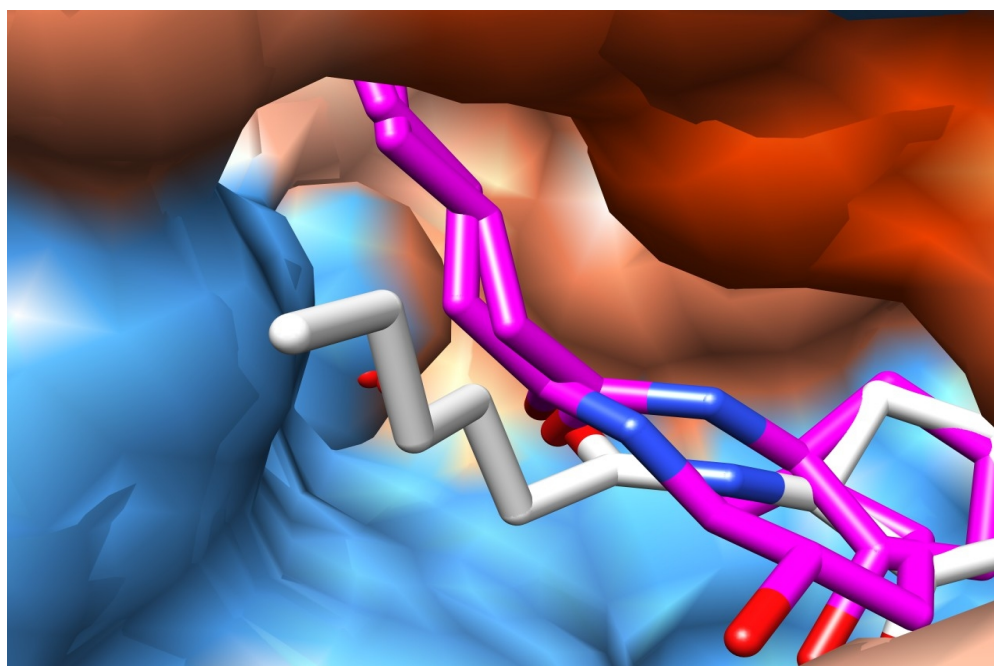


Figure 4.7 Overlay of the structures of *trans*-ACP bound to wild type dicobalt AHL lactonase (white ligand) and Y194F mutant AHL lactonase (pink ligands). The acyl chain is found to locate to an alternative pocket in the Y194F mutant enzyme. Figure prepared using UCSF Chimera (64).

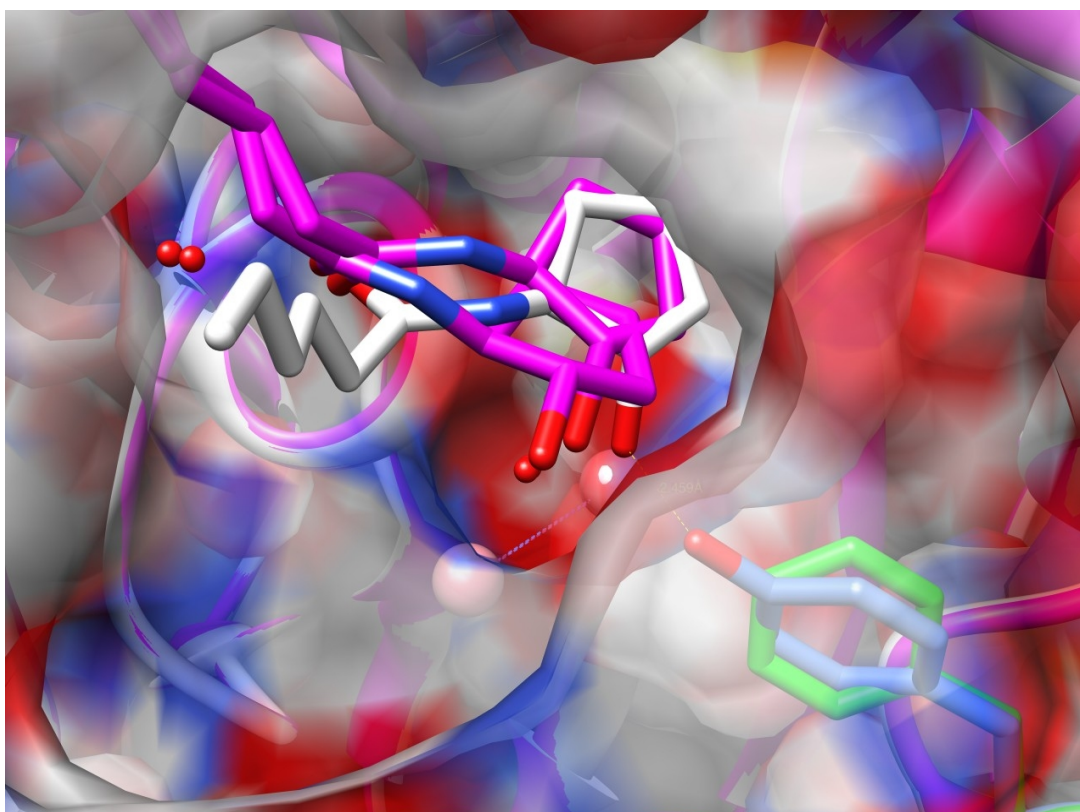


Figure 4.8 Overlay of the structures of *trans*-ACP bound to wild type dicobalt AHL lactonase (white ligand) and Y194F mutant AHL lactonase (pink ligands). The interaction between the hydroxyl of *trans*-ACP is not present in the structure with Y194F mutant enzyme, resulting in differences in binding, notably the localization of the hexanoyl chain to an adjacent hydrophobic groove. Tyr194 is colored cyan, and Phe194 is colored green. Figure prepared using UCSF Chimera (64).

Interestingly, the *N*-decanoyl tail of the ring-opened product of C10-HSL in complex with dicobalt AHL lactonase Y194F enzyme was also seen to locate to this alternative hydrophobic groove (Figure 4.9) which will be referred to as the “long acyl binding site”. While there is the possibility that this binding mode is an artifact of the

Y194F mutation, crystal structures of ring-opened C10-HSL with an F107W and Y194A mutant show that the decanoyl tail locates to the long acyl binding site in these mutants as well (D. Liu, C. F. Liu, and D. Ringe, personal communication).

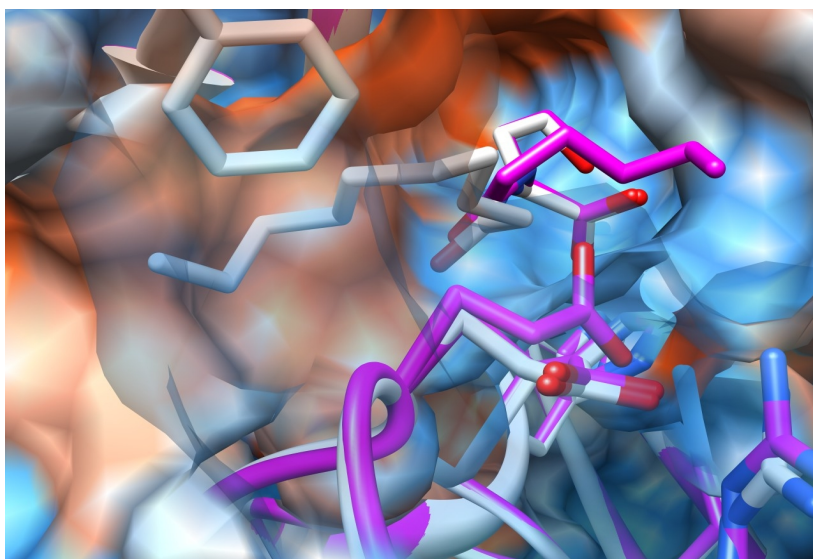


Figure 4.9 Overlay of wild type dicobalt AHL lactonase complexed with C6-Hse (pink ligand) and dicobalt Y194F AHL lactonase complexed with C10-Hse (white ligand). Figure prepared using UCSF Chimera (64).

DISCUSSION

Several observations suggest that the *N*-acyl chain binding pocket of the *B. thuringiensis* AHL lactonase is not fully optimized for AHL substrates. Typical AHL substrates have millimolar K_M values (Table 4.4). Specificity constants reveal that this enzyme does not show much selectivity between acyl chains of varying lengths (Table

4.4) or substitutions (Table 4.3). Molecular dynamics simulations show considerable motion and conformational flexibility for the *N*-hexanoyl tail of enzyme-bound C6-HSL (93). Despite this lack of selectivity, the acyl chain is required for efficient hydrolysis of AHL substrates. Comparison of the hydrolysis kinetics of the unsubstituted lactone γ -butyrolactone (GBL) with substrates incorporating longer acyl chains (Table 4.3) reveals that GBL behaves as a very poor substrate with high K_M values and is processed only very slowly. C5-HSL and C10-HSL were both much better substrates, exhibiting lower K_M values (800 μM for C5-HSL and 150 μM for C10-HSL) and higher k_{cat} values leading to an increase in k_{cat}/K_M values of 4 orders of magnitude. The physiological concentrations of AHLs used by Gram-negative bacteria during quorum-sensing are typically in the μM -nM range (16), so these enzymes would be expected to operate under second-order conditions. For this reason, it is useful to compare the apparent substrate discrimination energies ($\Delta\Delta G$) derived from k_{cat}/K_M values (Table 4.3).

In comparison to the unsubstituted lactone GBL, the addition of a five carbon amide substitution in C5-HSL results in a 6 kcal/mol improvement in substrate discrimination (Table 4.3). Addition of five more carbon units in the C10-HSL substrate only translates into an additional 1.2 kcal/mol of discrimination energy. This lengthening of the substrate's acyl chain improves substrate discrimination by only 0.24 kcal/mol per carbon increment. As a comparison, the transfer of *n*-alkyl alcohols from water into *n*-octanol is favorable by approximately 0.38 kcal/mol per carbon unit, and the binding of

hydrophobic groups to enzymes may be even more favorable due to displacement of waters from the binding site (105). This indicates that the acyl chain binding site of AHL lactonase is considerably less hydrophobic than *n*-octanol and does not appear to be fully optimized for acyl chain binding. This is consistent with the binding surface observed in C6-HSL product bound structures of dicobalt and dizinc AHL lactonases (Chapter 2), and with the movement seen in a QM/MM simulation of an enzyme-substrate complex with C6-HSL (93).

Using these structures as a guide, large nonconservative mutations were introduced to increase (A206W and G207W) and decrease (G207D) the hydrophobicity of the binding surface. The G207W mutant displayed a considerably lower K_M value for the longer C10-HSL substrate, which presumably could take advantage of the increased hydrophobicity of the binding cavity. Similarly, the more polar G207D mutant had an increased K_M for C5-HSL, a shorter substrate that presumably cannot compensate for this lost hydrophobic interaction. In general, however, mutations of the shallow binding surface resulted in only modest alterations in k_{cat}/K_M values, consistent with the multivalent interactions predicted to occur between the acyl chain of the substrate and the wide binding surface. The hydrophobic pocket occupied by the *N*-acyl moiety upon binding of AHL substrates may be dependent upon acyl tail length, however, as indicated by crystal structures with dicobalt Y194F mutant AHL lactonase and *trans*-ACP or ring opened C10-HSL (Figures 4.7 and 4.9). These structures reveal an alternative

hydrophobic binding groove for acyl chains, which may represent a long acyl chain binding site.

A similar hydrophobic groove for substrate binding is observed in a complex of the phosphotriesterase *SsoPox* from *Sulfolobus solfataricus* with a long acyl thiolactone substrate (106). Although this enzyme is not predicted to be related to *B. thuringiensis* AHL lactonase, it is notable that both contain dinuclear metal centers and an active site tyrosine that interacts with the carbonyl oxygen of the lactone or thiolactone ring (106). *SsoPox* displays lactonase and phosphotriesterase (PTE) activities, and it has been proposed that this enzyme has evolved from an enzyme whose primary function was as a lactonase (107). In light of the proposed evolutionary pathway for *SsoPox*, we can hypothesize that the duplicity of acyl binding sites seen in AHL lactonase may also be vestigial, related to a function performed by a distant relative. These two binding pockets may also be associated with a developing activity, or to binding an unknown non-AHL substrate.

While more investigation into the nature and location of acyl group binding to AHL lactonase is necessary, it is clear that this enzyme can efficiently hydrolyze both short and long chain AHL substrates, as indicated by k_{cat}/K_M values in Table 4.4. This promiscuity is further evidenced by the facile hydrolysis of artificial substrates possessing nonnatural *N*-acyl substitutions with similar hydrophobicity similar to AHLs but with very different steric constraints, BOC-HSL and CBZ-HSL (Table 4.3). Crystal

structures may provide an additional clue to the ability of AHL lactonase to accept a variety of substrates as the active site has been observed to tighten around the open homoserine moiety, but not the acyl chain, in the C6-Hse dizinc AHL lactonase product complex (48).

It should be noted that although the enzyme's binding site does not appear to be fully optimized for a particular substrate's acyl chain, the presence of this acyl substituent does appear to be required to prevent the nonproductive binding orientation observed with the inhibitor L-homoserine (37), which lacks this acyl substitution. The unsubstituted GBL substrate can presumably access both orientations and is subject to hydrolysis. On the basis of this broad specificity, it is possible that the AHL lactonase can also hydrolyze many non-natural *N*-substituted homoserine lactone quorum-sensing agonists and antagonists (108), and may also reflect a selective pressure to hydrolyze a diverse set of naturally occurring AHLs that exist in *B. thuringiensis* growth environments.

Chapter 5 AHL Lactonase Hydrolyzes a New Class of Quorum-Sensing Signals

INTRODUCTION

AHL lactonase from *B. thuringiensis* can efficiently hydrolyze the lactone ring of a wide array of AHLs as discussed in Chapter 4. Steady-state kinetics reveal that this enzyme will accept AHL substrates possessing acyl chains from 5 to 10 carbon atoms in length, although it appears not to be particularly well optimized for hydrolyzing substrates with *N*-alkyl chains. In addition to a range of naturally occurring AHLs, the lactonase can also hydrolyze the non-natural compounds *N*-(carboxybenzyloxy)-L-homoserine lactone and *N*-(*tert*-butyl)-L-homoserine lactone (Chapter 4). The recent discovery of a new class of homoserine lactone based quorum-sensing molecules (109) prompted investigation into the ability of AHL lactonase to degrade these compounds. This new class of signals is comprised of *N*-aryl homoserine lactones (ArHLs). The first ArHL discovered is the compound *N*-(*trans*-*p*-coumaroyl)-L-homoserine lactone, produced by *Rhodopseudomonas palustris* (pC-HSL, Figure 5.1) (109). A second ArHSL quorum sensing signal, *N*-(*trans*-cinnamoyl)-L-homoserine lactone (cinnamoyl-HSL, Figure 5.1) was found to be used for quorum sensing by an undisclosed *Rhodopseudomonas* species (Caroline Harwood, personal communication).

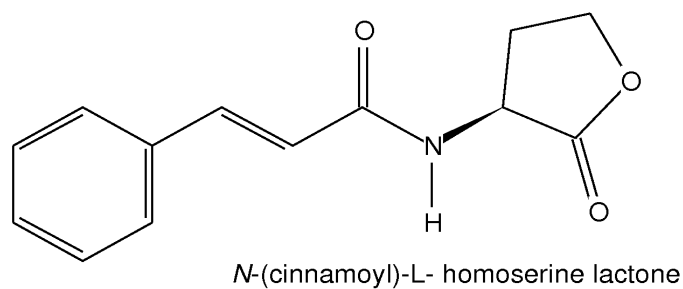
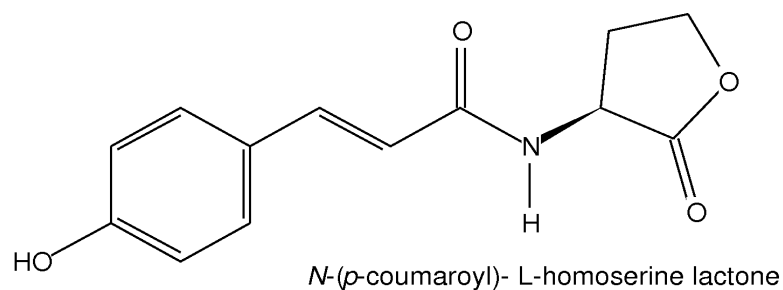


Figure 5.1 *N*-(*p*-coumaroyl)-L-homoserine lactone (pC-HSL) and *N*-(cinnamoyl)-L-homoserine lactone (cinnamoyl-HSL), novel ArHL signaling agents.

The two ArHSL signals thus far discovered, pC-HSL and cinnamoyl-HSL (Figure 5.1) are formed from homoserine lactone and the respective acids, *p*-coumaric acid or cinnamic acid. These acids are derived in part from a highly diverse set of aromatic plant degradation products (110). The utilization of plant degradation products for production of quorum sensing signals may illustrate one of the complex interactions that occur between the bacterial and plant kingdoms. Alternatively, the bacteria may simply be

making use of available chemicals for their own devices. Notably, the discovery of this new class of homoserine-based quorum sensing signals suggests the potential existence of a variety of previously undetected quorum sensing signal molecules consisting of various organic acids connected to homoserine lactone.

As a tool to investigate the ability of AHL lactonase to block signaling by ArHLs, we used *N*-(cinnamoyl) homoserine lactone in this study to discover that this enzyme does process these types of ArHLs both *in vitro* and *in vivo* by using steady-state kinetic assays and a previously established bioassay (109).

METHODS

Synthesis of *N*-(Cinnamoyl)-L-Homoserine Lactone (cinnamoyl-HSL)

All synthetic reagents were purchased from Sigma-Aldrich Chemical Co. (St. Louis, MO) with the exception of *trans*-cinnamoyl chloride which was purchased from Acros Organics (Geel, Belgium). In a procedure similar to those previously described (44, 45), (*S*)- α -amino- γ -butyrolactone hydrobromide (7.4 mmole) was dissolved in dimethylformamide (25 mL) to which triethylamine (10 mmole) was added. This mixture was stirred for 30 minutes at 0 °C, at which time *trans*-cinnamoyl chloride (8.3 mmole) was added. The reaction was allowed to come to room temperature and stirred for an additional four hours. Solvent was removed by reduced pressure rotary evaporation with heating ≤ 55 °C, and the resulting residue was dissolved in methylene

chloride (50 mL). This mixture was extracted sequentially with sodium sulfate (0.5 M, 100 mL), saturated sodium bicarbonate (100 mL) and saturated sodium chloride (100 mL). The organic layer was dried with anhydrous magnesium sulfate, filtered and solvent was then removed by reduced pressure rotary evaporation at ambient temperature. The final compound was afforded by recrystallization from a solution of ethyl acetate and hexanes (50:50 v/v). Calculated yield: 55%. $R_f = 0.75$ in ethyl acetate; $T_m = 143-145$ °C (uncorrected). ^1H NMR (600 MHz, CDCl_3) δ 2.17-2.24 (m, 1H), 2.89-2.94 (m, 1H), 4.29-4.33 (m, 1H), 4.47-4.51 (t, 1H), 4.66-4.70 (m, 1H), 6.29 (broad, N-H), 6.42-6.44 (d, 1H, $J = 15.8$ Hz), 7.35 (m, 3H), 7.47 (m, 2H), 7.62-7.65 (d, 1H, $J = 15.6$ Hz). Vinyl proton coupling ($J = 15.7 \pm 0.1$ Hz) indicates retention of *trans* configuration (*cis* $J = 7-12$ Hz, *trans* $J = 13-18$ Hz); ^{13}C NMR (75 MHz, CDCl_3) δ 30.53, 49.47, 66.26, 119.15, 127.94, 128.84, 130.03, 134.36, 142.46, 166.35; EI-HRMS $\text{MH}^+_{\text{calc}} = 232.0974$, $\text{MH}^+_{\text{obs}} = 232.0976$. $[\alpha]^{20}_{\text{D, methanol}} = -22.9^\circ$.

Expression and Purification of Metal-Substituted AHL Lactonases

Wild type and D108N mutant AHL lactonase from *B. thuringiensis* (AiiA) was expressed in *E. coli* harboring the pMAL-t-aiiA plasmid or the pMal-D108N plasmid using containing CoCl_2 supplemented M9 minimal media as previously described (Chapter 3). All proteins were used without removal of the maltose binding protein fusion, as it has been shown that this fusion does not affect catalysis (35). Metal analysis

was determined by ICP-MS (School of Geological Sciences, The University of Texas at Austin).

Kinetic Assay of Cinnamoyl-HSL Hydrolysis

Kinetic analysis was performed as previously described (Chapter 3) using phenol red (35).

Mass Spectral Analysis of Products Formed in the AHL Lactonase Reaction

Cinnamoyl-HSL (500 μM) was incubated overnight at 25 °C with CoCl_2 supplemented AHL lactonase (150 nM) in Tris buffer (20 mM, pH 7.6). A control sample was prepared by omitting the enzyme from the incubation mixture. Reactions were desalted on a protein microtrap (Protein MicroTrap: Michrom, Auburn, CA) and analyzed by electrospray ionization mass spectrometry (ESI-MS) on a ThermoFinnigan LCQ ion trap spectrometer (Analytical Instrumentation Facility Core, College of Pharmacy, The University of Texas at Austin).

Bioassay for Quorum Quenching Using the *R. palustris* Quorum Sensing System

LB agar was supplemented with gentamicin (50 $\mu\text{g}/\text{mL}$), cinnamoyl-HSL (400 μM), X-gal (200 $\mu\text{g}/\text{mL}$), and a 100-fold dilution of an overnight culture of *P. aeruginosa* MW1 containing the plasmid pRpaR-pRpaI::lacZ (109), which encodes the quorum-sensing system of *Rhodopseudomonas palustris*, a pC-HSL receptor (RpaR) and synthase (RpaI). Wells (5 mm) were bored into the agar 2.5 cm apart, and 20 μL of sample was

added to each well and overlaid with 5 μ L of mineral oil to prevent evaporation. Samples loaded into the wells were as follows: buffer (20 mM Tris, 5 mM NaCl, pH 7.4), dicobalt AHL lactonase (1 μ M), dicobalt D108N AHL lactonase (1 μ M), CoCl₂ (2 μ M) or ZnSO₄ (2 μ M). Plates were incubated overnight at 30 °C and photographed the next day.

RESULTS

Protein Purification and Characterization

Wild-type and D108N AHL lactonase were expressed and purified as maltose binding protein fusion proteins and subsequently characterized for purity and metal content. When protein expression was completed from minimal medium supplemented with ZnSO₄, wild-type AHL lactonase was purified with 1.8 equiv of zinc, 0.1 equiv of cobalt and negligible amounts of other bound divalent metal ions. When expression cultures were supplemented with CoCl₂, the wild-type protein contained 2.0 equiv of cobalt, 0.1 equiv of iron and negligible amounts of other divalent metal ions. The D108N variant of AHL lactonase was cloned without a tobacco etch virus protease cleavage site, and it was expressed, purified, and characterized with its *N*-terminal MBP fusion tag intact. Previous experiments have shown that the rates of hydrolysis exhibited by the fusion protein do not significantly differ from those of the untagged version (35). When expressed in medium supplemented with CoCl₂, the D108N MBP-AHL lactonase complex was found to contain 1.3 equiv of cobalt and 0.1 equiv of zinc.

Kinetic Analysis of Cinnamoyl-HSL Hydrolysis

Steady-state kinetic parameters were determined for the hydrolysis of cinnamoyl-HSL by dizinc- and dicobalt- AHL lactonases (Tables 5.1 and 5.2, respectively). Examination of k_{cat}/K_M values reveals that cinnamoyl-HSL is the best substrate discovered for dicobalt AHL lactonase to date, and is on par with the best substrate known for dizinc AHL lactonase.

Substrate	K_M (mM)	k_{cat} (s^{-1})	k_{cat}/K_M ($M^{-1}s^{-1}$)	$\Delta\Delta G^b$ (kcal/mol)	logP (calculated ^c)
C6-HSL	5.6 \pm 0.6	91 \pm 3	1.6 x 10 ⁴	0	0.700
C10-HSL	0.6 \pm 0.3	33 \pm 7	9.1 x 10 ⁴	-0.91	2.721
cinnamoyl-HSL	0.36 \pm 0.08	23 \pm 3	6.4 x 10 ⁴	-0.72	0.603
CBZ-HSL	0.7 \pm 0.3	7 \pm 2	9.4 x 10 ³	0.28	2.174

Table 5.1 Kinetic parameters and substrate discrimination energies for hydrolysis of indicated substrates by dizinc AHL lactonase. ^aValues for C6-HSL, C10-HSL and CBZ-HSL hydrolysis (Chapters 2 and 4) are included for comparison. ^bApparent substrate discrimination values ($\Delta\Delta G$) were calculated using $\Delta\Delta G = RT\ln[(k_{cat}/K_M)_{WT:C6-HSL} / (k_{cat}/K_M)_{enzyme:substrate}]$ (104). ^cLogP values were calculated using the Mitools toolkit (www.molinspiration.com).

Substrate	K_M (mM)	k_{cat} (s^{-1})	k_{cat}/K_M ($M^{-1}s^{-1}$)	$\Delta\Delta G^b$ (kcal/mol)	logP (calculated ^c)
C6-HSL	0.36 \pm 0.04	510 \pm 10	1.4 x 10 ⁶	0	0.700
C10-HSL	0.15 \pm 0.02	650 \pm 20	4.3 x 10 ⁶	-0.59	2.721
cinnamoyl-HSL	0.26 \pm 0.02	2330 \pm 80	9.0 x 10 ⁶	-0.97	0.603
CBZ-HSL	0.48 \pm 0.04	790 \pm 20	1.7 x 10 ⁶	-0.10	2.174

Table 5.2 Kinetic parameters and substrate discrimination energies for hydrolysis of indicated substrates by dicobalt AHL lactonase. ^aValues for C6-HSL, C10-HSL and CBZ-HSL hydrolysis (Chapters 2 and 4) are included for comparison. ^bApparent substrate discrimination values ($\Delta\Delta G$) were calculated using $\Delta\Delta G = RT\ln[(k_{cat}/K_M)_{WT:C6-HSL} / (k_{cat}/K_M)_{enzyme:substrate}]$ (104). ^cLogP values were calculated using the Mitools toolkit (www.molinspiration.com).

Examination of the kinetic constants given in Tables 5.1 and 5.2 reveal that exchange of zinc with cobalt in the metal center results in more efficient hydrolysis of AHL (C6-HSL and C10-HSL) and ArHL (cinnamoyl-HSL and CBZ-HSL) substrates, with an approximately 100-fold increase in k_{cat}/K_M values upon substitution of zinc with cobalt. Interestingly, exchanging zinc for cobalt increases k_{cat} around 20-fold for AHL substrates, while ArHL substrates experience an approximately 100-fold increase in k_{cat} . Apparent substrate discrimination energies were calculated by comparing the k_{cat}/K_M values for each enzyme- substrate pair to the value for wild-type lactonase hydrolysis of C6-HSL (Tables 5.1 and 5.2).

Mass Spectral Analysis of Products Formed in the AHL Lactonase Reaction

A control incubation mixture containing cinnamoyl-HSL but omitting enzyme showed an $MH^+_{\text{obs}} = 232.2 \pm 0.3$ peak by ESI-MS, corresponding to the $MH^+_{\text{calc}} = 232.09$ for substrate. Incubation mixtures including dicobalt AHL lactonase showed a new peak at $MH^+_{\text{obs}} = 250.1 \pm 0.3$, corresponding to $MH^+_{\text{calc}} = 250.11$ for the ring opened product, *N*-cinnamoyl-L-homoserine. This result indicates that the expected open-ring product was produced, and that AHL lactonase from *B. thuringiensis* will accept and hydrolyze the lactone ring of this newly identified quorum sensing signal.

Bioassay for Quorum Quenching of the *R. palustris* Quorum Sensing System

Qualitative investigation of the ability of AHL lactonase to quench quorum sensing mediated by cinnamoyl-HSL, a bioassay reported by Schaefer et al (109) was modified for use in an agar-plate format. The reporter strain *Pseudomonas aeruginosa* harbors a plasmid encoding the pC-HSL dependent RpaR transcription factor and a *lacZ* gene under control of the *rpaI* promoter. In the presence of pC-HSL, β -galactosidase is produced due to interaction between pC-HSL and the pC-HSL receptor, RpaR. This complex can then bind to the *rpaI* promoter, which controls production of LacZ in this construct. Thus, a blue color in the presence of X-gal indicates that the RpaR-RpaI quorum sensing system is active. In this assay, wells are created in agar containing cinnamoyl-HSL, indicator strain and X-gal, and the wells are filled with solutions

containing AHL lactonase or control solutions in order to assess the quorum quenching activity of AHL lactonase. The results of the *R. palustris* quorum-quenching bioassay are presented in Figure 5.2.

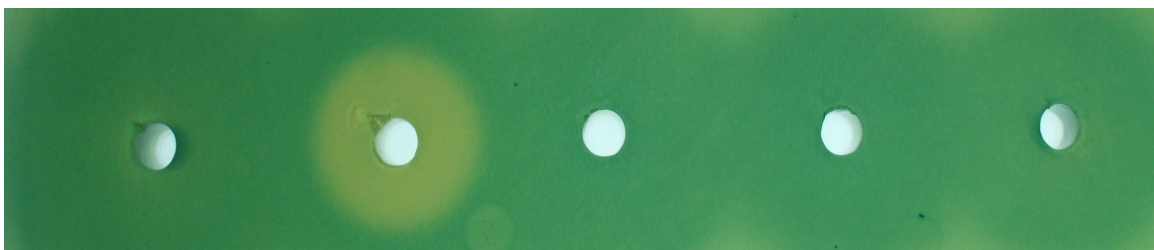


Figure 5.2 Assay for cinnamoyl-HSL hydrolysis using the *P. aeruginosa* pRpaR-pRpaI::lacZ reporter strain. Well contents left to right: buffer, dicobalt AHL lactonase (1 μ M), dicobalt D108N AHL lactonase (1 μ M), CoCl₂ (2 μ M) and ZnSO₄ (2 μ M). A blue color indicates the quorum sensing circuit is active, absence of blue is indicative of quorum quenching.

While cinnamoyl-HSL lacks the *para*-hydroxyl group that pC-HSL contains (Figure 5.1), it is able to bind RpaR and induce quorum sensing, as indicated by the blue color seen in the bioassay agar (Figure 5.2). The halo seen around the well containing wild type dicobalt AHL lactonase indicates that quorum-quenching occurs upon exogenous application of a solution of this enzyme in this bioassay format. Control wells containing buffer, cobalt (II) ions, zinc (II) ions, or a dicobalt AHL lactonase mutant with very low activity (D108N) do not display any quorum-quenching activity. The activity of the D108N mutant ($k_{cat}/K_M = 3.9 \times 10^4 \text{ M}^{-1}\text{s}^{-1}$, Table 3.2) is 145-fold less

than that of the wild-type enzyme ($k_{cat}/K_M = 1.4 \times 10^6 \text{ M}^{-1}\text{s}^{-1}$, Table 3.2), indicating that this low activity is not detected by the bioassay used in this experiment.

DISCUSSION

Previous steady-state kinetic analysis of AHL lactonase show that this enzyme will efficiently hydrolyze AHL substrates possessing *N*-acyl tails from 5 to 10 carbon atoms in length as well as the homoserine lactone-containing compounds CBZ-HSL and BOC-HSL (Chapter 4). Steady-state kinetic studies show that cinnamoyl-HSL is one of the best substrates of dicobalt AHL lactonase thus far characterized, with steady-state kinetic parameters for hydrolysis of this compound similar to those of C10-HSL (Table 5.2). There are interesting differences observed with steady-state hydrolysis kinetics of AHL and ArHL substrates by dizinc- and dicobalt AHL lactonases (Tables 5.1 and 5.2). While k_{cat}/K_M values are approximately $10^4 \text{ M}^{-1}\text{s}^{-1}$ for dizinc AHL lactonase and $10^6 \text{ M}^{-1}\text{s}^{-1}$ for dicobalt AHL lactonase for all substrates included in Tables 5.1 and 5.2, there are striking differences in k_{cat} values for the dizinc and dicobalt variants. While k_{cat} values are observed to decrease with hydrolysis of cinnamoyl-HSL and CBZ-HSL by the dizinc enzyme, k_{cat} values for the dicobalt enzyme increase dramatically with these ArHL substrates. This hyperactivity may simply be an artifact of substitution with an alternative metal, or it may indicate a metal ion/substrate pair that is preferred by AHL lactonase.

Other examples of activity enhancement upon substitution of zinc with cobalt have been observed in dihydroorotase (111), a related M β L (41), and other enzymes. Changes in metal ion ligation upon substitution of zinc with cobalt has been attributed to increases in specific activity for an alcohol dehydrogenase (112). Although EXAFS studies (35, 47) and crystal structures show identical metal environments for unliganded AHL lactonases, these different metalloforms of AHL lactonase may experience differences in second-shell metal ligand orientation that allow for increased k_{cat} values for hydrolysis of ArHLs compared to AHLs for dicobalt AHL lactonase. Although other explanations can be offered, changes in second-shell ligand orientation may allow the aryl ring of ArHLs to bind in a way that allows for more rapid hydrolysis of these substrates, however crystal structures are not available for ArHLs in complex with AHL lactonase preventing inspection of enzyme structure while interacting with these substrates.

Comparison of substrate discrimination energies for hydrolysis of C10-HSL and cinnamoyl-HSL relative to C6-HSL for dizinc and dicobalt AHL lactonases reveals that dizinc AHL lactonase favors C10-HSL by 0.2 kcal/mol compared to cinnamoyl-HSL (Table 5.1). In contrast, the dicobalt enzyme prefers cinnamoyl-HSL by approximately 0.4 kcal/mol compared to C10-HSL (Table 5.2).

The specificity constant (k_{cat}/K_M) for cinnamoyl-HSL hydrolysis by dicobalt AHL lactonase is the largest value measured for any *N*-substituted homoserine lactone

hydrolysis (Table 5.2). As noted in Chapter 4, a trend of k_{cat}/K_M values increasing from C5-HSL to C10-HSL with substrate hydrophobicity has been observed, however cinnamoyl-HSL hydrolysis does not follow this trend. Calculated logP (octanol/water partition coefficient) values show that cinnamoyl-HSL is less hydrophobic than the poorer substrate C6-HSL (Table 5.2). This may indicate that there is a specific compatibility between the binding pocket and cinnamoyl-HSL, and that the faster k_{cat} is not merely due to a better hydrophobic interaction. In support of this proposal, a structural overlay of ring-opened cinnamoyl-HSL with dizinc AHL lactonase bound with C6-Hse indicates that the cinnamoyl moiety is well accommodated at the shorter acyl tail binding site (Figure 5.3). Of course, the *N*-aryl groups of ArHLs may bind at the longer acyl tail binding site like C10-HSL (Chapter 4), more investigation is required to determine the exact mode of binding.

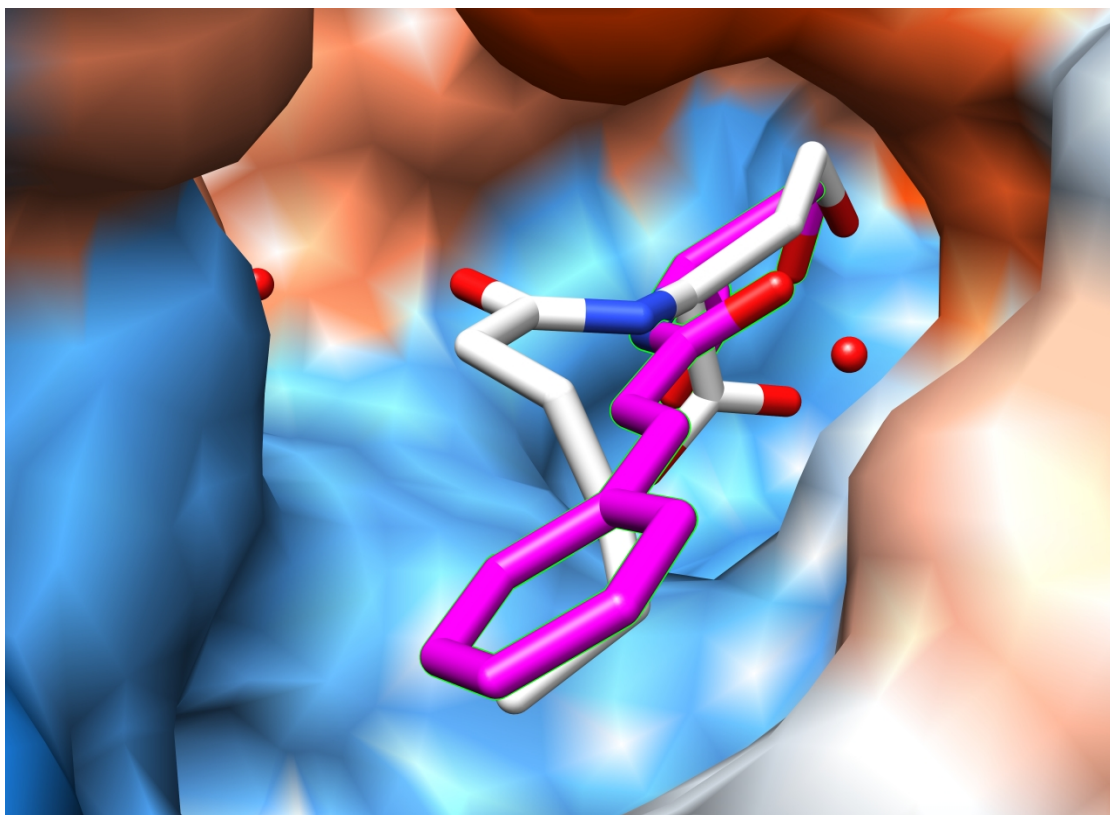


Figure 5.3 Structural overlay of ring-opened cinnamoyl-HSL (pink) with ring-opened C6-HSL (white) in complex with dizinc AHL lactonase. Figure was prepared manually using UCSF Chimera and the Protein DataBank coordinates 3DHB (48).

Another factor that may contribute to more rapid hydrolysis of ArHLs compared to AHLs is the compact shape of the *N*-aryl group. Acyl chain substrates are long and mobile, and are expected to have greater variation in binding mode. The fatty acyl chain of AHLs may require reorientation in order correctly locate the lactone ring for optimal hydrolysis, slowing catalysis relative to ArHL hydrolysis. AHL lactonase may

make favorable binding interactions with ArHL substrates via van der Waals interactions, pi-stacking, or hydrogen bonding with groups such as the *p*-hydroxyl moiety on pC-HSL (Figure 5.1). Prediction of the binding mode is further complicated by the multiplicity of binding sites for AHL acyl chains, necessitating additional investigations in order to determine the nature of ArHL binding.

Our studies have confirmed that *B. thuringiensis* AHL lactonase is able to hydrolyze a broad range of *N*-substituted homoserine lactone substrates. While the native substrates of this enzyme are not well defined, it is possible that the physiological function of this enzyme is to provide *B. thuringiensis* with a competitive advantage against other microorganisms in its natural environment by preventing competing organisms from coordinating gene expression. The role of ArHL mediated quorum sensing by *R. palustris* is not known, but it may modulate activities that pose a threat to nearby organisms. *B. thuringiensis*, *R. palustris* and *P. aeruginosa* are found in similar environments, residing in soil and on the surface of plants (113, 114). Application of exogenous AHL lactonase can quench quorum sensing *in vivo* for the *R. palustris* system, as described in this chapter, and also when heterologously expressed in organisms such as *P. aeruginosa* where it inhibits biofilm formation and virulence factor production (115, 116). While *R. palustris* is not specifically known to form biofilms, *Rhodopseudomonas* species have been identified in wound biofilms (117) and in biofouling in industrial wastewater treatment plants (118). There is evidence that

Bradyrhizobium sp. BTAi1 and *Silicibacter pomeroyi* DSS-3 have the ability to synthesize pC-HSL (109). *Bradyrhizobium* species have been detected in biofilms taken from PCB contaminated soil (119), and *Silicibacter pomeroyi* has been found associated with biofilms in a water pipeline (120). The presence of organisms that can produce ArHLs in biofilms suggests that this newly discovered class of homoserine lactone quorum sensing signals may be an attractive target for degradation. Our discovery of the broad specificity of AHL lactonase provides a useful tool for investigating both AHL and non-AHL quorum-sensing pathways. This enzyme may also find applications in medical and industrial settings where homoserine lactone based quorum-sensing is used to control virulence and biofilm formation.

References

1. Eberhard, A. (1972) Inhibition and activation of bacterial luciferase synthesis, *J. Bacteriol* 109, 1101-1105.
2. Nealson, K. H., Platt, T., and Hastings, J. W. (1970) Cellular control of the synthesis and activity of the bacterial luminescent system, *J. Bacteriol* 104, 313-322.
3. Visick, K. L., Foster, J., Doino, J., McFall-Ngai, M., and Ruby, E. G. (2000) *Vibrio fischeri* lux genes play an important role in colonization and development of the host light organ, *J. Bacteriol* 182, 4578-4586.
4. Eberhard, A., Burlingame, A. L., Eberhard, C., Kenyon, G. L., Nealson, K. H., and Oppenheimer, N. J. (1981) Structural identification of autoinducer of *Photobacterium fischeri* luciferase, *Biochemistry* 20, 2444-2449.
5. Kaplan, H. B., and Greenberg, E. P. (1985) Diffusion of autoinducer is involved in regulation of the *Vibrio fischeri* luminescence system, *J. Bacteriol* 163, 1210-1214.
6. Engebrecht, J., and Silverman, M. (1984) Identification of genes and gene products necessary for bacterial bioluminescence, *Proc. Natl. Acad. Sci. U.S.A* 81, 4154-4158.
7. Engebrecht, J., Nealson, K., and Silverman, M. (1983) Bacterial bioluminescence: isolation and genetic analysis of functions from *Vibrio fischeri*, *Cell* 32, 773-781.

8. Qin, Y., Luo, Z., Smyth, A. J., Gao, P., von Bodman, S. B., and Farrand, S. K. (2000) Quorum-sensing signal binding results in dimerization of TraR and its release from membranes into the cytoplasm, *EMBO J* 19, 5212-5221.
9. Stevens, A. M., Dolan, K. M., and Greenberg, E. P. (1994) Synergistic binding of the *Vibrio fischeri* LuxR transcriptional activator domain and RNA polymerase to the lux promoter region, *Proc. Natl. Acad. Sci. U.S.A* 91, 12619-12623.
10. Fuqua, C., Parsek, M. R., and Greenberg, E. P. (2001) Regulation of gene expression by cell-to-cell communication: acyl-homoserine lactone quorum sensing, *Annu. Rev. Genet* 35, 439-468.
11. Waters, C. M., and Bassler, B. L. (2005) Quorum sensing: cell-to-cell communication in bacteria, *Annu. Rev. Cell Dev. Biol* 21, 319-346.
12. Bjarnsholt, T., and Givskov, M. (2007) The role of quorum sensing in the pathogenicity of the cunning aggressor *Pseudomonas aeruginosa*, *Anal Bioanal Chem* 387, 409-414.
13. Van Houdt, R., Givskov, M., and Michiels, C. W. (2007) Quorum sensing in *Serratia*, *FEMS Microbiol. Rev* 31, 407-424.
14. Dong, Y. H., Xu, J. L., Li, X. Z., and Zhang, L. H. (2000) AiiA, an enzyme that inactivates the acylhomoserine lactone quorum-sensing signal and attenuates the virulence of *Erwinia carotovora*, *Proc. Natl. Acad. Sci. U.S.A* 97, 3526-3531.

15. Leadbetter, J. R., and Greenberg, E. P. (2000) Metabolism of acyl-homoserine lactone quorum-sensing signals by *Variovorax paradoxus*, *J. Bacteriol* 182, 6921-6926.
16. Wang, Y., Huang, J. J., and Leadbetter, J. R. (2007) Acyl-HSL signal decay: intrinsic to bacterial cell-cell communications, *Adv. Appl. Microbiol* 61, 27-58.
17. Zhang, H., Wang, L., and Zhang, L. (2002) Genetic control of quorum-sensing signal turnover in *Agrobacterium tumefaciens*, *Proc. Natl. Acad. Sci. U.S.A* 99, 4638-4643.
18. Kaufmann, G. F., Sartorio, R., Lee, S., Rogers, C. J., Meijler, M. M., Moss, J. A., Clapham, B., Brogan, A. P., Dickerson, T. J., and Janda, K. D. (2005) Revisiting quorum sensing: Discovery of additional chemical and biological functions for 3-oxo-*N*-acylhomoserine lactones, *Proc. Natl. Acad. Sci. U.S.A* 102, 309-314.
19. Schmidt, S., Blom, J. F., Pernthaler, J., Berg, G., Baldwin, A., Mahenthalingam, E., and Eberl, L. (2009) Production of the antifungal compound pyrrolnitrin is quorum sensing-regulated in members of the *Burkholderia cepacia* complex, *Environ. Microbiol* 11, 1422-1437.
20. Lowery, C. A., Dickerson, T. J., and Janda, K. D. (2008) Interspecies and interkingdom communication mediated by bacterial quorum sensing, *Chem. Soc. Rev.* 37, 1337.

21. Loh, J., Pierson, E. A., Pierson, L. S., Stacey, G., and Chatterjee, A. (2002) Quorum sensing in plant-associated bacteria, *Curr. Opin. Plant Biol* 5, 285-290.
22. Park, S., Park, S., Ryu, C., Park, S., and Lee, J. (2008) The role of AiiA, a quorum-quenching enzyme from *Bacillus thuringiensis*, on the rhizosphere competence, *J. Microbiol. Biotechnol* 18, 1518-1521.
23. Uroz, S., D'Angelo-Picard, C., Carlier, A., Elasri, M., Sicot, C., Petit, A., Oger, P., Faure, D., and Dessaux, Y. (2003) Novel bacteria degrading *N*-acylhomoserine lactones and their use as quenchers of quorum-sensing-regulated functions of plant-pathogenic bacteria, *Microbiology (Reading, Engl.)* 149, 1981-1989.
24. Park, S., Lee, S. J., Oh, T., Oh, J., Koo, B., Yum, D., and Lee, J. (2003) AhlD, an *N*-acylhomoserine lactonase in *Arthrobacter* sp., and predicted homologues in other bacteria, *Microbiology (Reading, Engl.)* 149, 1541-1550.
25. Park, S., Kang, H., Jang, H., Lee, J., Koo, B., and Yum, D. (2005) Identification of extracellular *N*-acylhomoserine lactone acylase from a *Streptomyces* sp. and its application to quorum quenching, *Appl. Environ. Microbiol* 71, 2632-2641.
26. Reimmann, C., Ginet, N., Michel, L., Keel, C., Michaux, P., Krishnapillai, V., Zala, M., Heurlier, K., Triandafillu, K., Harms, H., Défago, G., and Haas, D. (2002) Genetically programmed autoinducer destruction reduces virulence gene expression and swarming motility in *Pseudomonas aeruginosa* PAO1, *Microbiology (Reading, Engl.)* 148, 923-932.

27. Aravind, L. (1999) An evolutionary classification of the metallo-beta-lactamase fold proteins, *In Silico Biol. (Gedruckt) 1*, 69-91.
28. Daiyasu, H., Osaka, K., Ishino, Y., and Toh, H. (2001) Expansion of the zinc metallo-hydrolase family of the beta-lactamase fold, *FEBS Lett 503*, 1-6.
29. Costello, A. L., Sharma, N. P., Yang, K., Crowder, M. W., and Tierney, D. L. (2006) X-ray absorption spectroscopy of the zinc-binding sites in the class B2 metallo-beta-lactamase ImiS from *Aeromonas veronii* bv. *sobria*, *Biochemistry 45*, 13650-13658.
30. Crowder, M. W., Spencer, J., and Vila, A. J. (2006) Metallo- β -lactamases: Novel Weaponry for Antibiotic Resistance in Bacteria, *Accounts of Chemical Research 39*, 721-728.
31. Schilling, O., Wenzel, N., Naylor, M., Vogel, A., Crowder, M., Makaroff, C., and Meyer-Klaucke, W. (2003) Flexible metal binding of the metallo-beta-lactamase domain: glyoxalase II incorporates iron, manganese, and zinc in vivo, *Biochemistry 42*, 11777-11786.
32. Zang, T. M., Hollman, D. A., Crawford, P. A., Crowder, M. W., and Makaroff, C. A. (2001) *Arabidopsis* glyoxalase II contains a zinc/iron binuclear metal center that is essential for substrate binding and catalysis, *J. Biol. Chem 276*, 4788-4795.

33. Bebrone, C. (2007) Metallo-beta-lactamases (classification, activity, genetic organization, structure, zinc coordination) and their superfamily, *Biochemical Pharmacology* 74, 1686-1701.
34. Wang, L., Weng, L., Dong, Y., and Zhang, L. (2004) Specificity and Enzyme Kinetics of the Quorum-quenching *N*-Acyl Homoserine Lactone Lactonase (AHL-lactonase), *J. Biol. Chem.* 279, 13645-13651.
35. Thomas, P. W., Stone, E. M., Costello, A. L., Tierney, D. L., and Fast, W. (2005) The quorum-quenching lactonase from *Bacillus thuringiensis* is a metalloprotein, *Biochemistry* 44, 7559-69.
36. Liu, D., Lepore, B. W., Petsko, G. A., Thomas, P. W., Stone, E. M., Fast, W., and Ringe, D. (2005) Three-dimensional structure of the quorum-quenching *N*-acyl homoserine lactone hydrolase from *Bacillus thuringiensis*, *Proc Natl Acad Sci U S A* 102, 11882-7.
37. Kim, M. H., Choi, W., Kang, H. O., Lee, J. S., Kang, B. S., Kim, K., Derewenda, Z. S., Oh, T., Lee, C. H., and Lee, J. (2005) The molecular structure and catalytic mechanism of a quorum-quenching *N*-acyl-L-homoserine lactone hydrolase, *Proc. Natl. Acad. Sci. U.S.A* 102, 17606-17611.
38. Liu, D., Thomas, P. W., Momb, J., Hoang, Q. Q., Petsko, G. A., Ringe, D., and Fast, W. (2007) Structure and specificity of a quorum-quenching lactonase (AiiB) from *Agrobacterium tumefaciens*, *Biochemistry* 46, 11789-99.

39. Page, M. I., and Badarau, A. (2008) The Mechanisms of Catalysis by Metallo beta-Lactamases, *Bioinorg Chem Appl* 576297.
40. Garrity, J. D., Bennett, B., and Crowder, M. W. (2005) Direct evidence that the reaction intermediate of metallo-beta-lactamase L1 is metal bound, *Biochemistry* 44, 1078-1087.
41. Badarau, A., and Page, M. I. (2006) The variation of catalytic efficiency of *Bacillus cereus* metallo-beta-lactamase with different active site metal ions, *Biochemistry* 45, 10654-10666.
42. Kristelly, R., Earnest, B. T., Krishnamoorthy, L., and Tesmer, J. J. G. (2003) Preliminary structure analysis of the DH/PH domains of leukemia-associated RhoGEF, *Acta Crystallogr. D Biol. Crystallogr* 59, 1859-1862.
43. Kapust, R. B., Tözsér, J., Fox, J. D., Anderson, D. E., Cherry, S., Copeland, T. D., and Waugh, D. S. (2001) Tobacco etch virus protease: mechanism of autolysis and rational design of stable mutants with wild-type catalytic proficiency, *Protein Eng* 14, 993-1000.
44. Eberhard, A., and Schineller, J. B. (2000) Chemical synthesis of bacterial autoinducers and analogs, *Meth. Enzymol* 305, 301-315.
45. Chhabra, S. R., Harty, C., Hooi, D. S. W., Daykin, M., Williams, P., Telford, G., Pritchard, D. I., and Bycroft, B. W. (2003) Synthetic analogues of the bacterial

signal (quorum sensing) molecule *N*-(3-oxododecanoyl)-L-homoserine lactone as immune modulators, *J. Med. Chem* 46, 97-104.

46. Glasoe, P. K., and Long, F. A. (1960) Use of glass electrodes to measure acidities in deuterium oxide^{1,2}, *The Journal of Physical Chemistry* 64, 188-190.
47. Momb, J., Thomas, P. W., Breece, R. M., Tierney, D. L., and Fast, W. (2006) The quorum-quenching metallo-gamma-lactonase from *Bacillus thuringiensis* exhibits a leaving group thio effect, *Biochemistry* 45, 13385-93.
48. Liu, D., Momb, J., Thomas, P. W., Moulin, A., Petsko, G. A., Fast, W., and Ringe, D. (2008) Mechanism of the quorum-quenching lactonase (AiiA) from *Bacillus thuringiensis*. 1. Product-bound structures, *Biochemistry* 47, 7706-14.
49. Duerre, J. A., and Miller, C. H. (1966) Preparation of L-homocysteine from L-homocysteine thiolactone, *Analytical Biochemistry* 17, 310-315.
50. Rehm, T., Huber, R., and Holak, T. A. (2002) Application of NMR in structural proteomics: screening for proteins amenable to structural analysis, *Structure* 10, 1613-1618.
51. Wüthrich, K. (1986) *NMR of Proteins and Nucleic Acids*. Wiley, New York.
52. Risley, J. M., and Van Etten, R. L. (1989) Mechanistic studies utilizing oxygen-18 analyzed by carbon-13 and nitrogen-15 nuclear magnetic resonance spectroscopy, *Meth. Enzymol* 177, 376-389.

53. Llewellyn, D. R., and Bishop, C. O. (1964) 110. Tracer studies of carboxylic acids. Part I. Acetic and pivalic acid, *J. Chem. Soc.* 545-549.
54. Bond, M. D., Holmquist, B., and Vallee, B. L. (1986) Thioamide substrate probes of metal-substrate interactions in carboxypeptidase A catalysis, *J. Inorg. Biochem* 28, 97-105.
55. Sillén, L. G., and Martell, A. E. (1982) Stability constants of metal-ion complexes, Supplement. Chemical Society, London.
56. Copeland, R. A. (2005) Evaluation of Enzyme Inhibitors in Drug Discovery: A Guide for Medicinal Chemists and Pharmacologists. Wiley-Interscience, Hoboken, N.J.
57. Cheng, Y., and Prusoff, W. H. (1973) Relationship between the inhibition constant (K_i) and the concentration of inhibitor which causes 50 per cent inhibition (I_{50}) of an enzymatic reaction, *Biochem. Pharmacol* 22, 3099-3108.
58. Segel, I. H. (1975) Enzyme kinetics behavior and analysis of rapid equilibrium and steady state enzyme systems. Wiley, New York.
59. Cameron, A. D., Ridderström, M., Olin, B., and Mannervik, B. (1999) Crystal structure of human glyoxalase II and its complex with a glutathione thiolester substrate analogue, *Structure* 7, 1067-1078.
60. Concha, N. O., Janson, C. A., Rowling, P., Pearson, S., Cheever, C. A., Clarke, B. P., Lewis, C., Galleni, M., Frère, J. M., Payne, D. J., Bateson, J. H., and Abdel-

- Meguid, S. S. (2000) Crystal structure of the IMP-1 metallo beta-lactamase from *Pseudomonas aeruginosa* and its complex with a mercaptocarboxylate inhibitor: binding determinants of a potent, broad-spectrum inhibitor, *Biochemistry* 39, 4288-4298.
61. Kurosaki, H., Yamaguchi, Y., Yasuzawa, H., Jin, W., Yamagata, Y., and Arakawa, Y. (2006) Probing, inhibition, and crystallographic characterization of metallo-beta-lactamase (IMP-1) with fluorescent agents containing dansyl and thiol groups, *ChemMedChem* 1, 969-972.
62. Kurosaki, H., Yamaguchi, Y., Higashi, T., Soga, K., Matsueda, S., Yumoto, H., Misumi, S., Yamagata, Y., Arakawa, Y., and Goto, M. (2005) Irreversible inhibition of metallo-beta-lactamase (IMP-1) by 3-(3-mercaptopropionylsulfanyl)propionic acid pentafluorophenyl ester, *Angew. Chem. Int. Ed. Engl* 44, 3861-3864.
63. Nauton, L., Kahn, R., Garau, G., Hernandez, J. F., and Dideberg, O. (2008) Structural insights into the design of inhibitors for the L1 metallo-beta-lactamase from *Stenotrophomonas maltophilia*, *J. Mol. Biol* 375, 257-269.
64. Pettersen, E. F., Goddard, T. D., Huang, C. C., Couch, G. S., Greenblatt, D. M., Meng, E. C., and Ferrin, T. E. (2004) UCSF Chimera--a visualization system for exploratory research and analysis, *J Comput Chem* 25, 1605-1612.

65. Dragani, B., Cocco, R., Ridderström, M., Stenberg, G., Mannervik, B., and Aceto, A. (1999) Unfolding and refolding of human glyoxalase II and its single-tryptophan mutants, *J. Mol. Biol* 291, 481-490.
66. Periyannan, G., Shaw, P. J., Sigdel, T., and Crowder, M. W. (2004) *In vivo* folding of recombinant metallo-beta-lactamase L1 requires the presence of Zn(II), *Protein Sci* 13, 2236-2243.
67. Kaiser, E., and Kezdy, F. (1976) Hydrolysis of Cyclic Esters, *Progress in Bioorganic Chemistry* 4, 239-67.
68. Huisgen, R., and Ott, H. (1959) Die konfiguration der carbonestergruppe und die sondereigenschaften der lactone, *Tetrahedron* 6, 253-267.
69. Johnston, N. J., Mukhtar, T. A., and Wright, G. D. (2002) Streptogramin antibiotics: mode of action and resistance, *Curr Drug Targets* 3, 335-44.
70. Holmquist, B., and Bruice, T. C. (1969) Carbonion (ElcB)mechanism of ester hydrolysis. I. Hydrolysis of malonate esters, *Journal of the American Chemical Society* 91, 2993-3002.
71. Tobias, P. S., and Kezdy, F. J. (1969) Alkaline hydrolysis of 5-nitrocoumaranone. Method for determining the intermediacy of carbanions in the hydrolysis of esters with labile alpha protons, *Journal of the American Chemical Society* 91, 5171-5173.
72. Moore, J. A., and Schwab, J. M. (1991) Unprecedented observation of lactone hydrolysis by the AAl2 mechanism, *Tetrahedron Letters* 32, 2331-2334.

73. Dong, Y. H., Wang, L. H., Xu, J. L., Zhang, H. B., Zhang, X. F., and Zhang, L. H. (2001) Quenching quorum-sensing-dependent bacterial infection by an *N*-acyl homoserine lactonase, *Nature* 411, 813-817.
74. Aubert, S. D., Li, Y., and Raushel, F. M. (2004) Mechanism for the hydrolysis of organophosphates by the bacterial phosphotriesterase, *Biochemistry* 43, 5707-5715.
75. Murphy, B. P., and Pratt, R. F. (1989) A thiono-beta-lactam substrate for the beta-lactamase II of *Bacillus cereus*. Evidence for direct interaction between the essential metal ion and substrate, *Biochem. J* 258, 765-768.
76. Lopreore, C., and Byers, L. D. (1998) The urease-catalyzed hydrolysis of thiourea and thioacetamide, *Arch. Biochem. Biophys* 349, 299-303.
77. Bienvenue, D. L., Gilner, D., and Holz, R. C. (2002) Hydrolysis of thiono-peptides by the aminopeptidase from *Aeromonas proteolytica*: insight into substrate binding, *Biochemistry* 41, 3712-3719.
78. Sigel, H., and McCormick, D. B. (1970) Discriminating behavior of metal ions and ligands with regard to their biological significance, *Accounts of Chemical Research* 3, 201-208.
79. Wang, Z., and Benkovic, S. J. (1998) Purification, characterization, and kinetic studies of a soluble *Bacteroides fragilis* metallo-beta-lactamase that provides multiple antibiotic resistance, *J. Biol. Chem* 273, 22402-22408.

80. Chow, J. Y., Wu, L., and Yew, W. S. (2009) Directed evolution of a quorum-quenching lactonase from *Mycobacterium avium* subsp. *paratuberculosis* K-10 in the amidohydrolase superfamily, *Biochemistry* 48, 4344-4353.
81. Wang, Z., Fast, W., Valentine, A. M., and Benkovic, S. J. (1999) Metallo-beta-lactamase: structure and mechanism, *Current Opinion in Chemical Biology* 3, 614-622.
82. Melino, S., Capo, C., Dragani, B., Aceto, A., and Petruzzelli, R. (1998) A zinc-binding motif conserved in glyoxalase II, beta-lactamase and arylsulfatases, *Trends in Biochemical Sciences* 23, 381-382.
83. Spencer, J., Read, J., Sessions, R. B., Howell, S., Blackburn, G. M., and Gamblin, S. J. (2005) Antibiotic recognition by binuclear metallo-beta-lactamases revealed by X-ray crystallography, *J. Am. Chem. Soc* 127, 14439-14444.
84. Carenbauer, A. L., Garrity, J. D., Periyannan, G., Yates, R. B., and Crowder, M. W. (2002) Probing substrate binding to Metallo- β -Lactamase L1 from *Stenotrophomonas maltophilia* by using site-directed mutagenesis, *BMC Biochem.* 3, 4.
85. Hege, T., and Baumann, U. (2001) Protease C of *Erwinia chrysanthemi*: the crystal structure and role of amino acids Y228 and E189, *Journal of Molecular Biology* 314, 187-193.

86. Lees, J. G., Miles, A. J., Wien, F., and Wallace, B. A. (2006) A reference database for circular dichroism spectroscopy covering fold and secondary structure space, *Bioinformatics* 22, 1955-1962.
87. Whitmore, L., and Wallace, B. A. (2004) DICHROWEB, an online server for protein secondary structure analyses from circular dichroism spectroscopic data, *Nucleic Acids Res* 32, W668-673.
88. Whitmore, L., and Wallace, B. A. (2008) Protein secondary structure analyses from circular dichroism spectroscopy: methods and reference databases, *Biopolymers* 89, 392-400.
89. Khalifah, R. G. (1971) The carbon dioxide hydration activity of carbonic anhydrase. I. Stop-flow kinetic studies on the native human isoenzymes B and C, *J. Biol. Chem* 246, 2561-2573.
90. Hurt, J. D., Tu, C., Laipis, P. J., and Silverman, D. N. (1997) Catalytic properties of murine carbonic anhydrase IV, *J. Biol. Chem* 272, 13512-13518.
91. Schindler, J. F., Naranjo, P. A., Honaberger, D. A., Chang, C. H., Brainard, J. R., Vanderberg, L. A., and Unkefer, C. J. (1999) Haloalkane dehalogenases: steady-state kinetics and halide inhibition, *Biochemistry* 38, 5772-5778.
92. Sreerama, N., and Woody, R. W. (2004) Computation and analysis of protein circular dichroism spectra, *Meth. Enzymol* 383, 318-351.

93. Momb, J., Wang, C., Liu, D., Thomas, P. W., Petsko, G. A., Guo, H., Ringe, D., and Fast, W. (2008) Mechanism of the quorum-quenching lactonase (AiiA) from *Bacillus thuringiensis*. 2. Substrate modeling and active site mutations, *Biochemistry* 47, 7715-25.
94. Lu, X., Yuan, Y., Xue, X., Zhang, G., and Zhou, S. (2006) Identification of the critical role of Tyr-194 in the catalytic activity of a novel *N*-acyl-homoserine lactonase from marine *Bacillus cereus* strain Y2, *Curr. Microbiol* 53, 346-350.
95. Holz, R. C., Bzymek, K. P., and Swierczek, S. I. (2003) Co-catalytic metallopeptidases as pharmaceutical targets, *Curr Opin Chem Biol* 7, 197-206.
96. Bounaga S, Laws A, Galleni M, and Page M. (1998) The mechanism of catalysis and the inhibition of the *Bacillus cereus* zinc-dependent β -lactamase, *Biochem. J.* 331, 703-711.
97. Tioni, M. F., Llarrull, L. I., Poeylout-Palena, A. A., Martí, M. A., Saggi, M., Periyannan, G. R., Mata, E. G., Bennett, B., Murgida, D. H., and Vila, A. J. (2008) Trapping and characterization of a reaction intermediate in carbapenem hydrolysis by *B. cereus* metallo-beta-lactamase, *J. Am. Chem. Soc* 130, 15852-15863.
98. Davies, A. M., Rasia, R. M., Vila, A. J., Sutton, B. J., and Fabiane, S. M. (2005) Effect of pH on the active site of an Arg121Cys mutant of the metallo-beta-lactamase from *Bacillus cereus*: implications for the enzyme mechanism, *Biochemistry* 44, 4841-4849.

99. Xu, D., Xie, D., and Guo, H. (2006) Catalytic mechanism of class B2 metallo-beta-lactamase, *J. Biol. Chem* 281, 8740-8747.
100. Crisp, J., Conners, R., Garrity, J. D., Carenbauer, A. L., Crowder, M. W., and Spencer, J. (2007) Structural basis for the role of Asp-120 in metallo-beta-lactamases, *Biochemistry* 46, 10664-10674.
101. Garrity, J. D., Carenbauer, A. L., Herron, L. R., and Crowder, M. W. (2004) Metal binding Asp-120 in metallo-beta-lactamase L1 from *Stenotrophomonas maltophilia* plays a crucial role in catalysis, *J. Biol. Chem* 279, 920-927.
102. Llarrull, L. I., Fabiane, S. M., Kowalski, J. M., Bennett, B., Sutton, B. J., and Vila, A. J. (2007) Asp-120 locates Zn²⁺ for optimal metallo-beta-lactamase activity, *J. Biol. Chem* 282, 18276-18285.
103. Yamaguchi, Y., Kuroki, T., Yasuzawa, H., Higashi, T., Jin, W., Kawanami, A., Yamagata, Y., Arakawa, Y., Goto, M., and Kurosaki, H. (2005) Probing the role of Asp-120(81) of metallo-beta-lactamase (IMP-1) by site-directed mutagenesis, kinetic studies, and X-ray crystallography, *J. Biol. Chem* 280, 20824-20832.
104. Fersht, A. (1999) Structure and Mechanism in Protein Science: A Guide to Enzyme Catalysis and Protein Folding. W.H. Freeman, New York.
105. Fersht, A. R. (1987) The hydrogen bond in molecular recognition, *Trends in Biochemical Sciences* 12, 301-304.

106. Elias, M., Dupuy, J., Merone, L., Mandrich, L., Porzio, E., Moniot, S., Rochu, D., Lecomte, C., Rossi, M., Masson, P., Manco, G., and Chabriere, E. (2008) Structural Basis for Natural Lactonase and Promiscuous Phosphotriesterase Activities, *Journal of Molecular Biology* 379, 1017-1028.
107. Afriat, L., Roodveldt, C., Manco, G., and Tawfik, D. S. (2006) The latent promiscuity of newly identified microbial lactonases is linked to a recently diverged phosphotriesterase, *Biochemistry* 45, 13677-13686.
108. Geske, G. D., O'Neill, J. C., Miller, D. M., Mattmann, M. E., and Blackwell, H. E. (2007) Modulation of bacterial quorum sensing with synthetic ligands: systematic evaluation of *N*-acylated homoserine lactones in multiple species and new insights into their mechanisms of action, *J. Am. Chem. Soc* 129, 13613-13625.
109. Schaefer, A. L., Greenberg, E. P., Oliver, C. M., Oda, Y., Huang, J. J., Bittan-Banin, G., Peres, C. M., Schmidt, S., Juhaszova, K., Sufrin, J. R., and Harwood, C. S. (2008) A new class of homoserine lactone quorum-sensing signals, *Nature* 454, 595-9.
110. Boudet, A. Evolution and current status of research in phenolic compounds, *Phytochemistry* 68, 2722-2735.
111. Brown, D. C., and Collins, K. D. (1991) Dihydroorotase from *Escherichia coli*. Substitution of Co(II) for the active site Zn(II), *J Biol Chem* 266, 1597-604.

112. Kleifeld, O., Rulisek, L., Bogin, O., Frenkel, A., Havlas, Z., Burstein, Y., and Sagi, I. (2004) Higher Metal–Ligand Coordination in the Catalytic Site of Cobalt-Substituted *Thermoanaerobacter brockii* Alcohol Dehydrogenase Lowers the Barrier for Enzyme Catalysis, *Biochemistry* 43, 7151-7161.
113. Saleh, S. M., Harris, R. F., and Allen, O. N. (1970) Recovery of *Bacillus thuringiensis* var. *thuringiensis* from field soils, *Journal of Invertebrate Pathology* 15, 55-59.
114. Harwood, C. S., and Gibson, J. (1988) Anaerobic and aerobic metabolism of diverse aromatic compounds by the photosynthetic bacterium *Rhodospseudomonas palustris*., *Appl. Environ. Microbiol.* 54, 712-717.
115. Reimmann, C., Ginet, N., Michel, L., Keel, C., Michaux, P., Krishnapillai, V., Zala, M., Heurlier, K., Triandafillu, K., Harms, H., Défago, G., and Haas, D. (2002) Genetically programmed autoinducer destruction reduces virulence gene expression and swarming motility in *Pseudomonas aeruginosa* PAO1, *Microbiology (Reading, Engl.)* 148, 923-932.
116. Wang, Y., Dai, Y., Zhang, Y., Hu, Y., Yang, B., and Chen, S. (2007) Effects of quorum sensing autoinducer degradation gene on virulence and biofilm formation of *Pseudomonas aeruginosa*, *Science in China Series C: Life Sciences* 50, 385-391.
117. Dowd, S. E., Sun, Y., Secor, P. R., Rhoads, D. D., Wolcott, B. M., James, G. A., and Wolcott, R. D. (2008) Survey of bacterial diversity in chronic wounds using

- Pyrosequencing, DGGE, and full ribosome shotgun sequencing, *BMC Microbiol.* 8, 43.
118. Satoh, H., Yamakawa, T., Kindaichi, T., Ito, T., and Okabe, S. (2006) Community structures and activities of nitrifying and denitrifying bacteria in industrial wastewater-treating biofilms, *Biotechnology and Bioengineering* 94, 762-772.
119. Macedo, A. J., Kuhlicke, U., Neu, T. R., Timmis, K. N., and Abraham, W. (2005) Three Stages of a Biofilm Community Developing at the Liquid-Liquid Interface between Polychlorinated Biphenyls and Water, *Appl. Environ. Microbiol.* 71, 7301-7309.
120. Lopez, M. A., Serna, F. J. Z. D. D. L., Jan-Roblero, J., Romero, J. M., and Hernandez-Rodriguez, C. (2006) Phylogenetic analysis of a biofilm bacterial population in a water pipeline in the Gulf of Mexico, *FEMS Microbiology Ecology* 58, 145-154.

Vita

Jessica Momb was born in Walnut Creek, CA on September 3, 1979 along with her twin brother Andrew to Daniel and Kathy Momb. She graduated from Humboldt State University in 2004 with the degree of Bachelor of Science in Chemistry.

Publications:

Momb, J., Thomas, P. W., Breece, R. M., Tierney, D. L., and Fast, W. (2006) The quorum-quenching metallo-gamma-lactonase from *Bacillus thuringiensis* exhibits a leaving group thio effect, *Biochemistry* 45, 13385-93.

Liu, D., Thomas, P. W., Momb, J., Hoang, Q. Q., Petsko, G. A., Ringe, D., and Fast, W. (2007) Structure and specificity of a quorum-quenching lactonase (AiiB) from *Agrobacterium tumefaciens*, *Biochemistry* 46, 11789-99.

Liu, D., Momb, J., Thomas, P. W., Moulin, A., Petsko, G. A., Fast, W., and Ringe, D. (2008) Mechanism of the quorum-quenching lactonase (AiiA) from *Bacillus thuringiensis*. 1. Product-bound structures, *Biochemistry* 47, 7706-14.

Momb, J., Wang, C., Liu, D., Thomas, P. W., Petsko, G. A., Guo, H., Ringe, D., and Fast, W. (2008) Mechanism of the quorum-quenching lactonase (AiiA) from *Bacillus thuringiensis*. 2. Substrate modeling and active site mutations, *Biochemistry* 47, 7715-25.

Permanent address: 1200 Barton Hills Drive, #339; Austin, TX 78704

This dissertation was typed by Jessica Momb.